5-2016

Network Dynamics of Visual Object Recognition

Mehmet C. Kadipasaoglu

NETWORK DYNAMICS OF VISUAL OBJECT RECOGNITION

by

Mehmet Cihan Kadipasaoglu, B.Sc.

APPROVED:

_____
Nitin Tandon, M.D.
Advisory Professor

_____
Steven J. Cox, Ph.D.

_____
Valentin Dragoi, Ph.D.

_____
Harel Shouval, Ph.D.

_____
Edgar T. Walters, Ph.D.

APPROVED:

_____
Dean, The University of Texas
Graduate School of Biomedical Sciences at Houston

NETWORK DYNAMICS OF VISUAL OBJECT RECOGNITION

A

DISSERTATION

Presented to the Faculty of

The University of Texas

Health Science Center at Houston

and

The University of Texas

M. D. Anderson Cancer Center

Graduate School of Biomedical Sciences

in Partial Fulfillment

of the Requirement

for the Degree of

DOCTOR OF PHILOSOPHY

By

Mehmet Cihan Kadipasaoglu, B.Sc.

Houston, Texas

December 2015

Dedication

This thesis is dedicated to my family and to my wonderful wife (my pigeo), who is the drive behind all things for which I strive

Acknowledgements

If acknowledgements are to be given, I would certainly need to begin with my amazing parents, who have worked so hard, and for so long, so that my sister and I could have the richest possible experience growing up. It was they that taught me how to be emotionally intelligent and how to cultivate a love for knowledge. And of course to my wonderful and outrageously talented sister, gifted artist that she is. If it weren't for her, I probably never would have even considered this whole research thingamajig.

I don’t even know how to begin to thank my incredible wife - Jamie - without whom I probably never would have made it past my second year of school. She has put up with so much from me, and she has given up so much for me, and still, all that she does is love me without end. She is the light in my night that guides me through this life.

I must graciously thank my mentor and P.I., Dr. Nitin Tandon, who has given me the most incredible opportunity to study the mind by way of some truly awesome “*science-ing*”, and who has taught me to eschew obfuscation along the way. This thanks also extends to everyone in the Tandon lab (the Tandonites) for their help with getting me through this process in one piece: Chris Conner (who taught and molded me in the ways of the lab), Tom Pieters, Mike Disano, Meagan Whaley, Vatche Baboyan, Kiefer Forseth, Matthew Rollo, and of course, the many new Drs. in the house: Bartlett of the Blaise Moore, Eleonora Bartoli, Suganya Karunakaran, and Kamin Kim. Thanks should also reach my distant Californian brethren: Amber, Millie, and Andrew, and their faithful guardian, Dr. Arne Ekstrom, without whom SFN would not have been the same, and the chance to enjoy in-depth discussions on the finer points of Nicolas Cage’s raw talent might have never bloomed.

I want to thank the distinguished faculty that served on my advisory committee, and who helped shaped me into a more successful scientist: Drs. Valentin Dragoi, Harel Shouval, Edgar T Walters, and Steve Cox (along with his amazing BrainSTEM program). And I must thank everyone in the MD/PhD program at the UT-Health Science Center at Houston, with special acknowledgments for Dr. Walters, Jo Cheatwood and Dr. Dianna Milewicz for their constant support in helping me navigate this oh-so-fun affair.

I am especially grateful to all the patients who volunteered for participation in the countless hours of research experimentation, the neurologists at the Texas Comprehensive Epilepsy Program (Jeremy Slater, Giridhar Kalamangalam, Omotola Hope and Melissa Thomas) who participated in the care of these patients, Vips Patel, and all of the nurses and technicians in the Epilepsy Monitoring Unit at Memorial Hermann Hospital who helped make this research possible.

Penultimately, stepping away from the academic realm and into the social, I must express my deepest gratitude to my amazing friends and mentors from Awty International (the Cool Kidz and the endlessly supportive Namtvedt family); Carnegie Mellon (Ojo-Lippa and the Forbes House gang); Texas Heart (Drs. Frazier and Cohn, and the endlessly knowledgeable Jesse Rios); and the UT-HSC Medical School (the Rock-Sake-Chicken and In-Home-Country doctors). It is with these incredible folk that I have shared some of my proudest and most ridiculous experiences; and their support, advice, and love have played a non-trivial role in getting me where I am today.

And finally, because money is power (or something along those lines), I would like to thank my funding sources: The Center for Clinical and Translational Research

Award from the National Institute of Health, the Vivian Smith Foundation for Neurologic Research, and the Memorial Hermann Foundation.

NETWORK DYNAMICS OF VISUAL OBJECT RECOGNITION

Mehmet Cihan Kadipasaoglu, B.Sc.

Advisory Professor: Nitin Tandon, M.D.

Visual object recognition is the principal mechanism by which humans and many animals interpret their surroundings. Despite the complexity of neural computation required, object recognition is achieved with such rapidity and accuracy that it appears to us almost effortless. Extensive human and non-human primate research has identified putative category-selective regions within higher-level visual cortex, which are thought to mediate object recognition. Despite decades of study, however, the functional organization and network dynamics within these regions remain poorly understood, due to a lack of appropriate animal models as well as the spatiotemporal limitations of current non-invasive human neuroimaging techniques (e.g. fMRI, scalp EEG). To better understand these issues, we leveraged the high spatiotemporal resolution of intracranial EEG (icEEG) recordings to study rapid, transient interactions between the disseminated cortical substrates within category-specific networks. Employing novel techniques for the topologically accurate and statistically robust analysis of grouped icEEG, we found that category-selective regions were spatially arranged with respect to cortical folding patterns, and relative to each other, to generate a hierarchical information structuring of visual information within higher-level visual cortex. This may facilitate rapid visual categorization by enabling the extraction of different levels of object detail across multiple spatial scales. To characterize network interactions between distributed regions sharing the same category-selectivity,

we evaluated feed-forward, hierarchal and parallel, distributed models of information flow during face perception via measurements of cortical activation, functional and structural connectivity, and transient disruption through electrical stimulation. We found that input from early visual cortex (EVC) to two face-selective regions – the occipital and fusiform face areas (OFA and FFA, respectively) – occurred in a parallelized, distributed fashion: Functional connectivity between EVC and FFA began prior to the onset of subsequent re-entrant connectivity between the OFA and FFA. Furthermore, electrophysiological measures of structural connectivity revealed independent cortico-cortical connections between the EVC and both the OFA and FFA. Finally, direct disruption of the FFA, but not OFA, impaired face-perception. Given that the FFA is downstream of the OFA, these findings are incompatible with the feed-forward, hierarchical models of visual processing, and argue instead for the existence of parallel, distributed network interactions.

Table of Contents

Dedication iii

Acknowledgements iv

Abstract vii

Table of Contents ix

List of Tables xii

List of Figures xiii

List of Abbreviations xiv

Chapter I : Introduction 1

- **The functional organization of higher-level visual cortex in humans** 6
- **Network dynamics of object recognition** 9
- **Goals** 11
- **Structure of this dissertation** 15

Chapter II : Surface-Based Analysis of Intracranial EEG 16

- **Introduction** 17
- **Methods** 21
- **Results** 33
- **Conclusions** 38
- **Summary** 43

Chapter III : Functional Organization of the Ventral Temporal and Lateral Occipital Cortex: 44

Introduction **45**

Methods **48**

Results **56**

Conclusions **68**

Summary **74**

Chapter IV : Information Flow within the Ventral Temporal and Lateral Occipital Cortex **75**

Introduction **76**

Methods **78**

Results **90**

Conclusions **105**

Summary **111**

Chapter V : Conclusions and Future Directions **112**

Future Plans: **118**

Appendix A: The History of Visual Cortex **121**

Ventricular localization and the *Sensus Communis* **123**

Cortical localization and the discovery of the sensory-motor brain **125**

Discovery of association cortex and visual agnosia **128**

Discovery of inferotemporal cortex and its role in object recognition **129**

Appendix B: Disease Profile of Drug-Resistant Epilepsy **133**

Introduction **134**

Epidemiology **135**

Etiology **136**

Symptoms and Diagnosis **137**

Surgical Treatment **138**

Prognosis **140**

Translational Need **141**

References **143**

Vita **187**

List of Tables

Table II-1. Spatial Coordinates of ROI Peak and Mean Activation Sites 36

Table IV-1. Experiment 1 - Mixed-effects Multilevel Analysis of Face-selectivity 91

List of Figures

Figure II-1. Surface-electrode recording zone (sERZ) and ECoG datasets. 25

Figure II-2. Isotropic and Anisotropic Spatial Transformation of ECoG data 27

Figure II-3. Spatial Normalization Comparisons, Grouped MEMA, and Time-series Analyses 34

Figure II-4. Comparison of Volume- and Surface-based MEMA with Surface-based Normalizations 37

Figure III-1. Experimental Design and Analysis 49

Figure III-2. Population Coverage of Higher-level Visual Cortex 52

Figure III-3. Single Subject Category-selectivity Analysis 57

Figure III-4. Grouped SDE and *d*' Visualization 59

Figure III-5. Grouped *d*' Sensitivity vs. SDE Coordinates 61

Figure III-6. Linear Mixed Effects Model Results 63

Figure III-7. Spatial Organization of VTC and LOC Category-Selectivity 67

Figure IV-1. ECoG Spectral and Functional Connectivity Analyses 83

Figure IV-2. Single Subject Time-Series Analyses 92

Figure IV-3. Grouped Time-Series Representations 94

Figure IV-4. Grouped Functional Connectivity: Faces 96

Figure IV-5. Summary Time-Series and Connectivity: Faces 97

Figure IV-6. Grouped Functional Connectivity: Non-Face Stimuli 99

Figure IV-7. Individual Structural Connectivity 101

Figure IV-8. Individual Cortical Stimulation Mapping 103

List of Abbreviations

AEC	Amplitude Envelope Correlation
BGA	Broadband Gamma Activity
BOLD	Blood-Oxygenation-Level Dependent
CCEP	Cortico-Cortical Evoked Potential
CSM	Cortical Stimulation Mapping
ECoG	Electrocorticography
EEG	Electroencephalogram
ERP	Event Related Potential
EVC	Early Visual Cortex
FDR	False Detection Rate
FFA	Fusiform Face Area
FFT	Fast Fourier Transform
FHM	Feedforward, Hierarchical Model
fMRI	Functional Magnetic Resonance Imaging
icEEG	Intracranial EEG
LOC	Lateral Occipital Cortex
LOS	Lateral Occipital Sulcus

MEMA	Mixed-Effects Multilevel Analysis
MFS	Mid-Fusiform Sulcus
N1	First Negative ERP
NHM	Non-hierarchical Model
OFA	Occipital Face Area
OTS	Occipitotemporal Sulcus
pSTS	posterior Superior Temporal Sulcus
ROI	Region of Interest
SB-MEMA	Surface-Based MEMA
SDE	Subdural Electrode
sERZ	Surface Electrode Recording Zone
VB-MEMA	Volume-Based MEMA
vERZ	Volumetric Electrode Recording Zone
VTC	Ventral-Temporal Cortex

Chapter I: Introduction

If the doors of perception were cleansed every thing would appear to man as it is, infinite. For man has closed himself up, till he sees all things thro' narrow chinks of his cavern.

William Blake, 1790

The world is an uncertain place, within which humans and other animals must find a way to extract meaning from noise in order to survive. Our (human) experience of the world is a distinctly visual one, for which we have evolved dedicated machinery to extract useful 3D mental representations from 2D images on the retina. For the vast majority of people, it appears to work flawlessly. After all, "seeing is believing" and "vision is a certain route to knowledge"[1]. Or, as Plato has Theaetetus respond to Socrates, "Knowledge *is* perception." Such belief has obvious selective advantages: you are more likely to remain alive, and out of some predator's stomach, if you believe that the tiger ahead is really there.

The problem, as a variety of visual illusions make painfully clear, is that what we see is not necessarily what is really there[a]. There are many different ways that a visual scene can be reconstructed from a 2D retinal projection, which makes the "inverse optics" required by the brain an ill-posed problem, without a unique solution[1]. But competition for survival does not afford the luxury of pondering the myriad of possible solutions to the ambiguous input from our eyes. Thus, the human brain evolved to use prior knowledge about the world to filter irrelevant information and convert ill-posed problems into rapidly solvable ones.

The apparent ease and automaticity of visual perception also belies its underlying complexity, which is manifest in the proportion of human cortex dedicated to vision (~1/2 of the brain)[2, 3]. But it is only recently that conceptual and technological advances have enabled neuroscientists to begin to make real progress towards

[a] This problem is fundamental issue in epistemology, the theory of knowledge. In an 1878 lecture on perception, Hermann Helmholtz (theory of unconscious inference), described this problem as fundamental to all science as well as epistemology, asking: *What is true in our sense perceptions and thought? And in what way do our ideas correspond to reality?*

deciphering these neural mechanisms that give rise to perception. One aspect of our visual experience that holds special interest to neuroscience is **object recognition**. In general terms, object recognition is what allows us to recognize the faces of our loved ones, find our car in a crowded parking, and to read the words on this page. More specifically, object recognition describes the process by which the brain's visual system interprets sensory input to detect and categorize[b] objects in our environment[2, 4].

To understand how the brain so effortlessly achieves object recognition, neuroscientists have turned to lesional and functional neuroimaging studies in both animals and humans (see Appendix A for historical overview). These studies suggest that the human visual system operates in a hierarchical and largely feedforward fashion, summarized here in three stages[2-8]:

1) Visual sensory input from the environment[c], encoded by retinal activity patterns, is relayed via thalamic intermediates to the occipital striate (i.e. V1/Brodmann's area 17), where visual information is transformed and re-represented in the population activity of neurons.

2) Neuronal output from occipital striate progresses along a "ventral visual stream" comprising a series of retinotopically-organized early and intermediate visual areas (e.g. V1 to V2 to V4). Within each area, visual information is re-represented in stages of increasing complexity[d].

---

[b] Visual categorization is the rapid extraction of different levels of information (general to specific) about an object (e.g. object category, identity)

[c] Object recognition occurs on retinal input from ~central 10 degrees of the visual field.

[d] Each of these early and intermediate visual areas is retinotopically organized, in which adjacent points on the retina mapping to adjacent points in the visual space of the cortex. Thus visual space in the world is fully represented in the brain (i.e. visuotopographic organization).

3) Output at the end of the ventral stream reaches higher-level visual areas in the ventral temporal and lateral occipital cortices (VTC and LOC, respectively). The VTC and LOC mediate object recognition through the activity of distinct neuronal clusters that differentially and selectively respond to specific categories of visual stimuli (e.g. faces, places, tools, animals, words)[e].

Evidence for a hierarchical visual system was first proposed by Hubel and Wiesel[f] in 1959[9, 10]. Using single-neuron electrophysiology, they demonstrated how information from the eye (i.e. retinal activity) mapped in a point-to-point fashion onto neurons in striate cortex to create an internal representation of the visual world (i.e. a retinotopic or visuotopographic map). They then demonstrated that neighboring visual areas in the brain could be modeled using hierarchical relationships, in which neurons at higher levels of the hierarchy integrated input from groups of lower-level neurons to produce larger and more complex representations of the visual field (e.g. points grouped into a line, and lines grouped into a box)[5, 6]. In this fashion, internal representations of the world would become progressively more complete at each stage along the visual hierarchy [10].

Hubel and Wiesel's hypotheses were impressively confirmed in the subsequent discoveries of the numerous early and intermediate visual areas (e.g. V2, V3, V4) that extended beyond the boundaries of the striate cortex[g], each containing its own

[e] Retinotopic organization is no longer present in these regions.
[f] Hubel and Wiesel's work revolutionized visual neuroscience, as they introduced the first mechanism for understanding how perception could result from organized neural activity.
[g] At the time (~1950s) vision was still commonly believed to occur entirely within primary visual cortex (occipital striate)

increasingly complex visuotopographic representation[6, 11, 12]. These regions were eventually consolidated and organized within two parallel, but tightly interrelated visual processing streams: a dorsal visual stream for spatial information (*where pathway*) and a ventral visual stream for object information (*what pathway*)[7, 13].

In 1969, the final stage in the ventral visual stream was discovered by Charles Gross[14]. Recording single-neuron activity in monkey inferior temporal (IT) cortex, Gross reported clusters of neurons that selectively responded to complex and salient objects[h] – specifically hands and faces[14-17]. Importantly, these neurons were the first in the visual stream thus far to *not* demonstrate visuotopographic organization. Rather, they were foveally biased and had bilateral visual field representation (i.e. unified percepts of central vision). They also consistently activated to their preferred stimulus, regardless of changes in stimulus size, contrast, and color (i.e. invariant responses)[18]. Finally, recent lesional studies in monkeys had demonstrated that injury to these same IT regions could produce unique perceptual deficits – visual agnosia[i] – in which the monkey would be unable to recognize objects by sight, despite the absence of any impairment in visual acuity[19-24]. Taken together, this evidence overwhelmingly suggested that Gross' category-specific neuronal clusters mediated the final stage in

[h] Gross' decision to test face and hand stimuli was inspired by the Polish neuroscientist, Jerzy Konorski. Konorski had recently proposed (nearly presciently) the concept of "gnostic" neurons and fields, which were regions responding to 'unitary percepts' of ecologically relevant stimuli (e.g. faces) that he thought would be in IT.

[i] Visual agnosia was first reported by Hermann Munk in 1881, during his historic "battle for the visual cortex" with David Ferrier. At the time he used the term "psychic blindness", which was popularized by William James in his 1890 *Principles of Psychology*. This was later renamed "visual agnosia" by Sigmund Freud in 1891. At the time, under the British associationism movement in psychology, the agnosias were not considered to be a visual sensory deficit. Instead, it was a problem of "associating" a sensory input with "what it stands for" due to damage to the "visuopsychic" regions in the association cortex.

visual object recognition – the interface between sensory and conceptual knowledge[18, 25, 26].

In humans, the first reports of category-specific activity were not made until almost 20 years later, in the early 1990s, following the introduction of non-invasive functional neuroimaging technology – e.g. positron emission topography (PET) and functional magnetic resonance imaging (fMRI)[27-31]. Within a few years, however, early and intermediate visual areas in the human brain had become reliably mapped, and the existence of the human ventral visual stream was confirmed[32, 33].

Today, category-specific regions of higher-level visual cortex form the cornerstone of all object recognition research. However, despite 25 years of intensive research, two fundamental questions have yet to be resolved: a) what is the functional organization of these regions within higher-level visual cortex and b) do multiple regions sharing the same category-preference (i.e. a category-specific network) interact in a serial or parallel fashion to perform object recognition.

The functional organization of higher-level visual cortex in humans

The first model of category-specific organization was the modular hypothesis, introduced by Nancy Kanwisher in 1997[34], which argued that the higher-level visual cortex was a heterogeneous structure containing a distinct set of specialized regions responsible for the processing of specific object categories (e.g. faces). The first (and most famous) module to be described was the fusiform face area (FFA), a small (~3-5mm) region in the mid-fusiform gyrus believed to be specialized for the representation of facial identity[34, 35]. Work from Kanwisher's laboratory soon discovered additional modules subserving different category-specific functions, such as the parahippocampal

place area (PPA) – a region specialized for the representation of visual scenes[36]; and the fusiform body area (FBA) – a region specialized for body representation[37].

Although Kanwisher's modular hypothesis remains influential, it has been the focus of considerable criticism[33, 38-44]. Most relevant to this discussion are criticisms pertaining to its heavy emphasis on single regions. With respect to faces, at least two other face-selective regions were typically observed in addition to the FFA: an occipital face area (OFA), localized posteriorly in the inferior occipital cortex[39], and another region in the posterior aspects of the superior temporal sulcus (pSTS)[45]. Similarly, multiple place- and body-selective foci have also been reported throughout the lateral and occipital cortical regions [46-48].

An alternative to modular hypothesis (for faces) was proposed in the distributed model of face-perception, introduced by James Haxby in 2000[40]. Haxby's distributed model suggested that the three distinct face-selective regions – the OFA, FFA, and pSTS – formed a 'core network" for face-perception, in which each region was responsible for a different aspect of face processing (detection, identity, and gaze, respectively). Since Haxby's original proposal, the distributed model has become widely accepted and has since been extended to other behaviorally relevant categories (e.g. body-parts) [4, 41, 49].

A second criticism of the modular hypothesis has been with its failure to explain a larger-scale organizational principle for these category-specific regions, beyond their rough localization within different gyri[33, 50]. This was problematic since the size and location of a category-selective region (e.g. FFA) could demonstrate considerable variability between individuals, both within and across studies. Additionally, within a

single individual, multiple foci of category-selective activity were often observed within the anatomical boundaries a single gyrus (e.g. multiple face-selective areas along the length of the lateral fusiform). Without established criteria, researchers were forced to either choose one activation focus (arbitrarily), or to average them together into one larger region of activation[33]. This produced discrepancies in the reported locations of these regions between different groups, which were often further exacerbated by the poor imaging resolution of earlier fMRI studies, the larger voxel sizes measured (i.e. volumetric pixels of the brain activity imaged), and the failure to account for gyral/sulcal folding patterns during data visualization – all of which resulted in a spatial blurring of activity across the cortex.

In the early 2000s, focus shifted towards identifying potential organizational principles for these regions [51-57]. Notably, outside of object recognition, more recent studies have shown that specific anatomical features (e.g. sulcal landmarks) could predict transitions in cyto-/ receptor- architectonics, distinct white-matter (i.e. structural) connectivity networks, as well as in large-scale functional maps, such as visual eccentricity bias (i.e. a regions preference for foveally vs. peripherally presented images) [4, 58-65]. When subsequently compared with reported locations for different category-selective regions, a consistent alignment with these same anatomical landmarks could also be observed (although much more inconsistently, for the reasons discussed above).

In 2014, Kalanit Grill-Spector consolidated these findings into a new model of hierarchical information coding, based around the preservation of structure-function relationships[4]. Grill-Spector suggested that the spatial organization of category-selective regions, with respect to cortical anatomy as well as relative to each other,

should be related to the underlying micro- and macro-anatomical organization (e.g. the spatial layout of different cyto-architecture and white-matter connectivity networks, respectively). Grill-Spector argued that the difference in underlying neural circuitry likely reflects different processing demands for distinct functional representations (e.g. peripherally-biased scenes vs. foveally-biased faces). By segregating unrelated category-specific regions into their respective functional networks (place and face-network, respectively), higher-level visual regions could parallelize visual processing streams to optimize information extraction. And by grouping category-specific regions that have related stimulus preferences (e.g. faces and body-parts), wiring costs and computational lag-times could be minimized between regions that have shared neural circuitry. Furthermore, the spatial clustering and segregating of related and unrelated category-specific regions (e.g. faces and animals vs. places and tools), respectively, around anatomical landmarks would implicitly generate larger-scale functional maps (animacy vs. inanimacy), which could enable the visual system, as well as downstream higher cognitive areas (e.g. speech centers in prefrontal gyrus) to rapidly extract categorical information at multiple levels of extraction[4, 66].

Although promising in its explanatory scope, Grill-Spector's hierarchical information coding model has not yet been fully validated, due in part to its relative novelty, but also to the fine-scale distinctions it makes, which are beyond the capacity of non-invasive neuroimaging methods to resolve[67].

Network dynamics of object recognition

Following the introduction of Haxby's distributed model for face processing, another shift in focus occurred, moving away from *which* brain regions activated for a specific category[32, 68], towards how multiple, distributed brain regions that all responded

to the same category might *interact* to achieve the task. The first systematic proposal for a category-specific network was introduced by Haxby to explain how the three different regions in his 'core' face network – the OFA, FFA, and pSTS – worked together to achieve face perception[40]. However, while prior studies had identified differential aspects of face-processing for the FFA (identity) and the pSTS (gaze and expression), the OFA's function at that time was still largely unknown[40].

Given the hierarchical organization in earlier visual systems, Haxby argued that face processing should follow similar principles, and be achieved in stages of increasing complexity. Thus, feature detection (e.g. eyes, mouth, nose) should precede facial representation (i.e. a complete face), which should precede facial recognition (identity)[40, 42]. Haxby further argued that the relatively posterior anatomical location of the OFA made it the likely candidate for early feature detection, as it was positioned to provide input to both the downstream FFA and pSTS. Haxby's feed-forward, hierarchical (FHM) model of face processing has remained influential since its inception[2, 43, 69-71]. However, recent findings from studies in individuals with uni- or bilateral OFA lesions have posed serious issues for FHM accounts of face processing[69, 72-74].

According to FHM models, the loss of the OFA (as the primary input to FFA) should preclude normal FFA function. However, subjects with OFA lesions not only demonstrated normal FFA function, but their performance during basic-level categorization tasks (e.g. detect face vs. car) matched those of healthy individuals[72]. Information was reaching the FFA of these individuals in an independent fashion, indicating that while the OFA may be a critical node in the face-network, it is not

necessarily the entry node[42]. Notably, where their performance did suffer was in the *differentiation* of faces (i.e. identity discrimination).

To account for these findings, Bruno Rossion introduced an alternative, non-hierarchical model (NHM) of face processing in 2003[43]. He argued that the FFA must be able to independently detect faces, using at least a coarse level of visual detail, while the OFA, in contrast, would be crucial for identity discrimination through a finer-level analysis of facial features[74]. Therefore, information flow within this network would not be rigidly serial (e.g. OFA to FFA only). Instead, Rossion proposed that input from early-visual areas was more likely independently delivered to both the OFA and FFA in parallel. Following coarse face detection by the FFA, facial representations could be progressively refined through the FFA's re-entrant interactions with the OFA[72, 74].

Unfortunately, non-invasive neuroimaging methods have been unable to critically evaluate feed-forward hierarchical and non-hierarchical accounts of face-perception, as the transient interactions between these regions occur at shorter time scales than can currently be resolved[75, 76].

Goals

Until only recently, our understanding of visual function[j] has been rooted in the study of neurological deficits due to brain-lesions and single-neuron recordings from the monkey brain[77, 78]. However, the uncontrolled, anatomically imprecise nature of brain lesions limits their spatial resolution and validity, while animal models invariably fall short in modeling human cognitive function. Thus, our insight into *human* visual

[j] It has only been 125 years since visual areas in the brain were first localized to the occipital striate (~1880-1890).

function – specifically the category-selectivity of higher-level human visual cortex – has only begun to evolve within the last 25 years[78].

The advent of non-invasive imaging modalities (e.g. fMRI, scalp EEG) rapidly advanced our ability to study the human visual system. However, the questions currently being asked have begun to exceed the spatiotemporal resolution of these modalities[76, 79]. An alternative approach for studying higher-level visual function, which surmounts most of these limitations, is provided by human intracranial EEG (icEEG) recordings, using subdural electrodes (SDEs) that measure local neuronal activity directly from the cortex with high spatial (1-3 mm) and temporal (sub- millisecond) resolution [75, 80-83]. As such, icEEG recordings offer an unmatched ability to study rapid, transient neural interactions across local and disseminated brain networks.

My research proposal seeks to investigate the functional and network properties of category-selective regions in the VTC and LOC utilizing icEEG data from a large patient cohort (*n*=42), collected during a visual object recognition task. Five ecologically relevant categories of visual stimuli[84, 85] (faces, animals, places, tools, and words) will be used to determine: **whether ventral temporal and lateral occipital cortical regions exhibiting category-selectivity form distinct, independent functional modules or are topologically organized into large-scale functional maps; and whether information flow into these regions relies upon serial, feed-forward or parallel, distributed input from early visual cortex.** These hypotheses will be evaluated through the following specific aims:

Specific Aim 1: To develop a topologically accurate approach for grouped icEEG analysis: Despite remarkable advantages, the broader application of icEEG to

cognitive science has been hindered by difficulties in data analyses at the individual and population-level. This is largely due to challenges from spatially variable and sparse electrode placement, which is clinically determined for each patient. To resolve these issues, a method for precise inter-subject data co-registration and statistically robust grouped analysis will be developed[80, 81]. Topologically accurate population-level activity maps using grouped icEEG data will be generated to enable comprehensive electrophysiological investigation of VTC and LOC category-selectivity in Aim 2.

Specific Aim 2: To determine if category-selective regions in VTC and LOC are organized within larger-scale functional maps**:** icEEG measures of task-induced cortical activity will be used to identify SDEs recording from category selective regions in the VTC and LOC. Individual and grouped-level analyses will be used to determine whether the spatial coordinates of SDEs over cortical regions exhibiting similar category-selective preferences (e.g. faces & animals) are arranged with respect to cortical anatomy into larger-scale functional maps (e.g. animacy). **Our hypothesis was that category-selective regions will be arranged on lateral-to-medial and ventral-to-dorsal axis in the VTC and LOC, respectively, within which large-scale functional maps (for animacy) will be implicitly generated.**

Specific Aim 3: To model information flow within VTC and LOC during visual processing: Measures of functional and structural connectivity as well as

disruptive cortical stimulation mapping, will be used to investigate information flow between early visual cortex and category-selective regions identified within the VTC and LOC. Directionality estimates of connectivity will be used to determine whether information flow is rigidly feed-forward and serial or parallelized and distributed in nature. **Our hypothesis was the information flow from early visual cortical regions to category-selective regions would occur in a parallel, distributed fashion, and that re-entrant interactions between category-selective regions would mediate subsequent visual processing – consistent with non-hierarchical model of higher-level visual networks.**

The application of icEEG to the study of visual networks presents unique opportunities to resolve long-standing theoretical debates, and generate new cognitive models that may direct future neural prosthetics and rehabilitation efforts. Importantly, a more accurate understanding of patients' brain networks will assist clinicians in planning safer interventional therapeutic strategies.

Structure of this dissertation

This dissertation is organized into 5 chapters and 2 appendices:

Chapter 1 (current chapter) provides an introduction to visual object recognition, as well as the specific aims and hypotheses of my research.

Chapter 2 is methodological in nature, relating to the application of icEEG for the study of human cognition, as well as the techniques I have developed to address existing limitations of icEEG as described in *Specific Aim 1*.

Chapters 3 and 4 provide the results of my research on the objectives outlined in *Specific Aims 2 and 3*, respectively.

Chapter 5 provides an overall summary and discussion of the dissertation, as well as future research directions.

Appendix A provides a broader historical review of visual neuroscience, describing the field's progress from antiquity to the modern era.

Appendix B provides an epidemiological review of pharmaco-resistant (i.e. drug resistant) focal epilepsy. This is the condition common across patients undergoing icEEG recordings as part of a pre-surgical evaluation to localize epileptogenic brain tissue.

Chapter II: Surface-Based Analysis of Intracranial EEG

Introduction

Note: This chapter is based upon: Kadipasaoglu C.M., Baboyan V.G., Conner C.R., Chen G., Saad Z.S., Tandon N. *Surface-based mixed effects multilevel analysis of grouped human electrocorticography*. NeuroImage, 101, 215-224 (2014). doi:10.1016/j.neuroimage.2014.07.006. Reprinted with permission from Elsevier

Intracranial EEG (icEEG) recordings are a frequent part of the evaluation of pharmaco-resistant epilepsy at specialized centers. In the United States, there are about a million patients with epilepsy who are likely surgical candidates. icEEG is commonly carried out using subdural grid electrodes (SDEs), yielding summed local neuronal activity around each electrode- termed electrocorticography (ECoG) [83]. In order to precisely delineate the epileptogenic network, SDEs are implanted over both pathologic and functionally normal cortical tissue. While abnormal ECoG is used to make clinical decisions regarding the resection of brain regions, ECoG recordings of local cortical network processes over uninvolved brain areas in these patients can provide multi-lobar, high spatio-temporal resolution sampling from disseminated brain regions [86-88]. These data provide an optimal convergence of coverage and fidelity compared to the spatially limited sampling of microelectrodes [89], the poor temporal resolution of fMRI, and the poor signal qualities of scalp EEG [76, 79].

Cognitive operations are reflected precisely by ECoG recordings of event related broadband activity in the mid-to-high gamma frequency range (60-120 Hz) [76, 90-94]. This broadband gamma activity is thought to bind remote regions during cognitive processes [95] such as episodic memory retrieval [86], semantic decoding and confrontation naming [96, 97]. Gamma-band activity also robustly correlates with the blood oxygen level dependent (BOLD) signal commonly used to provide insight into similar cognitive

processes using functional MRI techniques [96, 98-103]. The comparison of ECoG with the BOLD signal [96, 104, 105] in patients with intracranial electrodes additionally offers an opportunity to elucidate the relationship between hemodynamic and electrophysiological signals, during cognitive processes that cannot be replicated in animal models [106].

Despite its remarkable properties, the broader application of ECoG to cognitive neuroscience has been limited by three significant disadvantages: 1) Concerns that data collected from epileptic subjects may not reflect normal cognitive function. 2) Electrode coverage in each subject is variable and sparse (i.e. limited) due to the fact that clinical criteria dictate electrode placement. 3) The relative scarcity of such data that minimizes the potential for broad application to the study of human cognition [76].

Concerns about the applicability of these recordings to “normal” human cognition have been addressed by patient inclusion criteria based on pre-operative neuropsychological evaluation (e.g. IQ>80), the use of non-complex paradigms that optimize likelihood of response parameters overlapping with those seen in healthy volunteers, and the inclusion of only those ECoG data that are free of electrophysiological abnormalities [76, 79, 90, 107]. We have previously compared patient fMRI and ECoG recordings against fMRI obtained in healthy volunteers, under identical task conditions, further validating the reliability of such recordings [97]. This work specifically seeks to address the sparse sampling problem.

To develop icEEG for the generation of broad-field, high-resolution brain activity maps, as well as to contribute meaningfully to multimodal comparisons, the field urgently needs novel methods for individual data representation and grouped analyses

[108, 109]. Challenges for individual data representation arise, in large part, as a result of the convoluted geometry of the brain surface. Intracranial electrodes sample discrete patches of cortex related to the type of electrode used – in the case of SDEs this is the crown of the gyrus. Existing techniques for mapping ECoG activity onto cortical models, both volumetric [97, 110] and surface-based [105, 111], have been unable to fully address difficulties in the spatial transformation of electrode coordinates and ECoG activity onto the complex folding patterns of the surface. These include errors introduced during localization of electrodes situated over sulci, and failures to account for local topology when utilizing isotropic Euclidean distance measures for spatial smoothing of ECoG activity. These errors undermine icEEG's high spatial resolution and confound interpretations through the spatial aliasing of activity across functionally distinct regions.

A bigger problem arises with respect to inter-subject comparisons. Individual effect sizes measured by SDEs are robust, but single-subject recordings cannot capture all cortical regions involved in a particular task. Due to the discrete nature of the recordings, ECoG activity will likely underestimate functional representation at the individual level. Circumventing the sparse sampling problem requires combining data across large numbers of subjects to achieve widespread coverage. In this manner, continuous maps of functional activation can be generated that provide a more comprehensive view of underlying cortical networks [79]. Differences in cortical surface anatomy across subjects complicate grouped analyses due to poor alignment of functionally homologous brain regions [105, 111-114]. Errors of inter-subject co-registration render grouped ECoG data imprecise, or worse, inaccurate. Recently, however, advances have introduced the use of surface-based normalization [115] with ECoG

datasets [105, 111, 116, 117]. This approach offers a practical and computationally efficient method to correct for anatomical variability across subjects [113-115].

At the group-level, the application of traditional statistical models to neuroimaging datasets has recently been called into question [97, 118, 119]. Conventional group analysis strategies operate on the assumption of negligible, or equivalent, intra-subject variance. Additionally, effect-estimates are assumed to follow Gaussian distributions, without outliers. ECoG data frequently violate these two assumptions, the consequences of which are exacerbated by small sample sizes. Furthermore, conventional grouped-analysis strategies are not equipped to handle missing data from subjects with unsampled cortical regions [97, 119]. Given the sparse nature of icEEG, even after combining data across many subjects, much of the cortex remains unsampled [107]. Failure to correct for large-scale missing data will distort group effect estimates and inflate statistics [119]. Thus the analysis of grouped ECoG data requires a multi-level approach that is capable of incorporating individual subject effect sizes and their variances, correcting for missing data, and modeling outliers[118, 119]. Such comprehensive statistical approaches have been largely lacking in icEEG literature[86, 101, 105, 110, 116, 120-123].

To overcome these limitations, we have developed a pipeline for the topologically accurate and statistically robust surface-based analysis of individual and population-level ECoG data. We developed novel methods to accurately represent recording electrode coverage sites and to depict high frequency ECoG activity on cortical surface models. We integrated these methods with surface-based co-registration to correct for variability in cortical anatomy across subjects, and have

adopted a mixed-effects multilevel grouped analytic approach (n=22) to control for sparse sampling and outlier inferences, as well as intra- and inter-subject variability.

We extend prior work in this field in three ways: 1) the spatial transformation of individual SDE coverage to their cortical surface model incorporates the full diameter of each electrode. This preserves the true spatial resolution of the recording electrode, and avoids errors that occur when localizing SDEs situated over sulci with existing coordinate-to-nearest node approaches [97, 105, 111, 124, 125]. 2) The incorporation of local gyral and sulcal folding patterns during the spatial transformation of subject SDE coverage to the surface. By modeling underlying cortical geometry at each electrode, this approach prevents erroneous assignment of activity to neighboring cortical regions, which may be closely situated in Euclidean space but are in fact functionally distinct structures (e.g. opposing banks of a sulcus) [33, 114, 115]. 3) The adaptation of a mixed-effects multilevel analysis (MEMA) approach that avoids assumptions of equivalent or negligible intra-subject variability, corrects for missing data, and is capable of modeling outliers. Compared to conventional statistical models, the MEMA approach yields increased statistical power, more accurate grouped effect-estimates, and is better equipped to handle ECoG data [97, 119]. We validated our pipeline using data collected during a famous face-naming task and comparing our results against current methods of individual and grouped ECoG analysis.

Methods

22 patients (13 Female, mean age 35 ± 11 years, mean IQ 99.5 ± 8.5), scheduled for SDE implantation (14 LH, 5 RH, 3 Bilateral), were enrolled with informed consent. A total of 2518 (1799 LH, 719 RH) individual subdural electrodes were implanted (PMT Corporation; 4.5 mm diameter, 3 mm diameter contact with cortex)

using standard neurosurgical techniques [83]. Of these, we excluded 391 (286 LH, 105 RH) due to proximity to sites of seizure onset, inter-ictal spikes, or 60Hz noise; the remaining 2199 SDEs were analyzed.

Cortical Surface Models and Electrode Localization:

Cortical surface models were reconstructed from subject pre-implantation anatomical MRI scans (Phillips Medical; T1-weighted, 1mm isotropic resolution) using FreeSurfer software (v5.1) [126], and then imported to the SUMA module of AFNI [127]. SDEs were localized using intra-operative photographs combined with a recursive grid partitioning technique, and spheroids were generated to model the SDE location on the cortical surface model [109].

Experimental Design:

Patients participated in a proper name retrieval task wherein images of famous faces were presented for the experimental condition, and scrambled versions of the same stimuli were presented as a high-level control condition (1500 ms on screen, 3000 ms inter-stimulus interval). Patients were asked to overtly name faces in the experimental condition, and say “scrambled” for control images. A transistor-transistor logic pulse triggered by the stimulus presentation software (Python v2.7) at stimulus onset was recorded as a separate input during the ECoG recording to time lock all trials. Audio recording of each ECoG session was used to accurately measure the onset of articulation and to compute reaction time. Only trials in which the patient responded correctly in <2s were included.

ECoG Processing:

ECoG data were collected at 1-2000Hz using NeuroFax software (Nihon Kohden) or a NeuroPort NSP (Blackrock Microsystems). We performed spectral analysis using the Hilbert transform and analytic amplitude to estimate power changes in broadband gamma activity (BGA, 60-120 Hz). We derived the time course of power in both experimental (face naming) and control (scramble naming) conditions, for every trial, at each electrode [97]. These data were then imported into R [128], where composite variance and percent power changes (50 to 700 ms), with respect to baseline (-850 to -200ms), were computed at each electrode for task vs. scrambled control. Composite estimates were computed using a mixed-effects model with a restricted maximal likelihood estimator (rma, metafor package ver 1.4 in R) [129]. The Knapp and Hartung adjustment was employed to account for uncertainties in variance estimation [119, 129, 130].

Variance estimates were used to determine precision information at each electrode. Precision information (defined as reciprocal of the variance) served to weight the relative contribution of each electrode's effect estimate (composite percent change) at the group level. In this manner, we were able to avoid assumptions of equivalent intra-subject variability, or negligible intra-subject variability with respect to inter-subject variability [119]. See Section: *Grouped-Analysis and statistical corrections* for further discussion.

Subject Electrode Coverage Representation: Surface Electrode Recording Zone (sERZ):

The sERZ delineates cortical substrates that might contribute to activity at each electrode. This has previously been accomplished by projecting each electrode coordinate to the closest node in Euclidean space on the pial surface mesh [97, 105, 111,

[124, 125]. However, this approach fails to correct for electrodes positioned over a sulcus, which get incorrectly localized to the closer of two adjacent gyri (Fig 1a, left panel). This error effectively negates a primary strength of ECoG – the high spatial resolution. We addressed this issue by identifying the nearest node by Euclidean distance to each electrode coordinate on a smoothed-pial envelope mesh. We then grew an ROI radially outward to include all nodes within the recording electrode diameter (3mm). All of these nodes were assigned a value of one. All nodes outside of this region received a value of zero. The coordinates of the nodes within this ROI were then used to identify corresponding nodes on the pial surface, providing a topologically accurate representation of each SDE (Fig 1a, right panel).

To reflect signals originating from more distant neural sources, the sERZ was grown along the surface (Fig 1b, top). This growth traditionally uses isotropic Euclidean distances, which assumes that SDEs record from surrounding cortical regions in accordance with principles of volume conduction [97, 110, 122]. However, such isotropic Euclidean measures make the assumption that the cortical regions at every electrode form a homogenous medium for volume conduction.

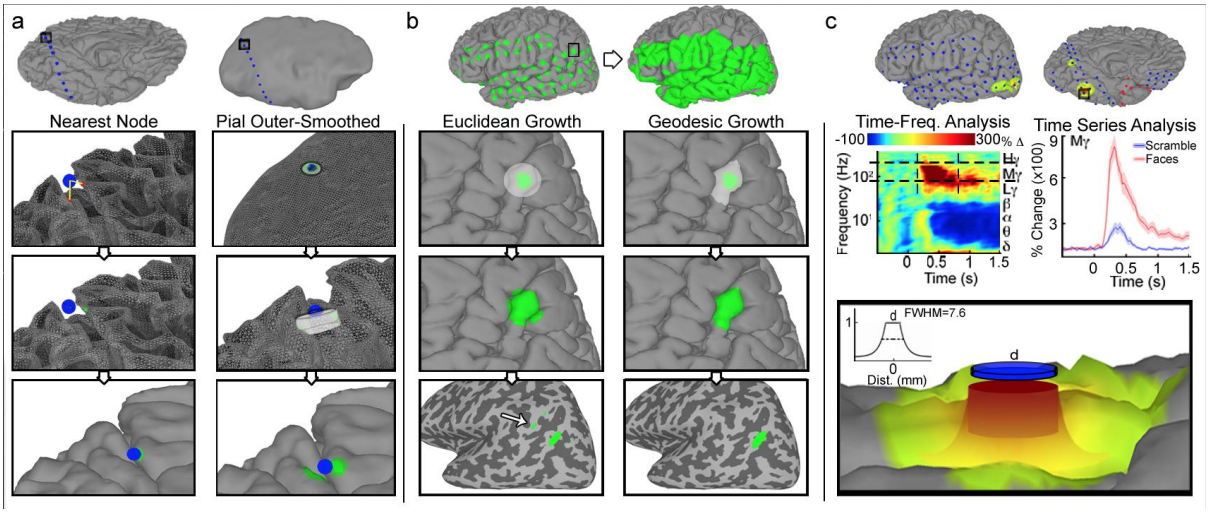

Figure II-1. Surface-electrode recording zone (sERZ) and ECoG datasets.

a) Subdural electrodes located on sulcus (blue sphere), localized to pial (left) and smoothed-pial envelope (right) surfaces. Nearest-node mapping techniques (left) erroneously localize electrode to closest node on pial mesh (green). Resulting ROI includes one gyrus, neglecting contribution from other. Using nearest-node mapping to smoothed-pial envelope, with subsequent radial growth to electrode's diameter, the sERZ correctly includes adjacent gyri.

b) sERZ generation comparing Euclidean distance expansion (left) vs. using geodesic growth (right) for a given electrode. The Euclidean technique creates an ROI that falsely includes topologically distant regions (arrow), which are close in space but not connected to the electrode. Geodesic growth along pial surface includes only nodes contiguous with the area electrode contacts.

c) Individual Surface ECoG representation: Percent power change compared to baseline. Electrodes in red discarded due to ictal activity. Time-frequency spectral and time-series analysis (broadband gamma: 60-120 Hz) of recorded ECoG signal computed using Hilbert transform. Dashed lines indicate data used to calculate composite ECoG activity (middle). ECoG activity applied to sERZ (bottom) using an exponential decay function (inset).

This assumption is only justified when considering electrodes situated strictly within gray matter [131]. Given that the intrinsic topology of the cortex is a highly convoluted 2-D sheet [115], most electrodes do not satisfy this criterion. Many electrodes are positioned near sulci, in close proximity to opposing sulcal banks. At these electrodes, volume conduction from the neighboring cortex occurs unequally through tissues with differing

conductivities: gray matter, pia-arachnoid, and cerebrospinal fluid (CSF). CSF has a much higher conductivity than gray matter, and can shunt currents [132-134]. The different conductivities of these cortical tissues preclude the assumption of homogeneity during assignment of neural activity along Euclidean principles around such electrodes.

Furthermore, for gamma frequency activity, the distance that potential neural sources could be located relative to the recording electrode is limited [135, 136]. The distances measured in Euclidean space substantially underestimate true separation along folded cortical surfaces, and neighboring regions often represent functionally distinct structures [33, 112, 114, 115]. For these reasons, the growth of the sERZ must take into account the underlying cortical geometry at each individual electrode. Geodesic (surface-based) growth is preferable to isotropic Euclidean measures, as distances are computed along the pial surface mesh [112].

Using geodesic distance metrics, the new boundaries of the sERZ included any node within 10 mm from the electrode center (7 mm from electrode edge) (Fig 1b, right panel). This resulted in a group of contiguous nodes, forming a mask on the pial surface mesh, which were then used to constrain the spatial transformation of activity at each electrode (see Section: *Spatial Transformation of Subject ECoG: Surface-ECoG Representation*). In this manner, we transformed recorded ECoG activity to the cortical ribbon using anisotropic Euclidean measures [114] that incorporate the local gyral and sulcal folding patterns on an electrode-by-electrode basis.

For an electrode located over a relatively lissencephalic region of cortex, the sERZ generated by either geodesic or isotropic Euclidean growth will be essentially identical, as will the resultant depiction of the recorded ECoG activity. However, for an SDE

located over a region with more complex topology, the differences between these methods are pronounced (Fig 2). Isotropic Euclidean measures often erroneously assign activity to proximate cortical regions (Fig 2b, right panel). In contrast the sERZ generated through geodesic growth avoids this errors (Fig 2b, left panel), and the resulting activity representation more accurately reflects the underlying electrophysiology (Fig 2a)

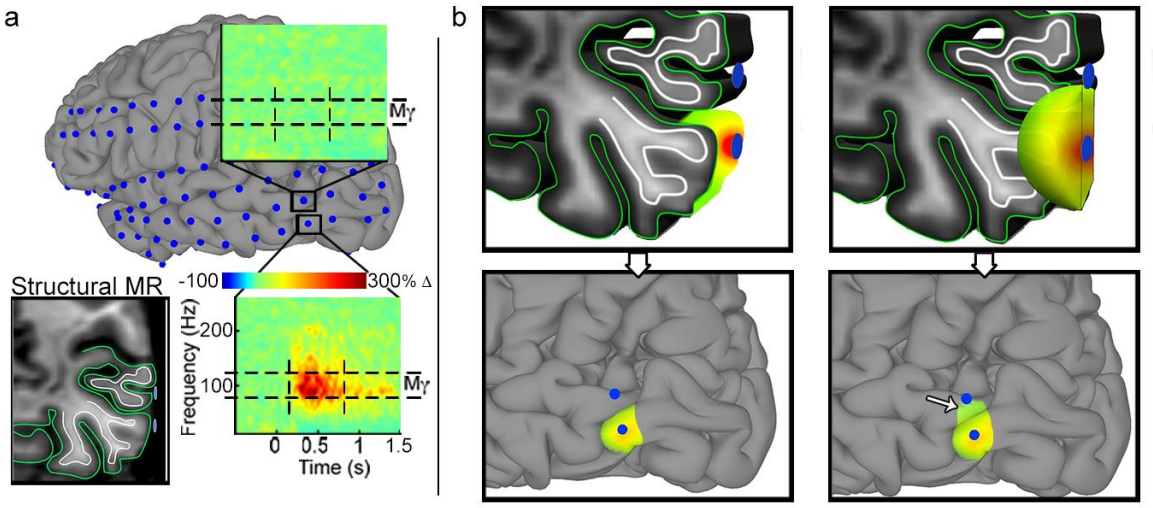

Figure II-2. Isotropic and Anisotropic Spatial Transformation of ECoG data

a) Spectrograms from two subdural electrodes (SDEs) over lateral temporal neocortex from a single subject. Spectral changes depicted as percent power change in broadband gamma activity (60-120 Hz). Dashed lines indicate data used to calculate composite ECoG activity during each epoch at each electrode.

b) “Anisotropic” Euclidean assignment (upper left) vs. “Isotropic” Euclidean assignment (upper right) of the site of activation measured by a given SDE in structural MR space. Anisotropic Euclidean assignment of activity spreads along surface to enter sulcus, whereas isotropic Euclidean assignment falsely localizes activity to neighboring gyri (arrow). SDEs with their respective surface ECoG representations on the cortical surface (below).

Importantly, a valuable secondary function of the sERZ is to enable corrections for sparse sampling at the grouped level. By combining subject-specific electrode coverage, a population-level coverage map can be generated. Population coverage maps can be used to constrain the grouped-analysis to only those cortical regions that contribute data, thereby correcting for missing data to yield significant gains in statistical power (See Section: *Grouped-Analysis and statistical corrections*).

A final note on geodesic vs. Euclidean growth strategies: While we have argued for the use of geodesic distance measures to delineate sERZ boundaries, our method does not critically hinge on this choice. The use of geodesic growth is one of many potential parameters that could be user-defined. Thus our strategy can easily be adapted to apply traditional isotropic Euclidean distance measures if desired.

Spatial Transformation of Subject ECoG: Surface-ECoG Representation:

After generation of the sERZ, we spatially transformed the recorded ECoG activity onto the underlying cortex to generate a surface ECoG dataset. Heretofore, data representation has typically been accomplished as a hemispherical volume under each electrode [97, 105, 110]. As discussed in Section: *Subject Electrode Coverage Representation: Surface Electrode Recording Zone (sERZ)*, this may result in activity being falsely assigned to nearby regions in Euclidean space (Fig 2b, right panel). We addressed this problem by using the sERZ to constrain the spatial transformation of ECoG activity only to those cortical regions located within its boundaries.

The spatial transformation was computed using an exponential activity-decay function for each electrode: Every node within the sERZ was assigned a weighted value of the ECoG activity, determined by its Euclidean distance from the center of the

electrode. In order to maintain the spatial resolution of SDEs, any node within the diameter of the electrode (3mm) received the peak ECoG amplitude. Peak ECoG amplitude was indicated by the full value of either the effect size (composite percent change) or the precision estimate (inverse of the composite variance) of the electrode. Nodes lying outside the electrode received a weighted value, decreasing by an exponential decay constant of .3 of their Euclidean distance from the electrode's edge (effective full-width half maximum of 7.6) (Fig 1c). Thus, the net activity at each node represented the weighted sum of all electrodes that contributed to it, in agreement with the current limited understanding of ECoG signal sources [105, 110, 137-139].

It is important to note that our method is independent of the assumptions made by our choice of activity-decay function. Similar to the flexibility in sERZ generation, our exponential decay function is a user-defined parameter, which can be replaced by other models in the future that are optimized for source localization– say a quadratic model or Gaussian kernel.

Finally, it is critical to clarify that use of an exponential decay (as well as the generation of the sERZ) does not address the inverse problem, and it is not within the scope of this dissertation to do so. Ultimately, the focus of this dissertation is to provide an ecologically valid method for surface-based representation of ECoG data, in order to enable co-registration across subjects and analysis of population-level intracranial data. The exponential function and decay constant were empirically determined to achieve a greater than 50% decay in activity within 3 mm from the electrode's edge. This distance was carefully chosen by considering inter-electrode distances (10 mm center-center; 7 mm edge to edge) and to limit spatial smoothing while simultaneously enabling inter-subject comparison. In doing so, we echo assumptions made by others in our field that

neural sources are proximate and geometrically distributed around each electrode [76, 97, 105, 138-140].

Surface-Based Normalization:

To optimize co-registration of the sERZ and surface ECoG datasets across individuals, we implemented surface-based normalization [113, 115, 141]. We inflated each subject's cortical surface to a sphere and warped the spherical mesh to align with the folding patterns of a population-averaged brain [115, 142]. Individual aligned surfaces, and therefore their associated sERZ and surface ECoG datasets, were resampled to a new standardized mesh with invariant node numbers, enabling a one-to-one node correspondence between node indices and anatomical locations across subjects [113]. Such surface-based techniques are better suited to cortical surface derived ECoG data, given that they maintain topological alignment and tissue-domain matching, increasing statistical power in grouped analyses [112, 113, 115, 141].

Volumetric-Representation of ECoG Data:

To compare our techniques against existing methods, we also generated volumetric electrode recording zones (vERZ) and volumetric ECoG representations that utilize isotropic Euclidean distance measure, unconstrained by cortical folding patterns (see Conner et al., 2013). Volumetric normalization (12-parameter affine) was used to transform subject vERZ and volumetric ECoG datasets into common space (MNI-N27).

Comparison of Surface-Based and Volume-Based Normalization:

To compare surface-based normalization against pre-existing volumetric techniques [97, 110, 143] we generated anatomical ROIs using auto-parcellation techniques [126], encompassing four gyri (pars-triangularis, precentral, superior temporal, and

fusiform), for each subject in the left hemispheric cohort (n=17). We then compared the co-registration accuracy on the N27 surface.

Grouped-Analysis and statistical corrections:

We introduce here the novel application of mixed effects multilevel-analysis (MEMA) to surface-based ECoG data. Unlike traditional statistical techniques at the group level, which assume that effect estimates across subjects have the same variance, MEMA uses both effect estimate and precision estimate (within-subject variance) at each electrode locus per individual as inputs. Higher weights are assigned to subject data with more reliable effect estimates (narrower confidence interval) and *vice versa*, and the impact of individual outliers and heterogeneities are minimized. By weighting effects estimates by their reliability, the final group effect-estimate is unbiased and robust. In this way, MEMA provides a more accurate statistical procedure in significance testing that maximizes group effect estimates, especially when sample sizes are small. We have previously published an ECoG analysis comparing MEMA against conventional approaches, and more in-depth comparisons are discussed elsewhere [97, 119].

The MEMA approach utilizes summarized data that intrinsically contain precision and effect size information: Suppose the effect estimate *yi* from the *i*th unit can be expressed in a model of mixed-effects multilevel analysis,

$$y_i = \alpha + \delta_i + \varepsilon_i,$$

where α, δ_i, ε_i are respectively the fixed effect (mean effect across all units), the random effect (deviation) of the *i*th unit, and the measurement error. The Gaussian assumption for random effects is $\delta_i \sim N(0,\tau^2)$ and $\varepsilon i \sim N(0, \sigma_i^2)$. The variance σ_i^2 for the

effect estimate y_i is typically known, and the unknown parameters are α and τ^2 that can be estimated through iterative algorithms such as restricted maximum likelihood [119].

Importantly, MEMA also allows us to handle missing data properly to prevent spurious inferences due to regions of the brain without coverage. By incorporating sERZ/vERZs, MEMA considers only the nodes, or voxels, contributing to the data in the analysis. In other words, a locus of a subject without coverage is not entered into the group analysis with a value of 0, but is instead excluded at node- or voxel-level. The number of nodes/voxels comprising the surface/volume datasets is in the hundreds of thousands. Because ECoG data is sparse, without constraining the analyses to the regions of coverage it will be much less likely for effect estimates, regardless of size, to survive statistical corrections [119]. Although originally designed for fMRI, MEMA is particularly appropriate for grouped ECoG analyses.

To correct for multiple comparisons, family-wise error correction by white-noise clustering analysis (Monte Carlo simulations, 5000 iterations) was applied, using the same number of nodes/voxels, dimensions, and smoothness as the data used for analysis. We applied an initial node/voxel-wise threshold of p=.05 (uncorrected), and only clusters greater than the minimum number of contiguous voxels/nodes needed for the corrected α =0.05 were considered significant.

Time-Series Analysis:

For each site of significant activation in the MEMA group results, we selected the location of maximum power change. We used these loci to identify corresponding electrodes across individuals, within an 8-9 mm radius, and computed the average percent changes in broadband gamma activity across these electrodes.

Results

Surface-based vs. Volumetric Normalization:

Following volumetric normalization, 21% of all transformed voxels lay within gyral bounds in target space. By contrast, 76% of nodes were correctly localized within the target gyrus using surface-based normalization (Fig 3a). Volumetric normalization led to only 0.08% of voxels overlapping across all 17 subjects, while surface-based normalization resulted in a 71.6% overlap of all subject nodes. Non-linear volume-based registration techniques might improve these co-registration results, but would not compare favorably with surface-based normalization to align homologous cortical topologies [113, 141].

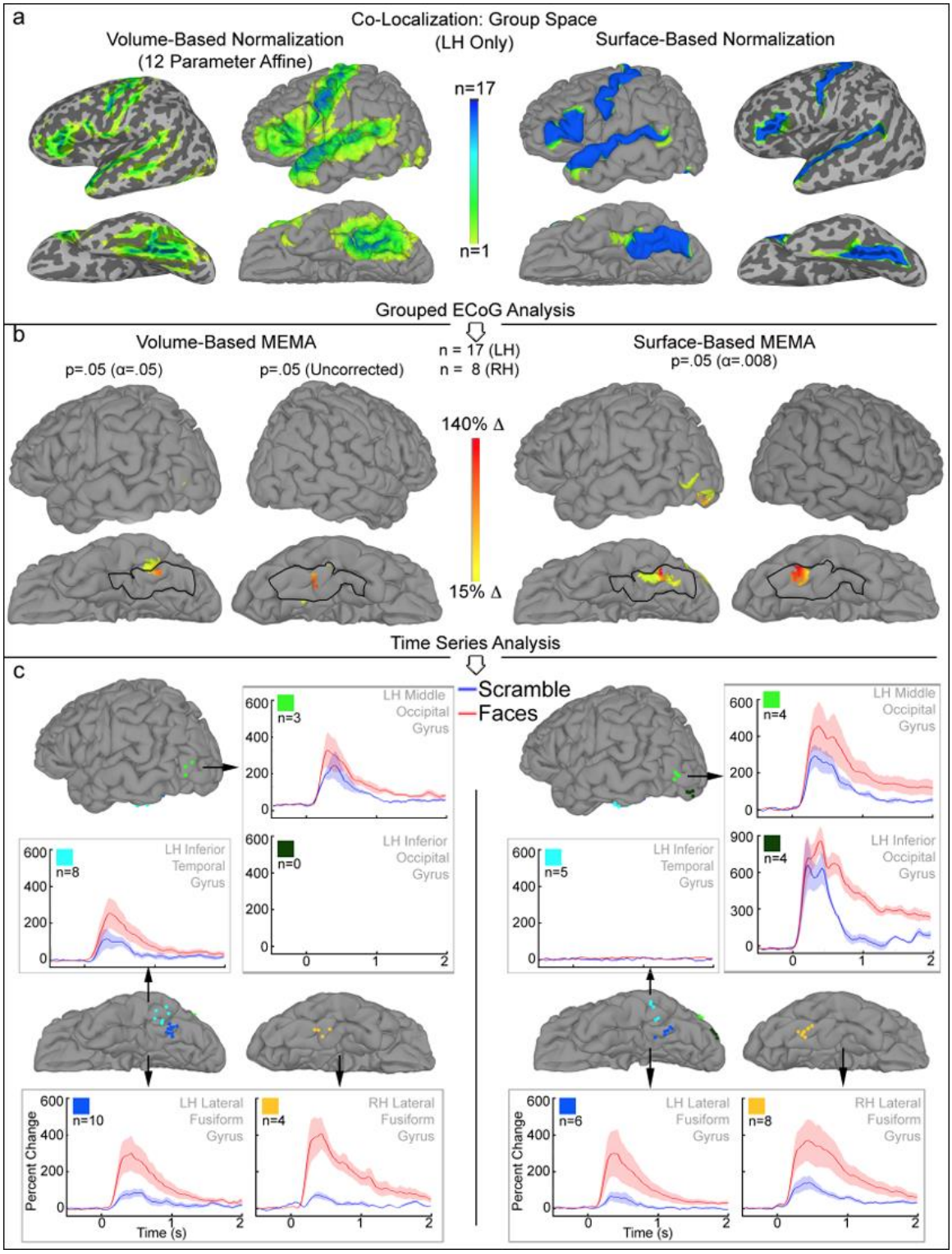

Figure II-3. Spatial Normalization Comparisons, Grouped MEMA, and Time-series Analyses

a) Individual normalized (n=17) anatomical ROIs of four gyri (pars-triangularis, precentral, superior temporal, and fusiform) co-registered using affine (left) vs. surface based (right) approaches.

b) Results of volume-based (VB) and surface-based (SB)-MEMA for left (n=17) and right (n=8) hemispheric cohorts. Figures display percent signal change in broadband gamma activity (60-120 Hz), for faces naming contrasted with scrambled images (*p*=.05, corrected). The time window chosen is 50 to 700 ms. The fusiform gyrus is outlined in black.

c) Time series analyses (-500 to 2000 ms). Electrodes are color-coded by region. Traces represent group-averaged response of electrodes to faces (in red) and scrambled face viewing (in blue) tasks, ± 1 sd (shaded). Bimodal peaks in left iOG from SB-MEMA are seen in individual traces as well, and may represent bottom up and top down modulation of local processes.

SB-MEMA vs. VB-MEMA:

SB-MEMA yielded significant power change from baseline, symmetrically in bilateral fusiform gyri (-40 -53 -20 left, 42 -51 -21 right), left mid-occipital cortex (-47 -77 0), and left inferior occipital gyrus (-34 -84 -14), after cluster correction for multiple comparisons (p=0.05, corrected). These loci are precisely consistent with co-ordinates for Fusiform Face and Occipital Face Areas [144, 145] (FFA and OFA, respectively) derived from meta-analyses. In contrast, VB-MEMA showed significant activity only in the left fusiform gyrus (-37 -49 -27), with spillover into the adjoining inferior temporal gyrus. The right fusiform gyrus showed non-significant activity located asymmetrically with respect to the left (Fig 3b).

We used published meta-analyses to place ROIs at the loci of left OFA and bilateral FFA (diameter 7mm ± 2 mm) [145, 146] (Table 1). With SB-MEMA, the left OFA had a significantly active surface area of 78 mm^2, with a peak percent power change over baseline of 83% in broadband gamma activity (mean 49.8%), that survived significance thresholding and corrections for multiple comparisons (p=.05). The left FFA ROI had a significantly active surface area of 81 mm^2, with an activity peak of 148% (mean 61.2%). The right FFA had a significantly active surface area of 38 mm^2,

with an activity peak of 162% (mean 96.6%). In contrast, VB-MEMA only showed significant activity in the left FFA in a volume of 14 voxels with a peak of 89% (mean 77.7%). VB-MEMA showed no significant activity for the left OFA and right FFA.

Region	Location by Meta-analysis	Surface-Based MEMA				Volume-Based MEMA			
		Locus	Surf. Area	Peak Activity	Mean Activity	Locus	Voxels	Peak Activity	Mean Activity
L. OFA	-33, -84, -13	-34, -84, -14	78	83	49.80	n/a	0	n/a	n/a
L. FFA	-36, -53, -20	-40, -53, -20	81	148	61.20	-37, -49, -27	14	89	77.70
R. FFA	37, -56, -21	42, -51, -21	38	162	96.60	n/a	0	n/a	n/a

Table II-1. Spatial Coordinates of ROI Peak and Mean Activation Sites

Talairach coordinates for right FFA, left Occipital and Fusiform Face areas (L. OFA and L. FFA) derived from meta-analyses. Locus and amplitude of peak percent change, spatial extent of activation (surface area in mm2 for SB-MEMA or number of voxels for VB-MEMA), and mean of all significant values (p=.05 corrected) are reported.

In order to clarify the extents to which the data representation techniques (v/s-ERZ and ECoG datasets) and normalization-techniques (volume vs. surface-based) individually contributed to the differences in these results, we also performed MEMA using surface-based normalization of volumetric ECoG data representation. There were substantial improvements in the results, with activity constrained bilaterally, within the fusiform gyri (-38 -53 -20 left, 39 -50 -21 right; p=0.05, corrected), similar to SB-MEMA (Fig 4). Critically, however, significant activity was still not visible in the left OFA.

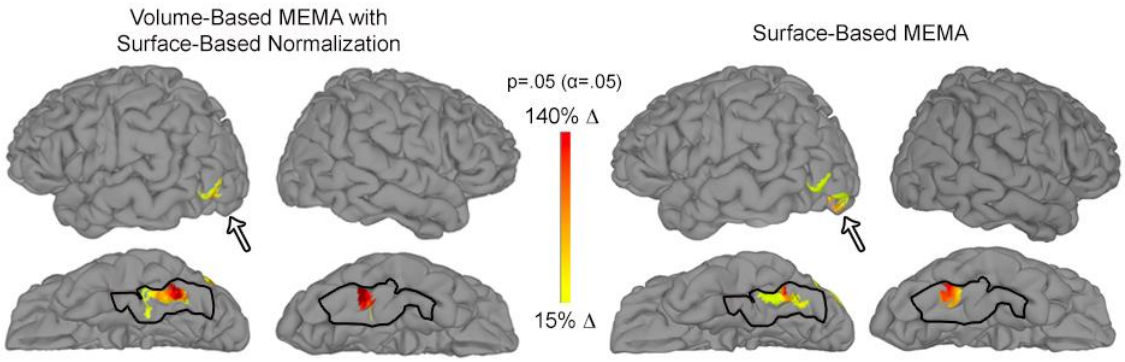

Figure II-4. Comparison of Volume- and Surface-based MEMA with Surface-based Normalizations

Compared with volume-based MEMA using affine transforms (Fig 3), a significant improvement was noted when surface-based co-registration was applied. This was evident for group activation in the left mid-occipital and bilateral fusiform gyri. Critically however, activity was absent in the left OFA (*left*, arrow) and was only evident when using surface-based MEMA with surface-based group normalization (*right*, arrow). This is due to failure of isotropic Euclidean methods to account for cortical topology during the spatial smoothing of subject data, which reduces spatial specificity and degrades group effect estimates.

Time-Series Analysis:

A major advantage of co-registration of ECoG data in this fashion is that it enables derivation of time series of activity from grouped data. Prominent early activity (< 150 ms) was seen in all regions. The left OFA revealed a bimodal activation profile, which likely represents signatures of bottom up and top down modulation of local processing [147]. This profile is not a result of group averaging, as identical temporal profiles were seen in individual subject electrode recordings. With VB-MEMA, this temporal profile of the OFA activity was lost. Additionally, activity was erroneously localized to the left inferior temporal gyrus (Fig 3c).

Conclusions

fMRI remains the most prevalent technique for the study of cognitive function in health and disease. Yet, it provides only an indirect measure of underlying neural activity and has poor temporal resolution. In contrast, the spatio-temporal features of ECoG yield invaluable information about the temporal dynamics of cerebral activity at the small scale and into hi-speed, transient interactions between broadly distributed neural modules [86, 148, 149]. The field has seen an exponential growth in the numbers of published articles. However, disadvantages of icEEG – most notably the sparse sampling problem- have precluded the broader application of ECoG data to the study of human cognition. Realistic solutions to address these disadvantages – including multimodal investigations and the generation of population-level functional maps – have been hindered by the limitations of current techniques to relate SDE recordings to the likely neural substrates that generate them, and to compare and analyze grouped datasets.

Prior efforts to represent icEEG data have used isotropic Euclidean measures at each electrode, assuming immediately proximate sources, identical signal decay across spectral components, and considering irrelevant the effects of cortical topology. Existing techniques of data representation, both volumetric and surface-based [97, 105, 110, 111] are unable to address problems in the spatial transformation of ECoG data to the complex folding patterns of individual cortical surfaces, specifically with electrodes located on or near sulci. They have also failed to address the “sparse sampling” issue related to the limited coverage, or to propose a statistical framework for grouped analyses that would also enable correction of these sparse data [86, 101, 105, 110, 120-123].

These issues have hindered grouped studies with smaller sample sizes, requiring large numbers of subjects to generate significant results. Even with larger numbers of subjects, however, grouped analyses still suffer from poor data alignment across individuals and unjustified assumptions concerning intra- and inter-subject variability. The importance of accurate inter-subject co-registration can be seen in the type 1 errors (presence of activity in the left inferior temporal gyrus) and type 2 errors (loss of activity in the left OFA) yielded by grouped affine transformed, volume-based analysis (VB-MEMA). Additionally, the poor alignment of individual datasets in the right hemisphere is reflected in the non-significant, asymmetrical activation identified for the right FFA. In contrast, SB-MEMA yielded statistically significant and topologically accurate results with sample populations of only 8 subjects (i.e. right FFA), as well as in regions with sparse coverage (i.e. left OFA). It should be noted, however, that group-size and degree of cortical coverage ultimately limit the improvement afforded by SB-MEMA, as is made clear by the lack of activity identified for the right OFA in both methods. From the 8 subjects contributing to data in the right hemisphere, only one had OFA coverage. In contrast, with OFA coverage from as few as 4 subjects in the left hemisphere, SB-MEMA was able to produce significant results that were consistent with individual activity profiles. Such limitations make clear the necessity for population-level analysis to be supported by data at the individual-level.

The introduction of surface-based normalization for grouped ECoG data offers a practical and computationally efficient method to correct for inter-subject anatomical variability [105, 111, 116, 117]. However, inter-subject co-registration is only an intermediary step between individual subject data representation and grouped-level analysis. The importance of accurate data representation is made clear by the results of MEMA

performed on volumetrically transformed data co-registered with surface-based normalization. Although the results were greatly improved, significant activity in the left OFA was still not present (Fig 4, left arrow). The OFA is a small and highly specialized region in the inferior occipital cortex, folded into close apposition with cortical regions exhibiting very different responses profiles to face stimuli [33, 43]. Isotropic Euclidean distance measures (e.g. volumetric smoothing) ignore such topological details and activity across functionally distinct regions gets smoothed together. At the individual level, errors in results arrived at in this fashion may appear to be trivial. When taken to the group level, these errors reduce spatial specificity and artificially degrade group effect estimates. The opposite effect, however, can also be seen when regarding activity differences in the FFA between SB- and VB-MEMA. Due to the greater degree of spatial smoothing, the activity in the FFA after VB-MEMA appears more focal and more intense (i.e. hotter colors, less extent). This is because, unlike the OFA, activity in the FFA is more uniform. Therefore, when greater smoothing across patients occurs, the result appears amplified. Although we cannot claim that this result from VB-MEMA is incorrect, and while it may be more visually compelling, it must be viewed as the flip side of increased spatial smoothing, with respect to the detriment of activity in the OFA.

The geodesic growth and exponential activity-decay strategies that we implement are not intended to function as true solutions to the inverse problem that incorporate biophysically realistic source and forward models. Rather, our strategies serve to approximate the functional localization of high-frequency gamma activity. This, in turn, enables a rapid and empirically consistent means of performing comparative analyses. We've chosen the geodesic growth strategy because we find that it provides

an estimate for SDE coverage and spatial ECoG transformation that is more consistent with the individual data than the current used models.

Importantly, our methodology has been designed to be separable from the assumptions we make in modeling neural sources, which are necessarily limited by available knowledge at this time. The parameters we implement here (geodesic growth and exponential decay) are simply one of many possible user-defined options, and can be seamlessly exchanged with alternative ECoG interpolation strategies if desired (e.g. Euclidean growth and Gaussian kernels). Our pipeline allows for each parameter in the generation of surface-based SDE coverage and ECoG activity representations (i.e. nearest-node or outer-pial localization, electrode radius, sERZ growth algorithm, activity decay function, decay constants, etc.) to be customized to a user-defined preference, and updated as new understandings of ECoG signals emerge. Thus, these techniques provide a flexible framework for individual data representation and statistically valid population-level ECoG analyses. Although neural source modeling is beyond the scope of this dissertation, our method can be readily applied to developing forward and inverse source-modeling solutions in future studies [139, 140].

In summary, the surface electrode recording zone (sERZ) and surface ECoG co-registration techniques offer, for the first time, tools for the representation of the recorded ECoG in a topologically accurate fashion onto a parcellated cortical surface with minimal errors in electrode localization. Using the sERZ, probable sources contributing to the activity at each electrode are independently estimated while controlling for local gyral and sulcal folding patters. The spatial transformation of ECoG activity is subsequently constrained to those regions. This preserves the spatial resolution of these data and enables precise intermodal comparisons [150]. By modeling

subject-specific electrode coverage, the sERZ additionally provides a means for SB-MEMA to correct for sparse-sampling and yield significant increases in statistical power. The integration of surface ECoG datasets with SB-MEMA combines the strengths of a MEMA approach with the topological precision of surface-based co-registration, thereby enabling the creation of multi-human brain activity maps of cognitive functions, such as language, that are impossible to study save in humans.

Summary

Electrocorticography (ECoG) in humans yields data with unmatched spatio-temporal resolution that provides novel insights into cognitive operations. However, the broader application of ECoG has been confounded by difficulties in accurately depicting individual data and performing statistically valid population-level analyses. To overcome these limitations, we developed methods for accurately registering ECoG data to individual cortical topology. We integrated this technique with surface-based co-registration and a mixed-effects multilevel analysis (MEMA) to control for variable cortical surface anatomy and sparse coverage across patients, as well as intra- and inter-subject variability. We applied this Surface-Based MEMA (SB-MEMA) technique to a face-recognition task dataset (n=22). Compared against existing techniques, SB-MEMA yielded results much more consistent with individual data and with meta-analyses of face-specific activation studies. We anticipate that SB-MEMA will greatly expand the role of ECoG in studies of human cognition, and will enable the generation of population-level brain activity maps and accurate multimodal comparisons.

Chapter III: Functional Organization of the Ventral Temporal and Lateral Occipital Cortex:

Introduction

Visual object recognition is a ubiquitous feature in our day-to-day lives, enabling us to recognize the faces of our loved ones, find a favorite snack in the grocery aisle, and even read the words on this page. Achieved with rapidity and accuracy, object recognition appears to us nearly effortless. Yet the apparent automaticity with which we perform this feat belies its underlying neural complexity, and damage to any part of the network of cortical regions involved may produce debilitating deficits – such as visual agnosias (e.g. face-blindness) – that can seriously affect social or vocational life [2, 151].

Extensive human and non-human primate research has identified putative higher-order visual areas in the ventral temporal and lateral occipital cortical complexes (VTC and LOC, respectively), which are believed to mediate object recognition via the activity of distinct neuronal clusters that differentially and selectively activate to specific categories of visual stimuli (e.g. faces/places/animals/tools/words) [14, 34, 36, 37, 39, 40, 152-161]. However, the functional and organizational principles of the VTC and LOC continue to remain a topic of debate. This is largely due to the considerable variability in anatomical location and spatial relation of different category specific regions reported in subjects, both within and across studies [33, 85, 162, 163].

Recently, advances in functional, structural, and anatomical neuroimaging have begun to yield new insights into structure-function relationships of the VTC and LOC [4]. Specifically, in the VTC, the mid-fusiform sulcus (MFS) has been revealed to predict lateral-to-medial transitions in receptor and cyto-architectonics, white-matter connectivity, and large-scale functional maps (e.g. eccentricity bias, object size, animacy); while in the LOC, dorso-ventral transitions in large-scale functional maps appear to be arranged around the lateral occipital sulcus (LOS). Subsequent

comparisons between the MFS/LOS and the relative locations of category-selective regions have revealed that these smaller-scale functional representations also align with the same sulcal landmarks [33, 46, 47, 56, 58-65, 163-170].

Taken together, these findings suggest that the MFS and LOS provide a structural framework for the organization of higher-order visual representations, in which opposing sides of these sulci contain neural hardware for processing distinct classes of visual information (foveal vs. peripheral, animate vs. inanimate, face vs. place) [4]. Importantly, the superimposition of large and small scale functional representations within this framework enables a hierarchical structure of visual information to mirror the organization of human conceptual knowledge: Concrete categorical information is embodied at smaller spatial scales (e.g. category selective regions reflect basic distinctions – faces vs. tools), while abstract categorical information is reflected at larger spatial scales (e.g. the MFS separates superordinate distinctions – animate vs. inanimate) [4, 163, 171]. This hierarchical structuring of visual information offers a biologically plausible mechanism to explain how the VTC and LOC may be optimized to achieve rapid object recognition and categorization [4].

While fMRI studies have made great strides towards understanding the organization of these visual areas, the spatio-temporal resolution and indirect nature of hemodynamic measures prevents a definitive assessment of their functional topography [76, 79]. Although newer analytic approaches have been developed to address the limitations of traditional localization-based techniques (e.g. multivariate pattern analysis) [38, 172-175], their relationships to the underlying neural population activity has not been validated in humans [176, 177]. Human intracranial EEG (icEEG) recordings provide

high spatiotemporal resolution neural recordings and offer a unique opportunity to validate hypotheses of VTC and LOC organization [75, 82, 83].

Despite recent work, a comprehensive icEEG investigation into the topology of VTC and LOC category-selectivity remains lacking for review see [67]. This is due largely to challenges arising from spatially variable and sparse electrode coverage within subjects. The discrete and clinically directed implantation of electrodes precludes evaluation of both small and large-scale functional organization in any single individual, requiring the combination of data across a large number of subjects to achieve adequate cortical coverage. However, current approaches for the spatial co-registration of datasets across individuals (e.g. affine/volumetric normalizations) are unable to preserve the topological alignment of homologous functional regions, due to the highly folded (nonlinear) cortical geometry [80]. As a result, prior icEEG studies have focused more on evaluating the functional properties of category-selective regions, but not their topological organization within the VTC and LOC but see [67, 120, 152, 160, 178-186].

Recently, new methodological advances have introduced surface-based normalization strategies for grouping icEEG data [80, 115, 141], which provide computationally efficient methods to correct for inter-subject anatomical variability and sparse-sampling [113]. In the current study, we utilized one such surface-based grouped icEEG approach [80] to investigate VTC and LOC category tuning across a large patient cohort (*n*=26). By generating topologically precise population-level maps of icEEG data, we directly evaluated whether: 1) large-scale animacy maps emerge from the relative arrangements of distinct category-selective regions in the VTC and LOC; and 2) transitions in multi-scale functional maps occur around specific sulcal landmarks (e.g. MFS and LOS, respectively).

Methods

Data were collected from 26 subjects (16 female, mean age 33 ± 11 years, mean IQ 100 ± 11) undergoing left (LH, *n* = 16) or right hemispheric (RH, *n* = 10) subdural electrode (SDE) implantation. Informed consent was obtained following study approval by our institution's committee for protection of human subjects.

Experimental Design:

Subjects participated in a visual confrontation-naming task using 5 categories[84]: famous faces, animate non-face (animals and body-parts; hereafter referred to as "animate"), famous places, tools, and word stimuli (Fig 1a; ~80 to 120 stimuli per category). A transistor-transistor logic pulse triggered by the stimulus presentation software (Python v2.7) at stimulus onset was recorded as a separate input during the experiments to time lock all trials during all tasks [97].

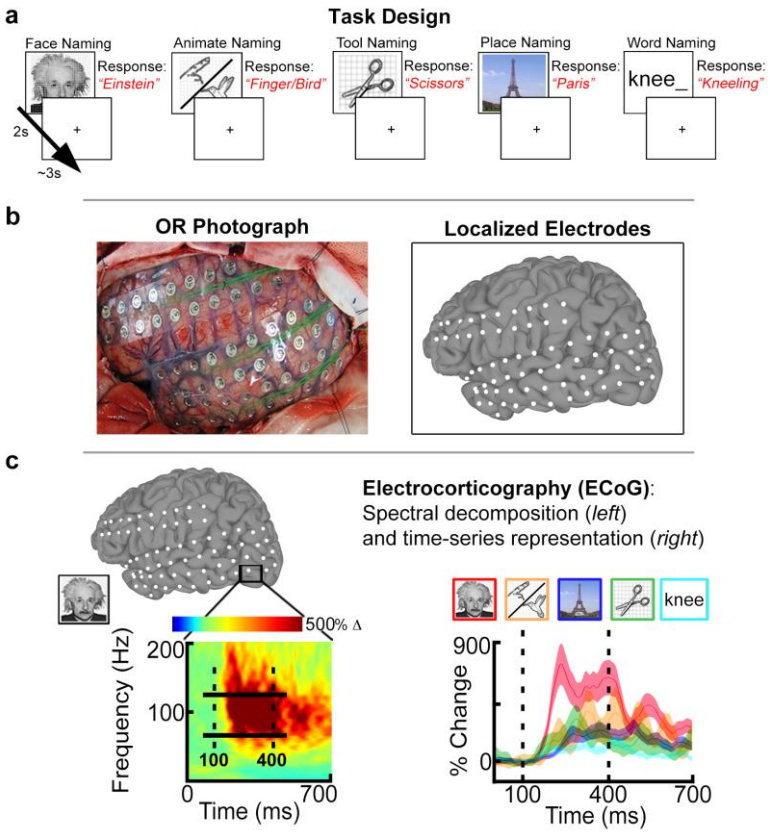

Figure III-1. Experimental Design and Analysis

a) Patients performed naming of 5 stimulus categories: faces, animate non-face (animals/body parts), places, tools, and words. Images were presented for 2 seconds followed by a jittered 3s inter-stimulus interval. Exemplar responses are indicated in red text.

b) Subjects were implanted with subdural electrodes (SDEs) in either the left (LH) or right hemisphere (RH). SDEs were localized to subject cortical surface models and represented as spheroids (white) centered on electrode coordinates.

c) Cortical activity was measured using electrocorticography (ECoG). (*Left)* ECoG data were spectrally decomposed to obtain percent-power change in the broadband gamma frequency range (BGA, 60 to 120 Hz; solid horizontal bars) relative to a pre-stimulus baseline window (-700 to -200 ms). The spectrogram depicts the response during face naming for a single SDE (black box) in the inferior occipital gyrus. (*Right)* For the same SDE, time-series representations of BGA are plotted per category. BGA for faces (red) is greatest compared to animate (orange), place (blue), tool (green), and word (cyan) stimuli. Shadings denote 1 SEM. Vertical dashed lines denote the time window (100 to 400ms; stimulus onset @ t = 0 ms) used to compute *d'* sensitivity indices.

Pictorial stimuli (face, animate, place, tool) were displayed at eye-level on a 15'' LCD screen placed at 2 feet from the patient (2000 ms on screen, jittered 3000 ms inter-stimulus interval; 500x500 pixel image size, ~10.8° x 10.8° of visual angle, with a grid overlay on 1300x800 pixel white background, ~28.1° x 17.3° of visual angle). Subjects were instructed to overtly name the stimuli during the experiment. Face stimuli consisted of gray-scale, real images of famous individuals shown in frontal view (celebrities, politicians, and historical figures). Place stimuli consisted of color, real images of famous landmarks (e.g. Eiffel tower, Grand Canyon). Animate and tool stimuli were from the Snodgrass and Vanderwart object pictorial set [187]. Word stimuli were presented as partial word stems (e.g. "kne_") to which subjects were instructed to respond with the first action word that came to mind (e.g. "kneeling"). Words consisted of black, lower-case text (2000 ms on screen, jittered 3000 ms inter-stimulus interval; font height of 100 pixels, Calibri font type, ~2.1° of visual angle) centered on a 1300 ´ 800 pixel white background.

For each category, images were randomly selected from our database and never repeated, so each subject saw a unique sequence of images. All subjects in both right and left hemispheric cohorts participated in the visual naming tasks with pictorial stimuli. However, given the strong hemispheric bias associated with word reading [159, 188-190], the word-naming task was only performed in the left hemispheric cohort. Due to clinical time constraints, 12 of 16 subjects in the left hemisphere cohort completed the word-naming task.

Cortical Surface Models

Pre-implantation anatomical MRI scans were collected using a 3T whole-body MR scanner (Philips Medical Systems, Bothell WA) equipped with a 16-channel SENSE head coil. Anatomical images were collected using magnetization-prepared 180-degree radio-frequency pulses and rapid gradient-echo (MP-RAGE) sequence, optimized for gray-white matter contrast, with 1 mm thick sagittal slices and an in-plane resolution of 0.938 x 0.938 mm [191]. Cortical surface models (Fig 1b) were reconstructed using FreeSurfer software (v5.1) [126], and imported to SUMA for visualization [113].

Electrode Localization and Selection Criteria

A total of 3506 SDEs (LH *n*=2101; RH *n*=1386) were implanted (PMT Corporation; top-hat design; 3 mm diameter contact with cortex) using previously published techniques [83]. 933 SDEs (LH *n*=482; RH *n*=451) were excluded due to proximity to seizure onset sites, inter-ictal spikes, or 60 Hz noise. The remaining 2573 SDEs (LH *n*=1619, RH *n*=935) were localized to cortical surface models using intra-operative photographs and an in-house recursive grid partitioning technique [109].

Using anatomical criteria, we identified all SDEs localized to the VTC and LOC for each individual in native anatomical space. The VTC includes the fusiform gyrus - bounded laterally by the occipitotemporal sulcus, medially by the collateral sulcus and anterior lingual gyri, posteriorly by the posterior transverse collateral sulcus, and anteriorly by the anterior tip of the mid-fusiform sulcus (MFS) [4]. The LOC includes the middle and inferior occipital gyri - bounded dorsally by the transverse occipital sulcus, ventrally by the occipitotemporal sulcus, posteriorly by the occipital pole, and anteriorly by the posterior superior temporal sulcus, as well as the posterior aspects of the inferior and middle temporal gyri (Fig 2) [33, 46, 57, 168].

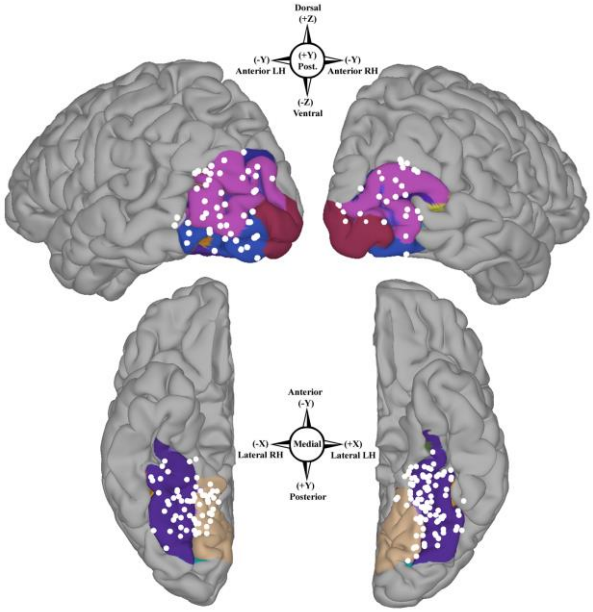

Figure III-2. Population Coverage of Higher-level Visual Cortex

Bilateral group-electrode coverage maps depict subdural electrodes (SDEs, white spheres) from all subjects (*n* = 26 subjects; LH *n*=16; RH *n*=10) on a common cortical surface (MNI N27 template brain aligned to Talairach coordinate space). A total of 3506 SDEs were implanted, from which 242 SDEs were localized to the lateral occipital cortex (LOC, top; LH *n*=48, RH *n*=35) and the ventral temporal cortex (VTC, bottom; LH *n*=95, RH *n*=64). Spatial transformation of individual SDE coordinates to Talairach space was performed in a surface-based fashion. Compass points denote SDE coordinates (Talairach space) and direction in each region. The VTC and LOC, and their respective boundaries, are highlighted using FreeSurfer's automated gyral and sulcal parcellation algorithm. The VTC consists of the fusiform gyrus (purple), occipitotemporal sulcus (orange), lingual gyrus (tan) and the posterior transverse collateral sulcus (teal). The LOC consists of the middle occipital (MOG, pink) and inferior occipital gyri (IOG, blue), lateral occipital sulcus (light purple, between IOG and MOG), transverse occipital sulcus (dark purple, dorsal to the MOG), occipitotemporal sulcus (orange), occipital pole (dark red), and posterior superior temporal sulcus (yellow).

To enable a population-level evaluation of category-selective topology, individual subject SDE coordinates were mapped to a standardized cortical surface (MNI N27 template brain aligned to Talairach coordinate space) using a surface-based normalization strategy (rather than affine or non-linear volumetric transformations) [80,

[113, 192-194], to maximize the overlap between topologically and functionally homologous regions across subjects [111, 112, 114]. A total of 159 SDEs (LH *n*=95, RH *n*=64) were localized to the VTC and 83 SDEs (LH *n*=48, RH *n*=35) to the LOC (Fig 2).

Electrocorticographic (ECoG) Processing:

In 14 subjects, ECoG data were collected at 1000 Hz using NeuroFax software (Nihon Kohden, Tokyo, Japan) (bandwidth 0.15-300 Hz). The other 12 subjects underwent ECoG data collection at 2000 Hz (bandwidth 0.1-750 Hz) using the NeuroPort recording system (Blackrock Microsystems, Salt Lake City, UT). Electrodes were referenced to a common average of all electrodes in a given subject, except for those with 60 Hz noise or epileptiform activity when initially referenced to an artificial 0V [195]. All electrodes with greater than 10 dB of noise in the 60 Hz band, inter-ictal epileptiform discharges, or localized to sites of seizure onset were excluded.

To focus only on perceptual processes, analyses were restricted to a period 100-400 ms after stimulus presentation [67, 183, 196, 197]. For all ECoG data, analyses were performed by first bandpass filtering raw ECoG data into the broadband gamma frequency range (60-120 Hz, following removal of 60Hz line noise and its harmonics; IIR Elliptical Filter, 30 dB sidelobe attenuation). A Hilbert transform was applied and the analytic amplitude was smoothed (Savitzky-Golay FIR, 5th order, frame length of 155 samples; Matlab 2013b, Mathworks, Natick, MA) to estimate the time course of broadband gamma activity (BGA) [97]. BGA provides precise estimates of task-specific cortical activity [75, 90, 148, 196, 198, 199], is tightly linked to the group activity of local neural populations [102, 200-202], and is strongly correlated with the BOLD signal [96, 102, 104-106, 185, 203, 204].

Time series representations of percent change in BGA were calculated by comparing post-stimulus BGA power to a mean pre-stimulus baseline activity (-700 to -200 ms) (Fig 1c) [80, 97]. For each category, trials with noise or artifacts during either the baseline or post-stimulus window were discarded, resulting in a mean (+/- sd) of 46 (18) face trials; 31 (9) animate trials; 29 (8) tool trials; 49 (6) place trials; and 38 (11) word trials used in the analyses.

Quantifying Category-Selectivity and Relationship to Cortical Topology:

To quantify category selective responses in each SDE, the *d'* (d-prime) sensitivity index was computed for each category per electrode (a total of 5 *d'* indices per electrode). The *d'* index is an established metric in signal detection used to determine how well a target can be discriminated from competing stimuli [67, 205-210]. For each category at each electrode, the mean BGA in the 100-400ms interval after stimulus onset was standardized by across trial standard deviation [67, 209]. The *d'* index was calculated as the difference between the standardized BGA for each category against all other categories:

$$d' = \frac{m_j - \frac{1}{N}\sum_{i}^{N} m_i}{\sqrt{\frac{1}{2}\left(s_j^2 + \frac{1}{N}\sum_{i}^{N} s_i^2\right)}}; i \neq j$$

where μ_j is the mean response to the current category *j*; σ_j is across-trial standard deviation of BGA activity to category *j*; and μ_i and σ_i denote the same for the other categories. Because 5 categories in all were evaluated, for each category *j, N* will be equal to 4. In this fashion, each electrode could be judged selective for multiple categories [208].

Significance thresholds were determined through permutation testing. For each electrode per subject, a null distribution was generated by randomly shuffling category labels across all trials and recomputing the *d'* index 10,000 times. The *p*-value for each category per electrode was determined as the fraction of shuffled *d'* indices that were greater than the actual *d'* index [209]. At the group-level, individual *p*-values were corrected for multiple comparisons (across categories and SDEs, per region and hemisphere) to an adjusted alpha level of 0.01. Corrections for multiple comparisons were performed using the false-detection rate (FDR) procedure [211].

To test for lateral-to-medial and ventral-to-dorsal functional gradients in the VTC and LOC respectively, grouped correlational analysis was performed using Spearman's rank correlations to evaluate the relationship between changes in category-selectivity (determined by the *d'* index) and SDE coordinates (in group, i.e. Talairach, space following surface-based normalization) [ggplot2 and stats packages in R] [128, 212]. Tests for significance were determined at an FDR-adjusted alpha level of 0.05 to correct for multiple comparisons across categories and SDEs (per region and hemisphere). Spearman correlations were selected (over Pearson's) for their robustness to outlier influence and smaller sample sizes. Furthermore, Spearman's correlations test for monotonic relationships, and the relationships between *d'* indices and SDE coordinates are not known *a priori* to be linear. Scatterplots were generated for each category to visually depict univariate relationships between grouped *d'* indices and SDE coordinates for each hemisphere in each region.

Next, linear mixed effects (LME) models were generated to more robustly quantify the relationship between category-selectivity (i.e. grouped *d*' index) and the cortical topology while controlling for individual subject effects. For each category, SDE

coordinates (in Talairach space) were modeled as a fixed effect, and patient ID modeled as a random effect to control for inter-subject variability as well as non-independence (e.g. one subject contributing multiple SDEs) [lme4 and lmerTest packages in R] [213-217]. To control for spatial multicollinearity, SDE coordinates per hemisphere in each region (VTC and LOC) were mean-centered prior to inclusion in the LME models. LME models were then fitted per category for each hemisphere in each region.

Finally, to visually evaluate the spatial organization of SDE category-selectivity relative to anatomical landmarks (the MFS and LOS), SDEs with significant *d'* indices ($p \leq 0.01$, FDR corrected) for each category were visualized on the MNI N27 cortical surface (aligned to Talairach space), and color-coded by category-preference.

Results

ECoG recordings of broadband gamma activity (BGA; 60 -120Hz) from 26 subjects (LH *n*=16; RH *n*=10) were analyzed to evaluate the relationship between category-selectivity and cortical topology in higher-level visual cortex. In total, 242 SDEs were evaluated: 159 SDEs were localized to ventral temporal cortex (VTC: LH *n*=95, median=5 SDEs/subject, interquartile range, IQR= 3 - 8.25; RH *n*=64, median=4.5 SDEs/subject, IQR=4-5), and 83 SDEs were localized to lateral occipital cortex (LOC: LH *n*=48, median=3.5 SDEs/subject, IQR=1.5-7; RH *n*=35, median = 7 SDEs/subject, IQR=3-10).

At the individual level, task-dependent increases in BGA peaked at ~350 - 400ms after stimulus onset (Fig 3). Category-selective BGA responses (significant *d'* index at an FDR corrected $p \leq 0.01$), organized with respect to the cortical topology,

were consistently seen at the single subject level. However, the sparse sampling in each individual case precluded a comprehensive evaluation of these relationships at the single subject level, and surface-based normalization was performed to transform all SDE coordinates across subjects to a common brain space (Fig 4).

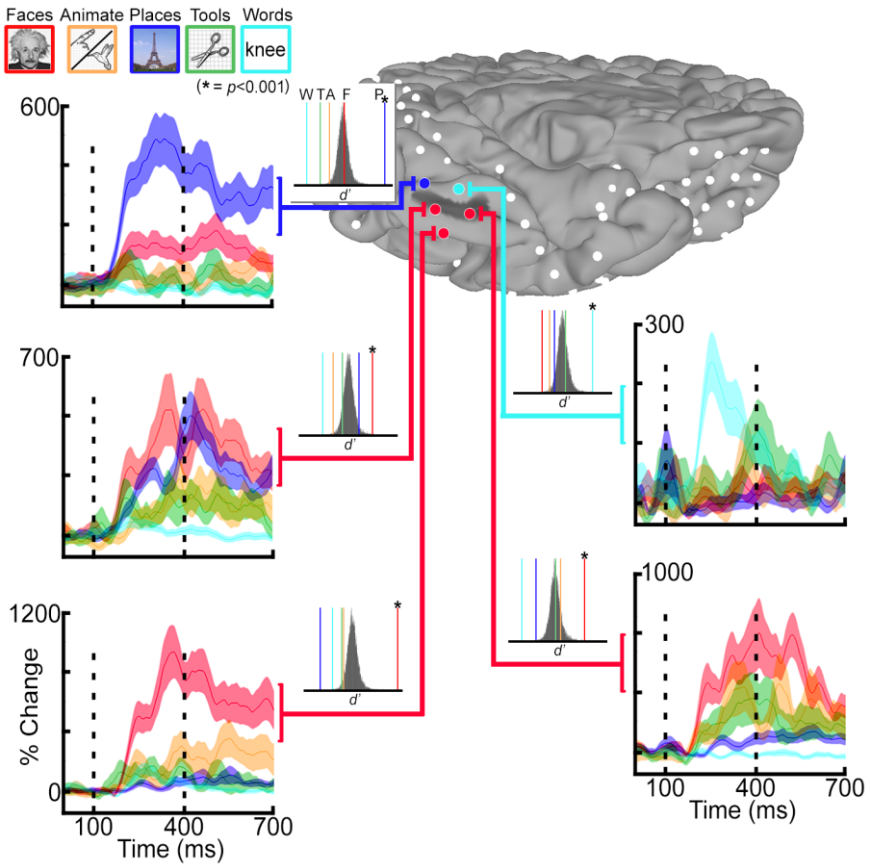

Figure III-3. Single Subject Category-selectivity Analysis

Single subject category-selectivity determined using the *d'* sensitivity index. 5 subdural electrodes (SDEs) were localized in this individual to the vicinity of the mid-fusiform sulcus (MFS, dark gray shading on cortical surface). Time-series representations of broadband gamma activity (BGA, 60 – 120 Hz) for face (red), animate (orange), place (blue), tool (green), and word (cyan) stimuli are depicted for each SDE. Vertical dashed lines denote the time window for *d'* analysis (100 to 400 ms after stimulus onset). *p*-values per category and per SDE were determined against a null distribution (insets; *n*=10,000 permutations). Colored vertical lines denote actual *d'* index per category (colors matched to tasks, asterisks denote $p \leq 0.001$). In this subject, all face-selective SDEs (*n*=3; red spheres) are localized at or lateral to the MFS, while place and word selective SDEs are localized postero-medially and antero-medially, respectively.

Of the 242 SDEs used in the analysis (VTC and LOC bilaterally), a total of 142 SDEs (~59%) had a significant *d*' index for at least one category ($p \leq 0.01$, FDR corrected). In the VTC, a total of 69/95 SDEs (~73%) in the left hemisphere and 34/64 SDEs (~53%) in the right hemisphere had a significant *d'* index (FDR corrected $p \leq 0.01$) for at least one category (Fig 4, left). In the LOC, a total of 26/48 SDEs (~54%) in the left hemisphere and 13/35 SDEs (~37%) in the right hemisphere had a significant *d'* index for at least one category (Fig 4, right). Notably, only 7 SDEs (VTC $n = 6$; LOC $n=1$) had a significant *d'* index for a second category (both faces and places), all of which were localized in the left hemisphere to the respective sulci of interest (MFS or LOS).

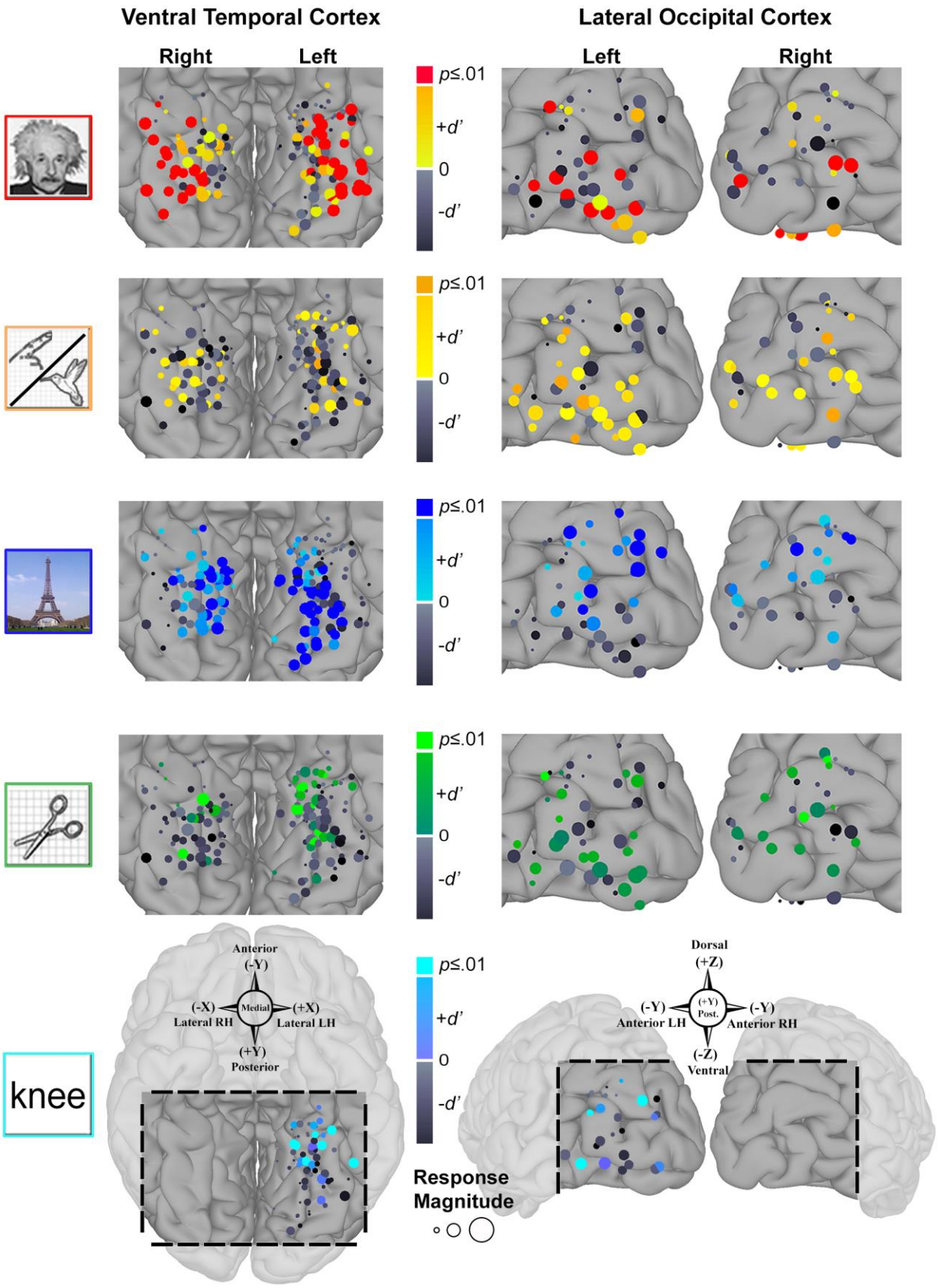

Figure III-4. Grouped SDE and *d'* Visualization

Responsivity and preference to each category for all subdural electrodes (SDEs) over ventral temporal cortex (VTC, *right*) and lateral occipital cortex (LOC, *left*), grouped across all 26 subjects (following surface-based normalization) and visualized on the MNI N27 template brain. Compass points denote SDE coordinates (Talairach space) and direction. SDE diameter reflects normalized BGA magnitude for each category (mean BGA divided by standard deviation), scaled by the largest normalized response across categories per region (VTC and LOC are scaled differently). SDE colors reflect their d' values per category. Positive, significant *d'* indices ($p \leq 0.01$, FDR corrected) are represented by the category-specific color-code at the top of the color bar (e.g. SDEs with significant face *d'* colored red). Positive, non-significant *d'* indices are represented as intermediate color-scales specific for each category. Negative *d'* indices are represented by gray color-scale (darker = more negative values).

Correlational analyses of d' indices with SDE coordinates

Spearman correlations were used to initially evaluate univariate relationships between grouped *d'* indices and spatially normalized SDE coordinate (Talairach space) for each category per region, and depicted as scatterplots (Fig 5). We note that in the VTC, x and z coordinates were highly correlated (RH: $r_{s,62} = .97$, $p = 2.2e\text{-}16$; LH: $r_{s,92} = -.83$, $p = 2.2e\text{-}16$). Therefore only the x and y coordinates were evaluated for the VTC (z coordinate was removed). Similarly, in the LOC, the x and y coordinates were highly correlated (LH: $r_{s,46} = -.94$, $p = 2.2e\text{-}16$; RH: $r_{s,33} = .865$, $p = 1.8e\text{-}14$). Therefore only the y and z coordinates were evaluated in the LOC (x coordinate was removed). The exclusion of the z and x coordinates as predictors for VTC and LOC category selectivity, respectively, remains consistent with the anatomical principles governing structure-function hypotheses currently being tested (e.g. animacy maps in the VTC are a function of a lateral-to-medial axis).

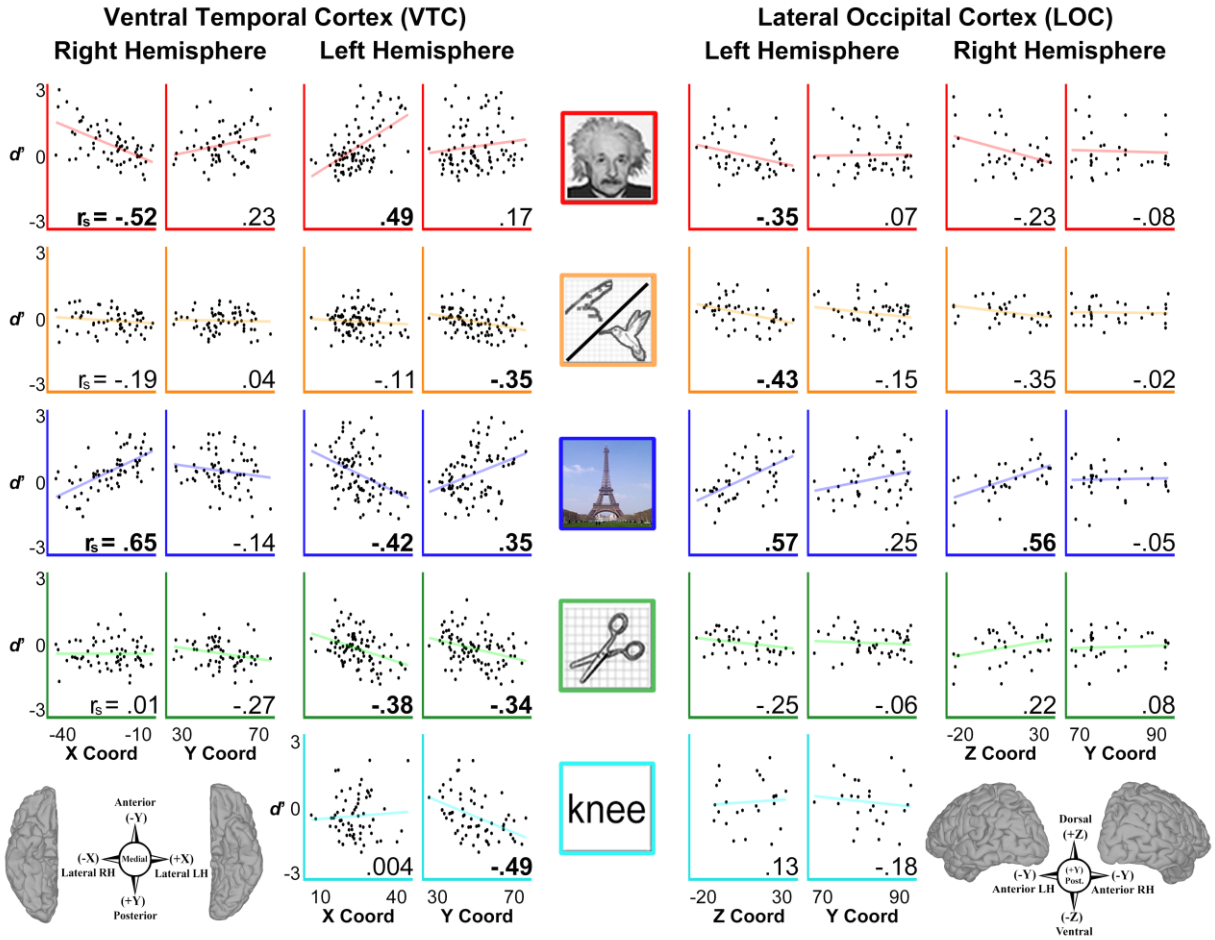

Figure III-5. Grouped *d*' Sensitivity vs. SDE Coordinates

Scatterplots depict grouped *d*' indices for each category plotted vs. subdural electrode (SDE) coordinates (in Talairach space) per hemisphere in each region. In the ventral temporal cortex (VTC; RH *n*=64, LH *n*=95), comparisons were made against the x and y coordinates. In the lateral occipital cortex (LOC; LH *n*=48, RH *n*=35), comparisons were made with the z and y coordinates. For each plot, regression lines were fitted (color-coded by category), and the strengths of association were estimated using Spearman correlations (bottom right, bold text denotes $p \leq 0.05$, FDR corrected).

For faces, significant correlations were noted between *d'* index and the x-axis in VTC bilaterally (RH $r_{s,62}$ = -.52, *p* = -1.2e-05; LH $r_{s,92}$ = .49, *p* = 3.3e-07), indicating lateral associations with face-selectivity (Fig 5). A significant correlation between face *d'* indices and the z-axis was also noted in the left LOC ($r_{s,46}$ = -.35, *p* = 0.014), indicating a ventral association with face-selectivity in this region. For animate stimuli,

significant correlations were found in the left hemisphere, between *d'* indices and the y-axis in the VTC ($r_{s,92}$ = -.35, *p* = 5.2e-04; anterior association) and the z-axis in the LOC ($r_{s,46}$ = -.43, *p* = 1.9e-03; ventral association). For place stimuli, significant correlations were found between *d'* index and the x-axis in the VTC bilaterally (RH $r_{s,62}$ = .65, *p* = 1.6e-08; LH $r_{s,92}$ = -.42, *p* =4.0e-05; medial associations), the y-axis in the left VTC ($r_{s,92}$ = .35, *p* = 5.7e-04; posterior association), and the z-axis in the LOC bilaterally (LH $r_{s,46}$ = .57, *p* = 2.9e-05; RH $r_{s,33}$ = .56, *p* = 4.0e-04; dorsal association). For tool stimuli, significant correlations were noted between *d'* index and the x- and y-axis in the left VTC only ($r_{s,92}$ = -.38, *p* = 1.4e-04; $r_{s,92}$ = -.34, *p* = 6.2e-04; medial and anterior associations, respectively). Finally, for word stimuli, a significant correlation was found only with the y-axis in the left VTC ($r_{s,63}$ = -.49, *p* = 2.4e-05; anterior association). No other relationships were observed to be significant.

Given that multiple SDEs could be contributed from each individual, we generated linear mixed effects (LME) models for each stimulus category to more robustly quantify the relationships between *d'* index and SDE coordinates (mm, in Talairach space) while controlling for non-independence of data within individuals. In the VTC, the x and y coordinates, and the interaction term (x*y), were entered as fixed effects into the models. In the LOC, the fixed effects were entered as the y and z coordinates, and the interaction term (z*y). All models included random-effect variable intercepts for subjects to control for inter-subject variability. Complete model results for the VTC and LOC are provided in Fig 6. For brevity, only significant LME results are discussed in the following section.

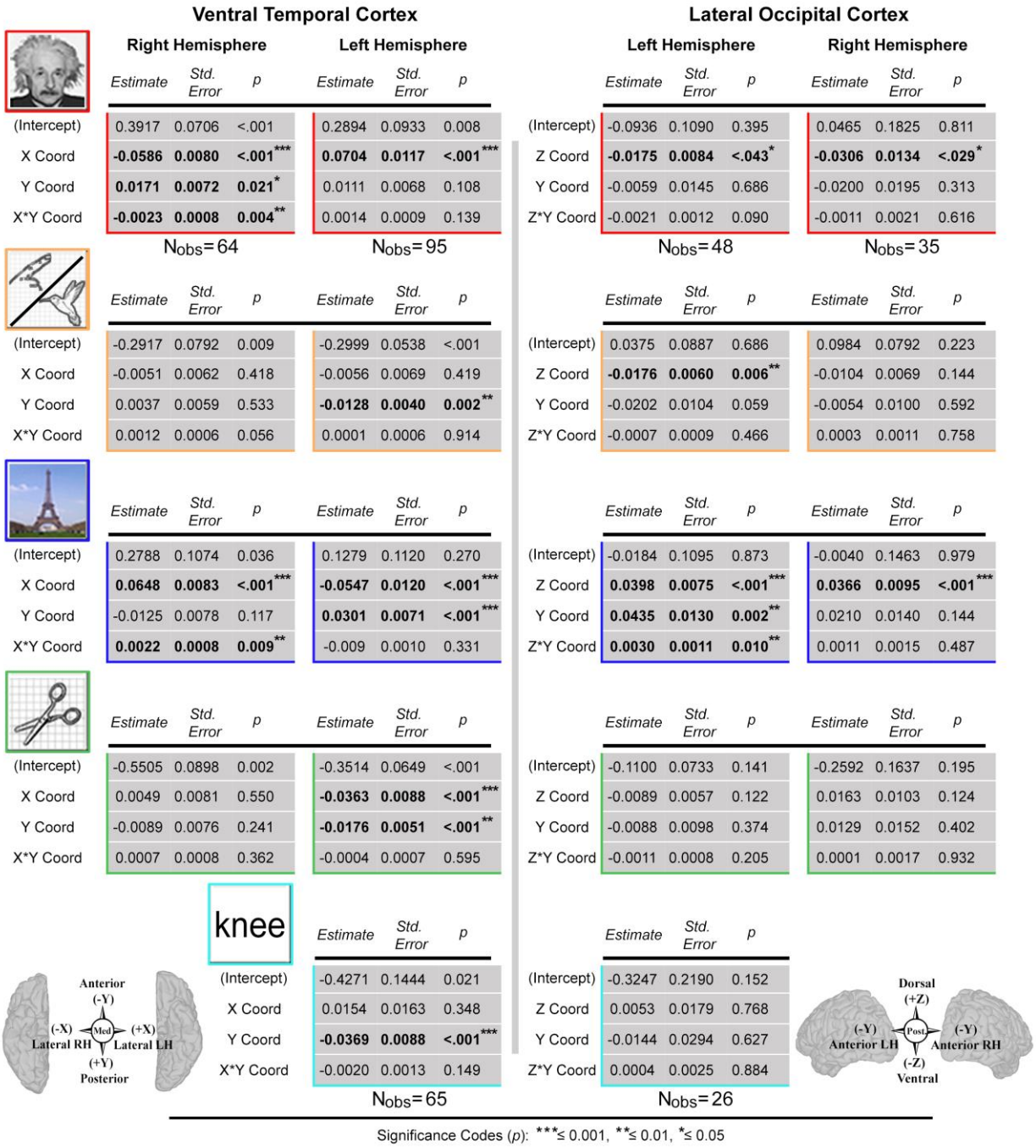

Figure III-6. Linear Mixed Effects Model Results

Linear mixed effects (LME) models computed to quantify relationship between *d'* sensitivity index (category-selectivity) and subdural electrode (SDE) coordinates (cortical topology) for each category per hemisphere in the ventral temporal cortex (VTC; left) and lateral occipital cortex (LOC; right). Tables provide coefficient estimates, standard errors, significance levels and number of observations (N_{obs}) for fixed effects predictors in each hemisphere per region. For face, animate, place, and tool LME models, the number of observations is consistent for each region and hemisphere, and thus listed once (under model results for faces). In the LOC, the fixed effects were: Z-Coord, Y-Coord, and Z*Y-Coord. In the VTC: X-Coord, Y-

Coord, and X*Y-Coord. All SDE coordinates (in mm, aligned to Talairach space using surface-based normalization) were mean-centered prior to being entered into the models. Bold text denotes significant predictors, with significance levels denoted by the asterisks (legend at bottom).

Linear mixed effects analysis: Ventral Temporal Cortex

In the right VTC, LME analysis was performed for 4 stimulus categories (faces, animate, places, and tools) using 64 SDEs (Fig 6). For face stimuli, a negative relationship was found with increasing *d'* index in the x-axis (*B* = -0.0586, *S.E.* = 0.0080, *p* = 6.5e-10; indicating selectivity increases laterally), a significant positive relationship with increasing selectivity in the y-axis (*B* = 0.0171, *S.E.* = 0.0072, *p* = .021; posteriorly), and a significant negative relationship between face-selectivity and the x*y interaction term (*B* = -0.0023, *S.E.* = 0.0008, *p* = 4.3e-03). For place stimuli, we found a significant positive relationship with increasing selectivity in the x-axis (*B* = 0.0648, *S.E.* = 0.0083, *p* = 1.2e-10; medially), and a significant positive relationship between selectivity and the x*y interaction term (*B* = 0.0022, *S.E.* = 0.0008, *p* = 9.2e-03). No significant associations were noted for tool- or animate-selectivity.

In the left hemisphere VTC, LME analysis was performed for 4 stimulus categories (faces, animate, places, tools) using 95 SDEs, and for 1 stimulus category (words) using 65 SDEs. For face stimuli, we found a significant positive relationship with an increasing *d'* index in the x-axis (*B* = 0.0704, *S.E.* = 0.0117, *p* = 3.32e-08; selectivity increases laterally). For animate stimuli, a negative relationship was observed for increasing selectivity in the y-axis (*B* = -0.0128, *S.E.* = 0.0040, *p* = 2.15e-03; anteriorly). For places, we found a negative relationship with increasing place-selectivity in the x-axis (*B* = -0.0547, *S.E.* = 0.0120, *p* = 1.53e-05; medially), and a

positive relationship with increasing selectivity in the y-axis (*B* = 0.0301, *S.E.* = 0.0071, *p* = 5.91e-05; posteriorly). For tools, we found a negative relationship with increasing selectivity in the x-axis (*B* = -0.0363, *S.E.* = 0.0088, *p* = 9.00e-05; medially), and a negative relationship with the y-axis (*B* = -0.0176, *S.E.* = 0.0051, *p* = 9.28e-04; anteriorly). For words, a negative relationship was observed with increasing selectivity in the y-axis (*B* = -0.0369, *S.E.* = 0.0088, *p* = 9.67e-05; anteriorly).

Linear mixed effects analysis: Lateral Occipital Cortex

In the left LOC LME analysis was performed for 4 stimulus categories (faces, animate, places, and tools) using 48 SDEs and for 1 stimulus category (words) using 26 SDEs (Fig 6). For both face and animate stimuli, we found significant negative relationships with increasing *d'* indices in the z-axis (face *B* = -0.0175, *S.E.* = 0.0084, *p* = 0.043; animate *B* = -0.0176, *S.E.* = 0.0060, *p* = 5.6e-03; selectivity increases ventrally for both). For places, we found a significant positive relationship with increasing selectivity in the z-axis (*B* = 0.0398, *S.E.* = 0.0075, *p* = 3.8e-06; dorsally), a significant positive relationship with the y-axis (*B* = 0.0435, *S.E.* = 0.0130, *p* = 1.7e-03; anteriorly), as well as a significant positive relationship with the y*z interaction term (*B* = 0.0030, *S.E.* = 0.0011, *p* =9.8e-03). No significant associations were noted for tool or word-selectivity.

Finally, in the right LOC, LME analysis was performed for 4 stimulus categories (faces, places, tools, and animate) using 35 SDEs. For faces, we found a significant negative relationship with increasing selectivity in the z-axis (*B* = -0.0306, *S.E.* = 0.0134, *p* = .029; selectivity increases ventrally), and for places we found a significant positive relationship with increasing selectivity in the z-axis (*B* = 0.0366, *S.E.* = 0.0095,

p = 6.0e-04; dorsally). No significant associations were noted for tool- or animate-selectivity.

Overall the LME provided a more rigorous quantification of the effects found by the exploratory analyses based on the Spearman's correlations, revealing three additional significant relationships: between the *d*' index for faces with the y-axis in the right VTC and the z-axis in the right LOC; as well between the *d'* index for places and the y-axis in the left LOC.

Topology of category-selectivity

To evaluate the spatial relationship of category-selective SDEs with respect to cortical folding patterns, all SDEs with significant *d'* indices were visualized on the MNI N27 brain surface (in Talairach space), and color-coded by category preference (Fig 7). Notably, all animate-selective (LH *n* = 3/3) and nearly all face-selective (LH *n* = 27/28; RH *n* = 15/17) SDEs were localized to or lateral to the mid-fusiform sulcus (MFS) in the VTC bilaterally. Similarly, all place-selective (LH *n* = 29/29; RH *n* = 14/14) and tool-selective SDEs (LH *n* = 7/7; RH *n* = 2/2) were localized to or medial to the MFS bilaterally. Additionally both tool-selective and word-selective (LH *n* = 7/7) SDEs were clustered along the anterior boundary of the mid-fusiform sulcus in the left VTC.

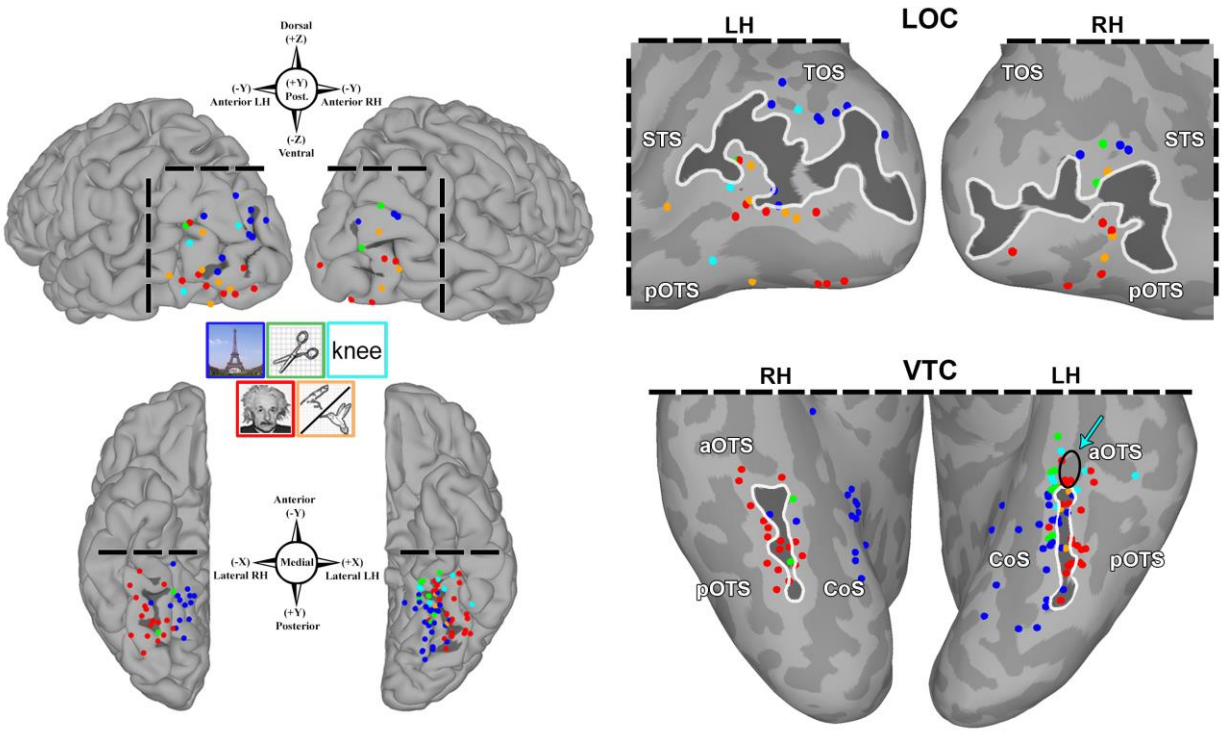

Figure III-7. Spatial Organization of VTC and LOC Category-Selectivity

All subdural electrodes (SDEs) with significant category-selectivity ($p \leq 0.01$, FDR corrected) are visualized on the MNI N27 template brain (aligned to Talairach coordinate space) after surface based normalization. SDEs are color-coded by the category of preference (matched to image legends). Compass points denote SDE coordinates (Talairach space) and direction. Left: Pial surface maps of lateral occipital cortex (LOC, *top*) and ventral temporal cortex (VTC, *bottom*). Right: inflated surfaces for these regions with the lateral-occipital sulcus (LOS) and mid-fusiform sulcus (MFS) delineated by dark gray shades and white contours, and adjacent sulci delineated by lighter gray shades (TOS, transverse occipital sulcus; STS, superior temporal sulcus; p/aOTS, posterior/anterior occipito-temporal sulcus; CoS, collateral sulcus). In the LOC, all 13 face-selective (red; LH *n* = 8; RH *n* = 5) and 9 animate-selective (orange; LH *n* = 6; RH *n* = 3) SDEs are localized at or below the LOS, while all 12 place- (blue; LH *n* = 9; RH *n* = 3) and 3 tool-selective (green; LH *n* = 1; RH *n* = 2) SDEs are localized at or dorsal to the LOS. In the VTC, all 3 animate- (LH only) and 42/45 face-selective (LH *n* = 27/28; RH *n* = 15/17) SDEs are localized to-or-lateral to the MFS, while all 43 place- (LH *n* = 29; RH *n* = 14) and 9 tool-selective (LH *n* = 7; RH *n* =2) SDEs are localized to-or-medial to the MFS.

In the LOC, bilaterally, a similar arrangement of category-selectivity with respect to the lateral occipital sulcus (LOS) was observed. All face-selective (LH *n*=8/8; RH *n*=5/5) and animate-selective (LH 6/6; RH *n*=3/3) SDEs were uniformly localized at or

inferior to the LOS, while all place-selective (LH *n*=9/9; RH *n*=3/3) and tool-selective (LH *n*=1/1; RH *n*=2/2) SDEs were localized at or superior to the LOS. However, no discernable spatial arrangement of word-selective (LH *n*=3) SDEs could be observed.

Conclusions

We utilized a surface-based grouped icEEG analyses, combined across a large cohort (*n* = 26; LH *n*=16, RH *n*=10), to provide a comprehensive electrophysiological evaluation of the topology of category-selectivity in higher-order visual cortex. We demonstrate a consistent spatial organization of category-selective regions with respect to specific anatomical landmarks in the ventral temporal and lateral occipital cortical complexes (VTC and LOC). Importantly, our findings advance prior work by demonstrating that the use of surface-based normalization strategies in grouped icEEG analyses preserves structure-function coupling in a common brain space. In doing so, we provide a method to circumvent the sparse-sampling problem that has constrained the broader application of icEEG to the study of cognitive function at the single subject level [80, 81].

Structure-function coupling in higher-level visual cortex

Our data reveal significant associations between category-selectivity with both lateral-to-medial and posterior-to-anterior axes in the VTC, as well as a dorsal-to-ventral axis in LOC, bilaterally. In the VTC, the mid-fusiform sulcus (MFS) provides a consistent boundary for transitions in selectivity between living (face and animate) and non-living (place and tool) stimuli: face and animate selective areas are constrained at or lateral to the MFS, while place and tool selective regions are constrained at or medial to the MFS. Furthermore, in the left VTC, the anterior aspect of the MFS

predicts the location of word, animate, and tool selective responses, suggesting that the VTC may possess additional functional gradients along the postero-anterior anatomical axis. Notably, regions demonstrating word-selectivity are clustered around the intersection of the occipito-temporal sulcus (OTS) and the anterior MFS (Figure 7). As prior studies of word selectivity have localized cortical regions sensitive to orthographic stimuli to the general vicinity of the OTS (i.e. the visual word-form area) [159, 160, 188-190, 208, 218, 219] – the intersection of the anterior MFS and OTS may be a more precise spatial descriptor, based on our data. The interspersed locus of word-selective regions with other categories in the anterior MFS is consistent with the interactive models of word reading developed to explain the spatial heterogeneity of responses elicited by this and other visual naming tasks [218].

In the LOC, the lateral-occipital sulcus (LOS) provides a consistent boundary for transitions between animate and face selective regions ventrally, and scene and tool selective regions dorsally. Notably, face- and animate selective SDEs are interspersed on the ventral aspects of the LOC in a fashion consistent with prior fMRI studies that demonstrate alternating regions of face and limb-selectivity [33, 220, 221]. Additionally, in the left LOC, tool stimuli elicit strong, but non-selective activations in SDEs localized ventral to the LOS. Although the ventral LOC exhibits an overall greater selectivity for living stimulus categories, the role of the LOC in more general visual form processing is well documented, and these findings remain consistent with models describing multiple, superimposed functional maps organized within the same expanse of cortical tissue [33, 53, 161, 167, 222].

While the locations of VTC and LOC category-selectivity reported here are consistent with an extensive body of invasive and non-invasive neuroimaging [35, 36, 84, 85,

[93, 155, 162, 168, 172, 178, 223-232], our findings provide novel electrophysiological support for hypotheses of hierarchical information structuring in higher-level visual cortex. Such hypotheses propose that small-scale functional representations are nested together within larger-scale functional maps, facilitating object categorization by the visual system (and possibly other higher-order cognitive systems) by enabling the extraction of different levels of categorical detail at different spatial scales (i.e. small scale for face information, larger scale for animacy information) [4, 163].

This hierarchical information structure is believed to arise from the distinct anatomical organization of these regions, as the MFS and LOS also predict transitions in cortical micro- and macro-architecture (e.g. cyto- and receptor architectonics and white-matter structural networks, respectively) [58, 60, 61, 166]. Such organization may speed visual categorization by directing unrelated visual information to distinct neural networks operating in parallel (e.g. details pertaining to scenes vs. faces), while related visual information (e.g. faces and body-parts) converge onto shared neural substrates [4, 66].

To date, evidence for hierarchical coding models has come almost exclusively from non-invasive neuroimaging studies. Although a recent electrophysiological study has also reported large-scale animacy distinctions along the MFS [67], the analysis in this study was restricted to a small sample size (*n*=6; LH 3, RH 3) and constrained to the individual level. Our work here validates their findings in a larger population, extends the investigation to the LOC, and broadens the stimulus classification to include tools and words. Notably, our observation that SDEs with dual-selectivity were localized within the MFS or LOS indicates that either our recordings average across multiple modules arranged in proximity to each other within the sulcus, or that the transitions

between neuronal clusters tuned to specific categories may be a gradual one [169]. While the recording scale of the SDEs used clinically does not allow us to distinguish between these two possibilities, our results nevertheless provide novel support that these sulci – the MFS and LOS – are critical to the functional topology of higher-level visual cortex.

Grouped icEEG: a solution to the sparse-sampling problem

The sparse-sampling problem has been a long-standing limitation of icEEG, to which the recent development of surface-based grouped techniques provides a viable and much-needed solution [75, 81, 105, 111]. In the current study, we combined data across 26 different subjects, each introducing a unique source of topological and pathological variability. The nonlinear transformation utilized here to map 242 SDEs into a common brain space preserved structure-function coupling across this heterogenous population, thus validating surface-based approaches to grouped icEEG. Furthermore, our findings also demonstrate a consistency of functional representation in our patient population – both amongst themselves and with respect to healthy subjects – thereby validating the use of patients with focal epilepsy for the study of cognitive function.

Limitations

Three main limitations of this work are apparent to us. The first is that we include only subjects implanted with SDEs, which record from the gyral crowns, and may be biased against activity arising from sulcal sources. Notably, prior literature focusing on limb- and body-selectivity in the VTC has reported regions localized in or near the OTS [33, 47, 48, 220]. The paucity of VTC animate selectivity reported in the current study may have resulted from this gyral bias. To investigate this possibility, future icEEG work will

integrate SDE data with data obtained from penetrating depth electrodes or stereotactic EEG [120].

A second limitation is the inconsistency in the low-level visual features of our stimuli (e.g. colored images for places vs. gray-scale face stimuli vs. line-drawings of tools/animate stimuli), which provide a potential confound in our analysis. However, higher-level visual regions are known to be invariant to changes in low-level visual features, and to maintain visual selectivity across a large spectrum of visual information, including color [4, 233-240]. This assumption is supported by the sharp changes in category-selectivity observed in the VTC and LOC. More specifically, while place and tool stimuli were the least similar in terms of low-level features (e.g. real color images of large, naturalistic stimuli vs. line-drawings of small, handheld objects) both were clustered together medial to the MFS. Similarly, in the LOC, face and animate stimuli (gray-scale vs. line-drawings, respectively) were clustered together ventrally with respect to the LOS.

The third limitation is that our stimulus set does not allow us to unequivocally claim that the abstract semantic concept of “animacy” is the driving force behind the topological organization we observe. Notably, prior studies have argued that animacy distinctions in higher-order visual areas may simply be a by-product of shape similarities between stimuli of related categories [241-243]. Nevertheless, category-specific functional gradients along abstract semantic boundaries (e.g. animacy) have been previously demonstrated in the congenitally blind [244]. Additionally, in a recent study describing the topographic representation of body parts in the VTC and LOC, shape similarities were found to be insufficient to explain the architecture of the body-maps observed. Specifically, the authors demonstrated that regions preferential to a specific

class of body-parts (e.g. upper limbs) were more responsive to within-class images, despite their greater dissimilarities in shape (e.g. hands and elbows), than to more similarly shaped images from distinct classes (e.g. feet and knees – lower-limbs) [47]. Finally, a recent computational study has suggested how functional representations along abstract semantic boundaries (specifically animacy) could be achieved via top-down influences (reflected in supervised learning models); with their most successful models incorporating both visual and semantic information [245]. Thus, a final account of the functional topology within higher-order visual regions will likely need to account for both low-level visual features as well as influences from semantic or categorical dimensions [4, 167, 169, 173, 245, 246].

In sum, we provide a comprehensive grouped icEEG investigation of VTC and LOC category-selectivity, and demonstrate unequivocal evidence for structure-function coupling in higher-level visual cortex through direct electrophysiological recordings in a large human cohort. Our findings support hypotheses of hierarchical information structuring in higher-level visual cortex via the generation of large-scale functional maps (e.g. animacy) from nested functional representations consequent to this structure-function coupling [4].

Surface-based strategies to icEEG analyses provide novel opportunities for researchers to pool ECoG datasets across centers. Given the relative rarity of icEEG data in many cortical regions of interest (e.g. the right occipital cortex), the adoption of such collaborative strategies could provide an invaluable tool to greatly expand the relevant application of high spatiotemporal resolution icEEG to the study of higher-level cognitive function.

Summary

Neuroimaging studies suggest that category-selective regions in higher-level visual regions are topologically organized with respect to specific cortical landmarks: the mid-fusiform sulcus (MFS) in the ventral temporal cortex (VTC) and the lateral occipital sulcus (LOS) in the lateral occipital cortex (LOC). To derive precise structure-function maps from direct neural signals, we collected broadband gamma activity (60 – 120 Hz) using intracranial EEG (icEEG) recordings in a large human cohort (*n*=26) undergoing implantation of subdural electrodes over each hemisphere. A surface-based approach to grouped icEEG analysis was used to overcome challenges arising from sparse electrode coverage within subjects and variable cortical anatomy across subjects. The topology of category-selectivity in bilateral VTC and LOC was assessed for five classes of visual stimuli – faces, animate non-face (animals/body-parts), places, tools, and words – using correlational and linear mixed effects analyses. In the LOC, selectivity for living (faces and animate non-face) and non-living (places and tools) classes was arranged in a ventral-to-dorsal axis along the LOS. In the VTC, selectivity for living and non-living stimuli was arranged in a latero-medial axis along the MFS. Selectivity for written words was reliably localized to the intersection of the left MFS and the occipito-temporal sulcus. These findings provide direct electrophysiological evidence for hierarchical information structuring in higher-level visual cortex [4]. These findings provide direct electrophysiological evidence for hierarchical information structuring of visual information within higher-order visual cortex.

Chapter IV: Information Flow within the Ventral Temporal and Lateral Occipital Cortex

Introduction

The recognition of a familiar face is fundamental to social dynamics. Seemingly effortless, this computational feat requires rapid object detection (the presence of a face) and feature discrimination (individuation) [247]. Converging evidence from behavioral, electrophysiological, functional, and lesional data have identified a subset of cortical regions, biased towards the right hemisphere, that form a distributed network responsible for the structural encoding of faces [40]. This network is comprised of the occipital face area (OFA) in the inferior occipital cortex [227] and the fusiform face area (FFA) in the postero-lateral fusiform gyrus [49]. While there is general agreement that these regions are important to face perception, their specific roles and the dynamics of information flow between them is a subject of continued debate [33, 74].

Contemporary theory posits that face perception operates via feed-forward mechanisms [13] with visual features serially processed in stages of increasing complexity along a postero-anterior axis in the ventral visual cortex [40, 49, 248]. However, recent work questions the validity of the Feed-Forward Model (FFM) [69]. Prosopagnosic patients with OFA lesions are able to categorize face stimuli (real and ambiguous), while fMRI studies of these subjects demonstrate face-specific FFA activity akin to healthy controls [72, 73]. These findings suggest that a Non-Hierarchical Model (NHM), relying on parallel, distributed network interactions, may better explain face perception [74]. According to the NHM, the FFA initially performs holistic face detection, independent of the OFA, via direct inputs from early visual cortex (EVC) [42, 249]. Following detection, reentrant interactions between the FFA and the OFA progressively refine facial representations to facilitate recognition.

Evidence for current models of face perception has been derived almost exclusively from non-invasive behavioral, functional, and stimulation studies. However, these approaches suffer from limited spatio-temporal resolution, and are ill-equipped to evaluate transient interactions between disseminated cortical regions [79]. Human intracranial EEG (icEEG) recordings improve upon these limitations [75, 82], but thus far have focused principally on the response properties (timing/distribution/selectivity) of the core face network [120, 179, 180, 183, 196, 206, 231, 250-256]. To date, a conclusive icEEG evaluation of the broader network dynamics responsible for face processing has not yet been performed. Specifically, a primary tenet of the widely accepted FFM – that the OFA relays EVC input to the FFA – has not been validated.

Using icEEG, we conducted a series of four experiments to investigate whether face perception invokes feed-forward or parallel interactions between EVC and the OFA and FFA. First, we measured task-dependent power changes in high frequency broadband activity [90] to compare relative onsets of face-selectivity in these regions. Second, we computed functional connectivity in high frequency bands to estimate directed information flow during face processing [257, 258]. Third, we utilized cortico-cortical evoked potentials [259] to compute task-independent estimates of electrophysiological connectivity between these regions. Lastly, we used high frequency cortical stimulation [260] to determine if transient OFA and FFA lesions produced perceptual deficits consistent with their predicted roles. We hypothesized that if the NHM correctly describes the mechanisms of face-perception, EVC should be directly and independently connected with both the OFA and FFA, and that the FFA should demonstrate face-selectivity no later than the OFA. In contrast, the FFM

predicts unidirectional information flow from EVC through OFA to the FFA, with sequential activation of these regions.

Methods

Data were collected from 11 subjects (5 female, mean age 38 ± 11 years, mean IQ 106 ± 9) scheduled for right hemispheric sub-dural electrode (SDE) implantation to localize seizure onset sites. Informed consent was obtained following study approval by our institution's committee for protection of human subjects.

Experimental Design:

10 of the 11 subjects participated in a visual confrontation naming task wherein images of famous faces were presented for the experimental condition and scrambled versions of the same stimuli were presented as a low-level visual control. Subjects were instructed to overtly name faces in the experimental condition, and say, "scrambled" for the control. The same subjects performed a subsequent visual naming task using inanimate (tools and non-tool objects) and animate, non-face stimuli (animals and body-parts) as high-level visual controls [97]. Stimuli were displayed at eye-level on a 15'' LCD screen placed at 2 feet from the patient (2000 ms on screen, 3000 ms inter-stimulus interval; 500x500 pixel image size, ~10.8° x 10.8° of visual angle, with a grid overlay on 1300x800 pixel white background, ~28.1° x 17.3° of visual angle).

Face stimuli consisted of gray-scale, real images of famous individuals shown in frontal view (celebrities, politicians, and historical figures taken from free online sources), and were cropped to show only the face and head. Scrambled control stimuli (referred to hereafter as "scramble") were generated by rearranging the grid overlay so

that low-level properties of the original face were preserved, while completely degrading any face-related information. Animate, non-face stimuli (referred to hereafter as “animate”) and inanimate stimuli were taken from the standardized Snodgrass and Vanderwart’s object pictorial set [187]. A transistor-transistor logic pulse triggered by the stimulus presentation software (Python v2.7) at stimulus onset was recorded as a separate input during the experiments to time lock all trials.

Cortical Surface Models:

Pre-implantation anatomical MRI scans were collected using a 3T whole-body MR scanner (Philips Medical Systems, Bothell WA) equipped with a 16-channel SENSE head coil. Anatomical images were collected using magnetization-prepared 180-degree radio-frequency pulses and rapid gradient-echo (MP-RAGE) sequence, optimized for gray-white matter contrast, with 1 mm thick sagittal slices and an in-plane resolution of 0.938 x 0.938 mm [191]. Cortical surface models were reconstructed using FreeSurfer software (v5.1) [126], and imported to SUMA [113].

Electrode Localization and Selection Criteria

A total of 1504 subdural electrodes were implanted (PMT Corporation; top-hat design; 3 mm diameter contact with cortex) using previously published techniques [83]. 286 electrodes were excluded due to proximity to seizure onset sites, inter-ictal spikes, or 60 Hz noise. SDEs were localized to cortical surface models using intra-operative photographs and an in-house recursive grid partitioning technique [109]. We then used both anatomical and functional criteria to identify all SDEs that were recording from early visual and face-selective inferior occipital and fusiform cortex.

To identify early visual cortex (EVC) electrodes, we first selected all SDEs localized over anatomically defined early visual regions (V1/V2/V3) on individually parcellated cortical maps [126, 261-263]. From these, we selected SDEs with response onset latencies less than 100 ms that also demonstrated equal or greater response for scramble compared to face stimuli [56, 123, 196, 198, 261, 264].

Occipital face area (OFA) electrodes were identified as SDEs showing face-selective responses, localized over the inferior occipital gyrus, lateral to the occipito-temporal sulcus and inferior to the lateral occipital sulcus [221, 227, 265, 266]. Fusiform face area (FFA) electrodes were identified as face-selective SDEs localized over fusiform cortex anterior to the posterior collateral sulcus, postero-medial to the occipito-temporal sulcus, and postero-lateral to the mid-fusiform sulcus [34, 44, 166].

Face-selectivity was defined as greater activation at an SDE for face stimuli compared with animate, inanimate, and scramble stimuli [34, 50, 171, 179, 181, 265]. We note here that non-invasive and intracranial neuroimaging provide substantial evidence to support the existence of multiple, distributed face-selective “areas” (or clusters/patches) in the human cortex [4, 267], and that the concept of a “single” FFA has been recently revised to consist of two smaller clusters - a middle and posterior face-selective fusiform cortex (termed mFus-faces and pFus-faces, respectively) [4]. Our goal here is to determine whether input from EVC reaches face-selective fusiform regions independently of the OFA. Therefore, we refer to any electrodes localized over either mFus or pFus-faces as an “FFA” electrode. The grouping of electrodes from these two fusiform regions is consistent with our goal, and provides a large enough sample size to enable meaningful analysis. We additionally took care to ensure that electrodes situated over pFus were not erroneously identified as OFA electrodes, again using

sulcal and anatomical boundaries from individually parcellated cortical surface models[33].

In the 10 subjects that participated in the visual naming tasks, 36 electrodes were localized over early visual cortex (EVC), OFA, or FFA. Of these, three subjects had concurrent EVC (11 SDEs), OFA (7 SDEs), and FFA (10 SDEs) coverage in the same individual. The remaining 7 subjects contributed an additional 8 FFA SDEs that were used in time-series and face-selectivity analyses. The last subject (no. 11) underwent cortico-cortical evoked potentials (CCEPs) and cortical stimulation mapping (CSM) recordings, but did not participate in the visual naming tasks. In this subject, EVC SDEs (n=4) were localized over the calcarine fissure (<2cm from occipital pole) [261, 263], while SDEs localized over the inferior occipital (n=3) and fusiform gyri (n=2) satisfied anatomical criteria for the OFA and FFA described above, and were determined to be face-selective by CSM (see Results: *Experiment 4 – Functional disruption through cortical stimulation mapping)* [83, 182, 184, 268-270]. Given that the cortical regions stimulated during CSM in subject 11 were not functionally classified as OFA and FFA, we refer to them here as OFA* and FFA*.

To visualize selected electrodes in a common reference space, we implemented a surface-based normalization strategy [80, 113] to map individual subject SDE coordinates to a standardized cortical surface (N27 brain). Due to individual anatomical variability, however, the group-level image may not accurately reflect the location of each SDE with respect to the native cortical surface.

Electrocorticographic (ECoG) Processing:

ECoG data were collected at 1000-2000 Hz using NeuroFax software (Nihon Kohden) or a NeuroPort NSP (Blackrock Microsystems) (Fig 1 a). ECoG data were visually inspected for inter-ictal epileptiform discharges and for electrical noise. For 6 subjects, ECoG data were collected at 1000 Hz using NeuroFax software (Nihon Kohden, Tokyo, Japan) (bandwidth 0.15-300 Hz). The other 4 subjects underwent ECoG data collection at 2000 Hz (bandwidth 0.1-750 Hz) using the NeuroPort recording system (Blackrock Microsystems, Salt Lake City, UT). Electrodes were referenced to a common average of all electrodes, except for those with 60 Hz noise or epileptiform activity when initially referenced to an artificial 0V [195]. All electrodes with greater than 10 dB of noise in the 60 Hz band were also excluded.

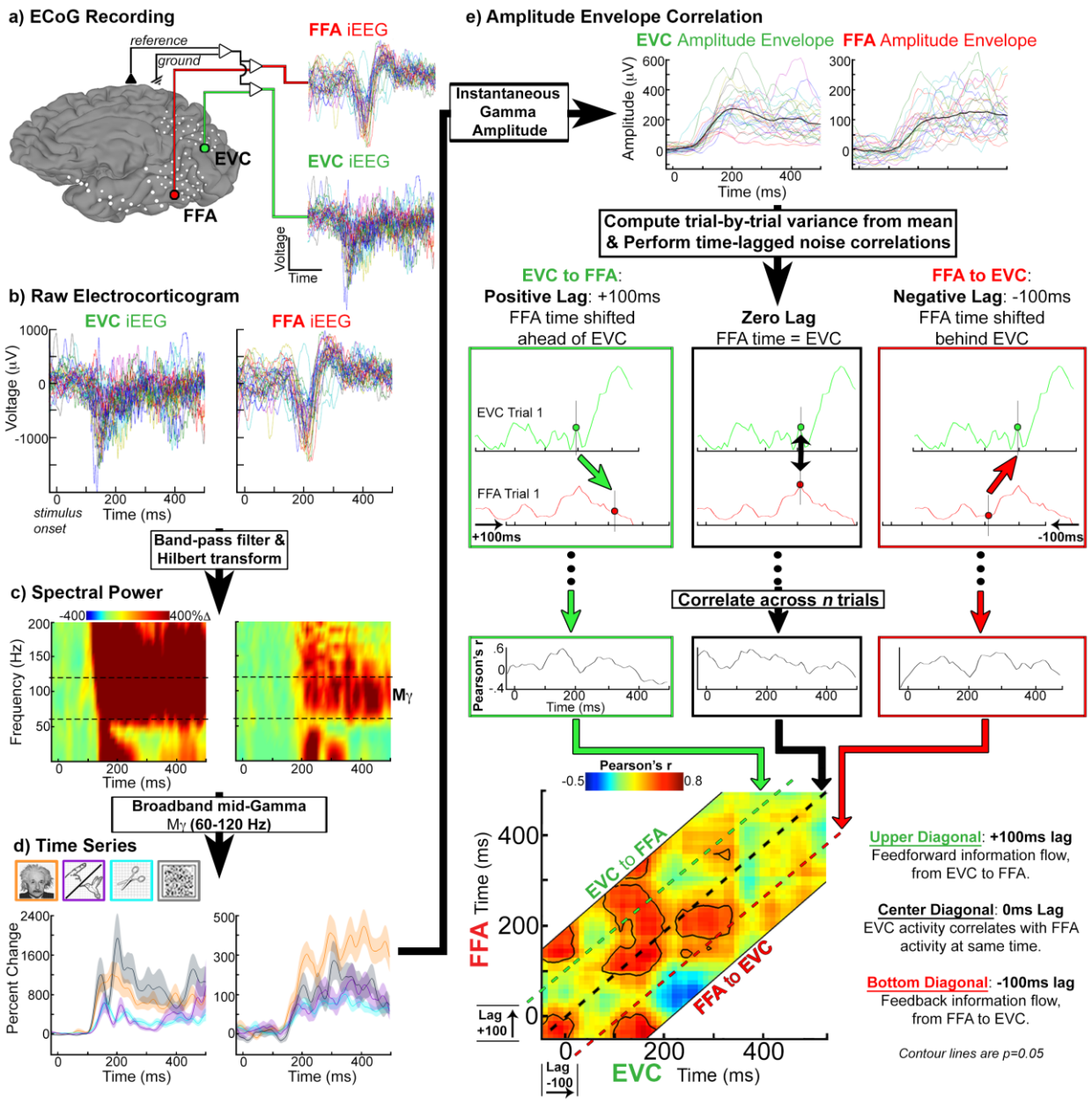

Figure IV-1. ECoG Spectral and Functional Connectivity Analyses

a) Subjects were implanted with subdural electrodes (SDEs) and electrocorticographic (ECoG) data recorded. SDEs recording from early visual cortex (EVC), the occipital face area (OFA), or the fusiform face area (FFA) were selected for further analysis. EVC (green) and FFA (red) electrode for a single subject are displayed.

b) Raw ECoG data from two SDEs: one in EVC and one in FFA. The N200 face-ERP can be seen in the FFA SDE.

c) To obtain spectral power, raw ECoG are band-pass filtered and Hilbert transformed. Mean percent power change (relative to pre-stimulus baseline; -700 to -200 ms) is visualized in time-frequency representations during perceptual processing (-50 to 500 ms; Stim onset at *t* = 0 ms; face stimuli only

shown). The broadband gamma frequency range (60 – 120 Hz) used throughout analyses is denoted by the dashed lines.

d) Time-series representation of mean broadband gamma power changes for faces (orange) vs. animate (purple) vs. inanimate (cyan) vs. scrambled (gray) stimuli. Shaded regions denote 1 SEM (*n*=30 trials per task).

e) Functional connectivity assessed using amplitude envelope correlations (AEC) between pairs of subject SDEs (face stimuli only). *(Top)* For each SDE, the instantaneous gamma amplitude envelope is obtained for every trial, and the average amplitude envelope (black trace*)* is subtracted to obtain trial-by-trial variance. *(Middle)* Noise correlations are performed across trials to compute connectivity between SDE pairs. To estimate information flow, correlations are computed at a zero time lag (black box), and repeated for both positive (green box) and negative (red box) lag values. (*Bottom*) Temporal cross-correlograms summarize connectivity across all time lags (-200 to +200 ms lags, 10 ms steps). Correlation coefficient values are plotted as a heat map. The black dashed line represents a lag of 0 ms. Above this line, EVC activity leads FFA (positive lag; information flow from EVC to the FFA), while below the dashed line FFA activity leads EVC (negative lag; information flow from FFA to EVC). Contours represent significant correlations (*p*=0.05, trial re-shuffling, 2000 resamples).

Experiment 1 – Face-Selectivity, Time Series Representation, and Movies:

Spectral analysis was performed by first bandpass filtering raw ECoG (Fig 1 b) data into the broadband gamma frequency range (Fig 1 c; 60-120 Hz; IIR Elliptical Filter, 30 dB sidelobe attenuation). A Hilbert transform was applied and the analytic amplitude was smoothed (Savitzky-Golay FIR, 5th order, frame length of 155 samples; Matlab 2013b, Mathworks, Natick, MA) to estimate the time course of broadband gamma power [97]. This broadband gamma frequency range was selected because it provides precise estimates of task-specific cortical activity [90, 148, 183, 196, 198, 199], is tightly linked to the global activity of local neural populations [102, 200-202], and strongly correlates with the BOLD signal [96, 102, 104, 106, 185, 203, 204].

Individual and grouped estimates of face-selectivity (faces > animate, inanimate, and scramble) were determined for EVC, OFA and FFA SDEs separately using a mixed-effects multi-level analysis (MEMA) of overall percent gamma power change across the analysis window (50 to 500 ms post stimulus onset; with respect to mean pre-stimulus baseline activity, -700 to -200 ms; false discovery rate corrected for multiple comparisons) [80, 97]. As previously described [80], MEMA uses both the effect estimate and precision estimate (within-subject variance) at each electrode per individual to provide an unbiased and statistically robust measure of grouped effects [119].

To determine relative onsets of gamma power and face-selective activity, a time-series representation of percent change in broadband power (n=30 trials per condition) was computed at each SDE for face, animate, inanimate, and scramble stimuli (Fig 1 d). The percent change at each time point was calculated by comparing power to mean pre-stimulus baseline activity (-700 to -200 ms). Grouped time-series for the EVC, OFA, and FFA were computed by averaging mean percent change from all electrodes in each functional zone [80, 97]. Gamma power onset was determined by the earliest time at which the percent change in gamma power significantly exceeded baseline levels using one-sided, non-parametric Wilcoxon sign-rank testing. Face-selectivity in OFA and FFA time-series was determined using two-sided, non-parametric Wilcoxon sign-rank testing for pairwise contrasts of gamma power differences between face and non-face stimuli (face vs. animate; faces vs. inanimate; face vs. scramble). Contrasts were repeated between animate, inanimate, and scramble stimuli to test whether any face-selective (i.e. domain-specific) activity observed also generalized to other animate stimuli (i.e.

domain-general) [271]. Comparisons were computed at each time point, and corrected using the false discovery rate (FDR) procedure for multiple comparisons [211].

Finally, in order to relate task-dependent changes in cortical activity to anatomical substrates of interest, we generated 4 dimensional representations of ECoG activity (Movie 1). Percent-change in broadband gamma activity (from mean baseline of -700 to -200 ms) were computed in 50 ms time bins, beginning 100 ms before stimulus onset and moving forward in 10 ms steps until 500 ms after stimulus onset (total of 61 bins). Using previously published techniques [80], surface-based ECoG representations were generated for each 50 ms bin, and then sequentially displayed on individual representations of lateral and ventral surfaces [113]. Importantly, by leveraging the high spatio-temporal resolution of ECoG, these movies enable the visualization of rapid task-dependent changes in cortical activity simultaneously across distributed cortical substrates, facilitating an intuitive insight into dynamical network behavior not readily appreciable through static images. However, we should clarify that these movies display unthresholded and uncorrected ECoG activity per subject. Therefore they are intended as visual aides, and not meant to supplant the results from our more rigorous, statistical analyses. In line with the focus of this dissertation, movies were only generated for ECoG data collected during face naming, and only in the 3 subjects with concurrent EVC, OFA, and FFA coverage. Movies for the other subjects and stimulus conditions were not generated because they do not provide essential insights into EVC-OFA-FFA network interactions during face-perception.

Experiment 2 - Amplitude Envelope Correlations (AEC):

A full description of network dynamics depends on both the patterns of cortical activation and the functional connectivity that underpins them [75, 272]. Traditional connectivity analyses that utilize phase relationships to study neural synchronization [273, 274] are poorly suited to asynchronous, high-frequency broadband activity [257, 258]. We therefore sought to categorize cortical interactions at higher frequency ranges using amplitude envelope correlations (AEC) (Fig 1 e), which circumvent such issues by computing coupling between power envelopes that are independent of phase [257, 275, 276].

For each SDE, ECoG data were initially filtered in the broadband gamma frequency band (60-120 Hz) using a square filter with sigmoid flanks (half amplitude roll off of 1.5 Hz), and subsequently Hilbert transformed. The amplitude envelope of each trial was smoothed using a moving average filter (100 ms) (Fig 1 e). The average across trials (n=30 per condition) was then subtracted from the amplitude envelope to obtain trial-by-trial variance for each SDE. Noise correlations between pairs of electrodes were computed using Pearson's correlation of the variance at each time point across trials. The low signal amplitude (2-5 microvolts in the 60-120 Hz band) in the gamma frequency range, together with the use of noise correlations, ensures that signal overlap and therefore spurious correlations between channels are unlikely [257, 258, 276, 277].

Given that connectivity between distant cortical regions may not be completely represented by instantaneous correlations (i.e. at zero time lag), we also calculated trial-by-trial correlations at more extended time lags. For each SDE pair, we lagged the time series on one channel prior to AEC, with a maximum lag of 200 ms. In this manner, AEC measures can estimate the directionality of information flow by

correlating activity in one region against activity in another region at an earlier or later point in time [276, 277]. Temporal cross-correlograms were used to summarize noise correlations calculated across all time lags between regions (Fig 1 e) [277]. Significance for AEC performed on individual subject SDE pairs was calculated using bootstrapping (p=0.05, trial re-shuffling, 2000 resamples using Matlab Parallel Computing Toolbox ver 6.1).

To achieve grouped estimates of connectivity, the SDEs localized in each region per individual (EVC, OFA, FFA) were used to generate a list of possible pairs between these regions. SDEs were selected only from the three subjects with concurrent coverage over the OFA (*n*=7 SDEs), FFA (n=10 SDEs), and EVC (*n*=11 SDEs). Analyses were carried out on a total of 25 EVC-OFA, 26 EVC-FFA, and 22 OFA-FFA SDE pairs. AEC results were computed at the individual level for all respective SDE pairs, transformed into a Fisher's z, averaged across subjects, and then assessed for significance using a two-sided, non-parametric Wilcoxon sign-rank test (*p*=0.01, FDR corrected for multiple comparisons).

Experiment 3 - Cortico-Cortical Evoked Potentials (CCEPs):

CCEPs can provide task independent and unbiased estimates of cortico-cortical connectivity [259, 278-280]. CCEPs were derived using bipolar stimulation of selected cortical regions (10 mA, 500 micro-second pulse width at 1 Hz for 50s) with a Grass Stimulator (Grass Technologies, West Warwick, RI USA) [279, 281]. Concurrent ECoG was collected at 1 kHz using NeuroFax software (Nihon Kohden). A subgroup of electrodes, located more than 2 cm from the stimulation site and with minimal stimulus artifact was used to generate an average reference. ECoG data were exported to Matlab, and time

locked to the beginning of each stimulus. Noisy trials containing inter-ictal epileptiform discharges or artifacts were excluded from further analysis. A high pass filter (10th order Chebyshev, 1 Hz cutoff, 30 dB side lobe attenuation) was applied to each channel to minimize the effects of voltage drift. Epochs were then averaged to derive the CCEP at each recording electrode.

Positive and negative deflections in the averaged CCEP response at each electrode were identified using an automated peak detection algorithm (in-house software) [279, 280]. Data within the first 8 ms were excluded to eliminate stimulation artifact. The first negative voltage deflection following the stimulus artifact was defined as an N1 response [259]. Only negative deflections within 40 ms of stimulus artifact were classified as N1 responses to minimize the influence of indirect connections. Channels with N1 peak amplitudes >1000 mV were excluded, as they likely reflected non-biological electrical transmission.

Experiment 4 - Cortical Stimulation Mapping (CSM):

Cortical stimulation mapping (CSM) was performed using constant current stimulation of adjacent pairs of electrodes with a Grass Stimulator [83]. Three second, 50 Hz trains of alternating polarity square-wave pulses (0.3 ms) were used. Stimulation intensity varied from a minimum of 2 mA to a maximum of 10 mA, in steps of 1 mA. During stimulation the patient was monitored for afterdischarges, dysnomia, and visual or somatic sensations.

It is important to clarify that CSM is dictated solely by clinical considerations for patient safety. Stimulation sessions can be exhausting, unsettling, and sometimes even upsetting to patients. Furthermore, results of CSM contribute significantly to

neurosurgical planning for cortical resection. As such, a primary goal is to localize essential language function with respect to pathological tissue as well as surrounding healthy cortex (i.e. eloquent cortex) [282, 283]. Therefore, CSM is performed under the strict guidance of the patient's neurologist, neurosurgeon, and neuropsychologist, while non-essential (i.e. non-clinical) personnel are kept to a minimum and testing for research purposes is severely limited. These limitations include the number of times a region may be stimulated, as well as the conditions under which stimulations are performed. Computer stimuli are rarely used, and during testing, patients are asked to describe perceptual changes they experience as they direct attention to environmental stimuli (e.g. people or objects in the room). Therefore, CSM reports are intrinsically limited by their subjective nature, but nonetheless, CSM has contributed immeasurably to our understanding of the human brain [83, 152, 230, 260, 270, 283-285].

Results

Behavioral results

Mean reactions times were 1771 ms (standard deviation, SD = 817 ms) for face naming, 1235 ms (SD = 415 ms) for inanimate naming, 1231 ms (SD = 373 ms) for animate naming, and 1152 ms (SD = 374 ms) for scramble naming. To focus on perceptual processes, all analyses were restricted to within 500 ms after stimulus onset[197].

Experiment 1- Face-selectivity and time-series analysis

The full list of MEMA effect sizes and statistics is shown in Table I. In summary, MEMA revealed no significant conditional differences across stimulus types in the EVC. In the OFA, MEMA revealed significant conditional differences between faces and all

other conditions, consistent with the face-selective nature of this region. Additionally it also revealed significant differences between animate vs. both inanimate and scramble stimuli [50]. In the larger FFA cohort (*n*=18 SDEs), MEMA revealed a significantly greater response to faces than all other conditions, consistent with the face-selective nature of this region. This finding was preserved when the analysis was repeated for the smaller FFA cohort (*n*=10 SDEs) using the three subjects with concurrent OFA and EVC coverage. No significant contrasts were observed for comparisons between animate, inanimate, or scramble conditions in either FFA cohort.

MEMA Contrast	Face vs Animate		Face vs Inanimate		Face vs Scramble		Animate vs Inanimate		Animate vs Scramble		Inanimate vs Scramble	
	p (FDR)	β (%Δ)	*p* (FDR)	β (%Δ)	*p* (FDR)	β (%Δ)	*p* (FDR)	β (%Δ)	*p* (FDR)	β (%Δ)	*p* (FDR)	β (%Δ)
EVC (*n*=11 SDEs)	0.423	-176	0.771	30.1	0.16	-193	0.372	65.6	0.154	-86	0.662	-175
OFA (*n*=7 SDEs)	0.015	169.7	0.015	263.5	0.015	293	0.0235	93.9	0.0124	137.9	0.23	20.8
FFA (*n*=10 SDEs)	0.014	248.7	0.014	254.6	0.0134	280.8	0.827	8.6	0.901	-9	0.767	-34
FFA (*n*=18 SDEs)	0.001	200.9	0.0005	222.5	0.0004	236.1	0.0894	24.4	0.869	2.6	0.232	-31

Table IV-1. Experiment 1 - Mixed-effects Multilevel Analysis of Face-selectivity

MEMA derived grouped effect-estimates (β, beta values) and statistics (*p*, FDR corrected for multiple comparisons) for conditional contrasts. Beta values denote difference in percent change of broadband gamma power (60-120 Hz) over the analysis window (50 to 500 ms after stimulus onset; percent change from mean pre-stimulus baseline of -700 to -200 ms). Rows are color-coded for SDEs from the three regions of interest: early visual cortex (EVC) in green, occipital face area (OFA) in blue, and fusiform face area (FFA) in red. FFA results are presented for the smaller cohort of 3 subjects (*n*=10 SDEs) with concurrent EVC, OFA, and FFA coverage, as well as for the full cohort of 10 subjects (*n*=18 SDEs) with FFA coverage. Face-selectivity (face > animate, inanimate, AND scramble stimuli) is noted in both the OFA and FFA. Notably, the OFA also demonstrates significant differences for animate vs. both inanimate and scramble stimuli.

On an individual basis (Fig 2) and across the group (Fig 3), time-series analyses revealed that peak percent change in gamma power was largest for SDEs over EVC, and decreased along a posterior-anterior gradient from OFA to FFA. Grouped time-series analysis (Fig 3) revealed that task-dependent increases in broadband gamma

power began earliest in EVC (~85 ms), followed by electrodes in the OFA and then FFA (~130 and ~140 ms, respectively). We note here that the millisecond temporal resolution afforded by ECoG does allow for precise estimates of latency [263]. In the individual ECoG movies, the parallel, distributed nature of this response manifests as a surge of broadband gamma activity across the lateral and ventral occipito-temporal cortices that is visible beginning ~100-130 ms (Movie 1).

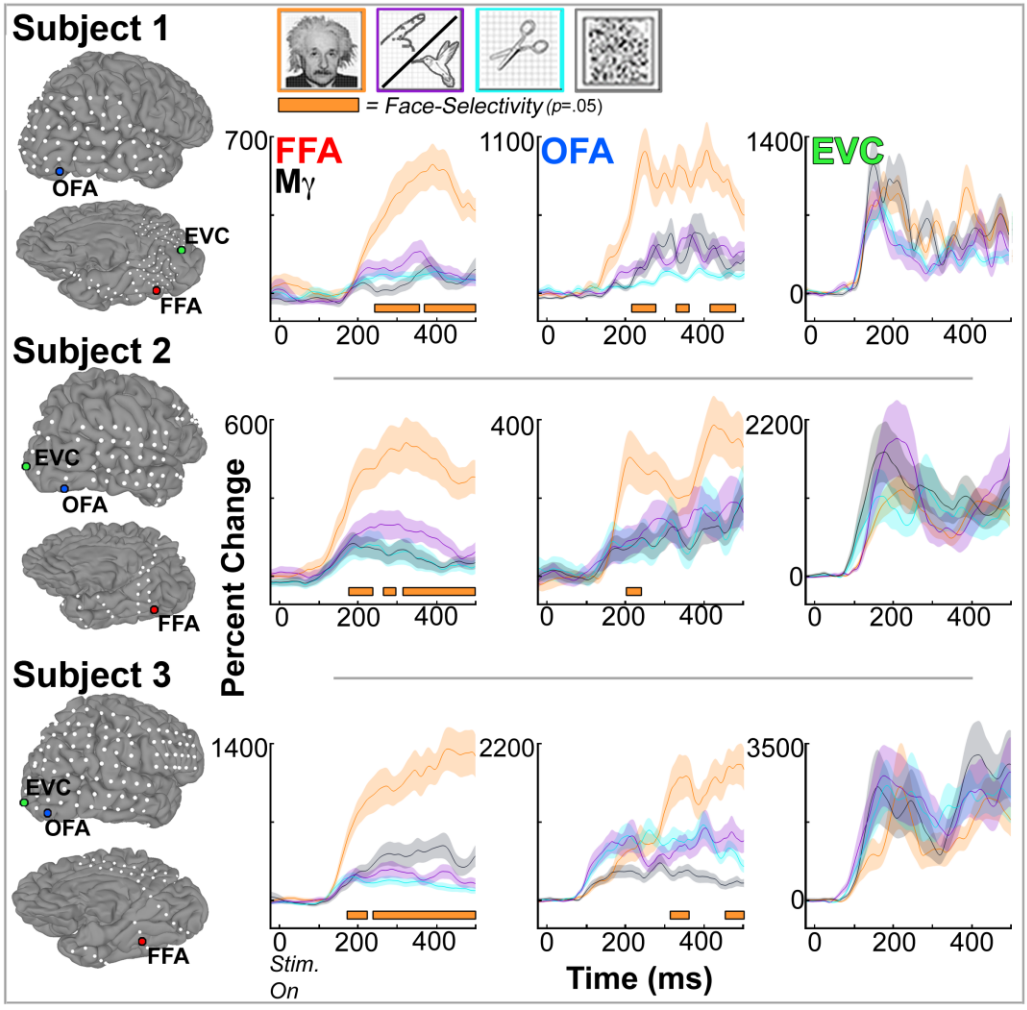

Figure IV-2. Single Subject Time-Series Analyses

Cortical surface models and subdural electrodes (SDEs - white spheres) are shown for the three subjects with coverage in all three regions of interest: early visual cortex (EVC, green), occipital face area (OFA, blue), and fusiform face area (FFA, red). Time-series representations of broadband gamma power changes (60-120 Hz) for faces (orange) vs. animate (purple) vs. inanimate (cyan) vs. scramble (gray) stimuli are shown for an SDE from each region per subject. Shadings denote 1 SEM (mean,

n=30 trials). Horizontal orange bars below each trace represent face-selectivity, defined as significantly greater percent change in gamma power for face vs. all non-face stimuli. Significance is *p*=0.05 (uncorrected) calculated using two-sided non-parametric Wilcoxon sign-rank testing for pairwise contrasts between each pair of conditions at each time-point.

Notably, earliest face-selectivity (faces >animate/inanimate/scramble) was observed in the FFA, beginning ~180 ms (p=0.01; Wilcoxon sign-rank, FDR corrected). In contrast, no face-selective activity was observed at any point in the OFA time-series (Fig 3). Despite the overall greater response to faces in OFA revealed by MEMA, the only significant differences in the OFA time-series were during the face-scramble contrast, also beginning ~180 ms (*p*=0.05; Wilcoxon sign-rank, FDR corrected). It might be conjectured that the absence of any face-selectivity in the OFA time-series was a result of the smaller sample size (*n*=7 SDEs), however the presence of a significant face vs. scramble contrast argues against this interpretation. Moreover in the FFA time-series, onset of face-selectivity remained unchanged following repeat analysis in the smaller FFA cohort (*n*=10 SDEs), demonstrating robustness of these contrasts with respect to sample size. Therefore, it is more likely that the absence of face-selectivity in the OFA time-series results from the obligate responses to salient, non-face stimuli (i.e. animate and inanimate), rather than low statistical power. These findings are supported by our MEMA results (Table I), which revealed a significantly greater OFA response to animate stimuli (vs. inanimate and scramble) in addition to face-selectivity. Importantly, this interpretation is consistent with prior fMRI studies that demonstrate earlier FFA face-sensitivity during dynamic visual stimulation [286], as well as the presence of both limb-selectivity and weaker face-selectivity in the OFA (with respect to face-selective

fusiform cortex) [33, 50]. No significant conditional contrasts were noted between animate, inanimate, and scramble stimuli at any point in the time-series analyses for any region.

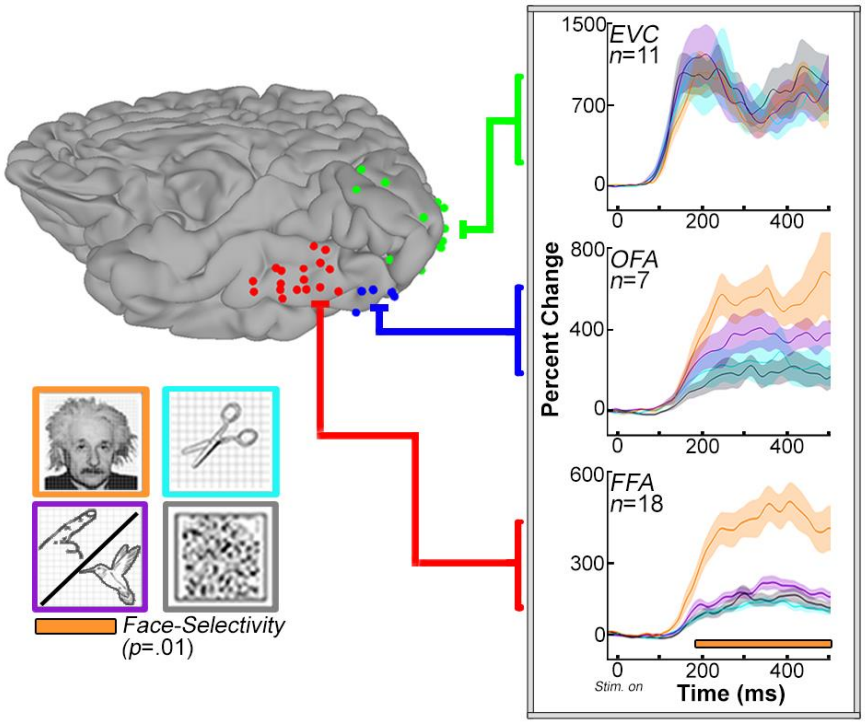

Figure IV-3. Grouped Time-Series Representations

(*Left*) SDEs from 10 subjects with recording sites over early visual cortex (EVC), occipital and/or fusiform face areas (OFA and FFA) co-localized onto a common brain surface (N27). Due to anatomical variability, the group-level representation may not accurately reflect the location of each SDE with respect to the native cortical surface. (*Right*) Group time-series representations of average broadband gamma power for faces (orange) vs. animate (purple) vs. inanimate (cyan) vs. scramble (gray) stimuli across SDEs per region (n=11 EVC; n=7 OFA; n=18 FFA). Shadings represent 1 SEM. Orange horizontal bars below traces denote presence of significant face-selectivity (faces vs. all non-face conditions, p=0.01, two-sided Wilcoxon signed-rank test, FDR corrected). Face-selectivity is only observed in the FFA beginning ~180 ms after stimulus onset. Absence of OFA face-selectivity was not due to low sample size, as FFA face-selectivity remained unchanged when analysis was repeated with only FFA SDEs (n=10) from the three subjects with concurrent OFA coverage.

Experiment 2 - Functional connectivity through amplitude envelope correlations (AEC):

All results observed at the group level were also notable in analyses performed between individual subject electrode pairs. Unless mentioned otherwise, all connectivity measures were tested at a significance level of p=0.01 using two-sided, non-parametric Wilcoxon sign-rank testing with FDR correction for multiple comparisons. In the three subjects with EVC, OFA, and FFA coverage, AEC was performed on a total of 25 EVC-OFA, 26 EVC-FFA, and 22 OFA-FFA SDE pairs. Positive unidirectional correlations identified using the AEC method are depicted using a symbol "⇒" that indicates the direction of presumed information flow. Bidirectional correlations are represented by the "⇔" symbol.

Connectivity during face stimuli:

In the pre-stimulus state, significant positive correlations were noted between all three regions. After stimulus onset, EVC⇒OFA connectivity was lost (Fig 4 a), whereas significant feed-forward EVC⇒FFA connectivity continued until ~70 ms, after which it was also lost briefly (Fig 4 b). At ~80 ms, feed-forward correlations re-emerged between the EVC⇒FFA, and rapidly became bidirectional. This was followed shortly after by feed-forward correlations EVC⇒OFA beginning ~100 ms. Significant connectivity between EVC and FFA ended by ~300 ms, followed by EVC⇒OFA connectivity (~380 ms). Both of these latencies are within the average saccade time [183, 287]. Notably, early (<100 ms) EVC⇒FFA connectivity is consistent with reports of predictive coding and expectation bias in higher visual cortex that facilitate perceptual processing of preferred stimuli [241, 288-290].

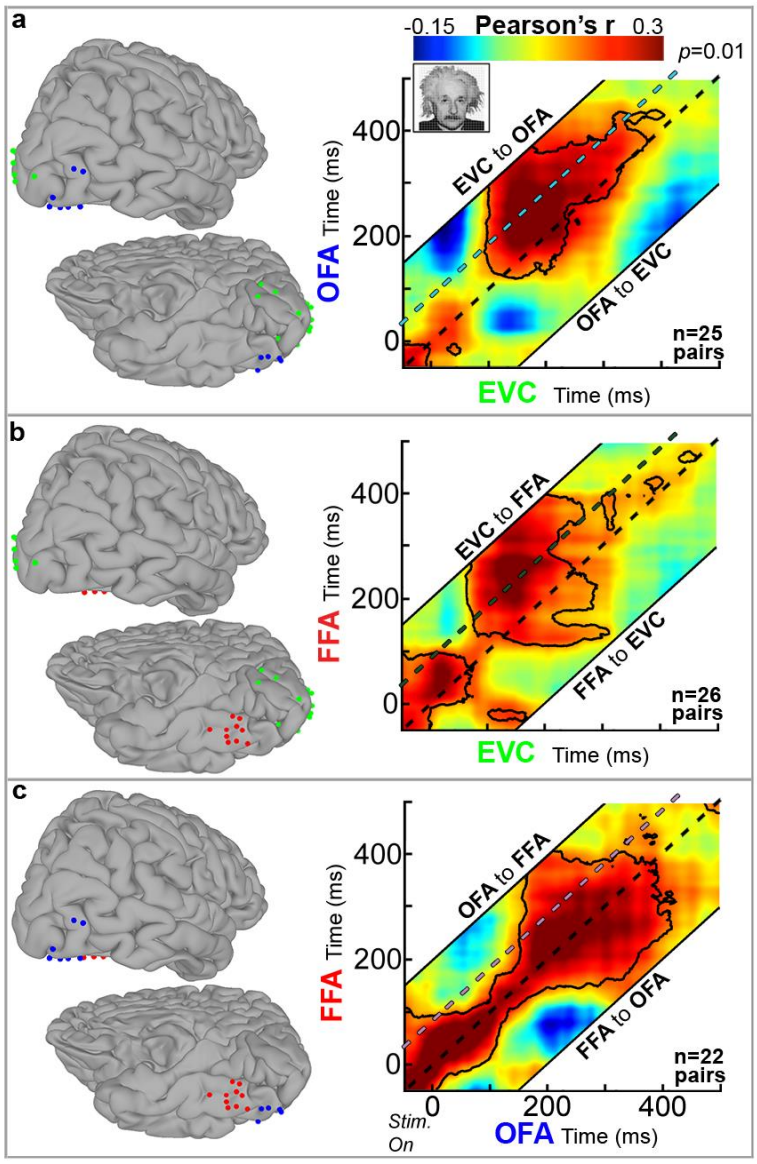

Figure IV-4. Grouped Functional Connectivity: Faces

a) Group temporal cross correlograms of EVC-OFA connectivity computed by averaging individual amplitude envelope correlations (AEC) (*n*=25 total pairs of SDEs, contours denote significant connectivity, *p*=0.01, two-sided Wilcoxon signed-rank test, FDR corrected) for face stimuli only. AEC is measured across lag ranges of -200 to +200 ms. The black dashed diagonal line represents a lag of 0 ms. Above the dashed line activity in EVC activity leads OFA (information flow from EVC to the OFA), while below the dashed line OFA activity leads EVC (information flow from OFA to EVC). Colored dashed lines identify the correlation coefficient values for a single feed-forward lag (+100 ms) plotted in Figure 5.

b) Connectivity between EVC and the FFA (*n*=26 SDE pairs). Onset of EVC-FFA connectivity is the earliest to appear between all regions.

c) Connectivity between OFA and FFA (*n*=22 SDE pairs).

Between the OFA and FFA, strong positive bidirectional correlations were also present at baseline. OFA⇔FFA connectivity was mostly unaltered for the first ~150 ms, after which connectivity became more robust bidirectionally (Fig 4 c). Significant OFA⇔FFA connectivity ended ~400 ms. Critically, the onset of feed-forward EVC⇒FFA connectivity significantly preceded OFA⇔FFA connectivity by ~70 ms (*p*=0.01, Wilcoxon rank-sum test, FDR corrected). The time-course of connectivity between these regions, as well as their time-series for face stimuli, is summarized in Fig 5 at a single positive lag value (+100 ms).

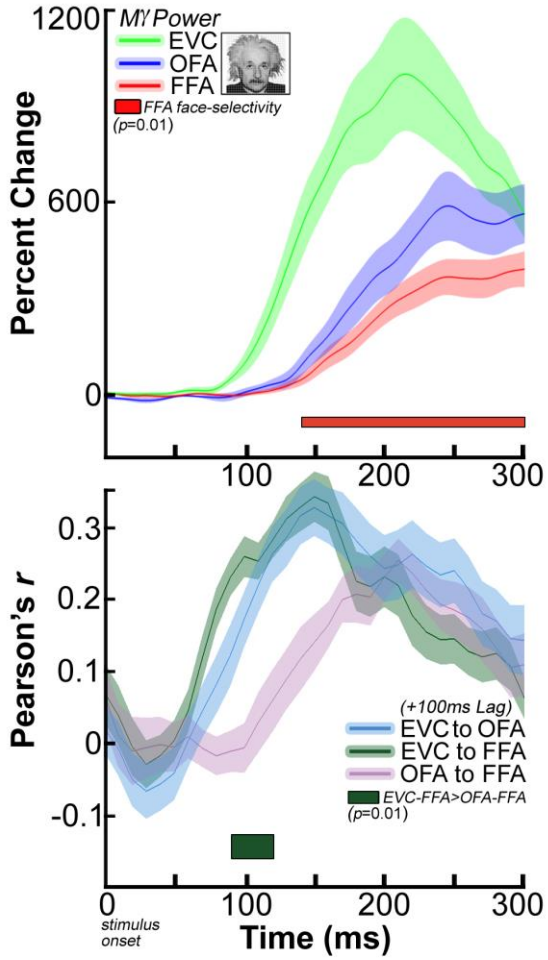

Figure IV-5. Summary Time-Series and Connectivity: Faces

a) Summary time-series representation for mean percent change in broadband gamma power across all SDEs per region of interest from Figure 3, face stimuli

only (0 to 300 ms; t=0, stimulus onset; shading denotes 1 SEM). Red horizontal bar below traces denote presence of significant FFA face-selectivity (faces vs. all non-face conditions, *p*=0.01, two-sided Wilcoxon signed-rank test, FDR corrected). Only FFA demonstrated face-selectivity during this period.

b) Feed-forward connectivity between all three regions for face-stimuli only (0-300 ms). Each trace plots change in correlation coefficient values between each pair of regions from Figure 5 for a positive lag of 100 ms (Denoted by dashed color lines offset from diagonal in Figures 5a-c; mean across group ± 1SEM). Horizontal bar below traces denotes significant EVC-FFA vs. EVC-OFA contrast (p=0.01, Wilcoxon rank-sum test, FDR corrected). There were no other significant regional differences.

Connectivity during non-face stimuli:

Overall, functional connectivity was much weaker during perceptual processing of animate and scrambled stimuli, while no significant connectivity was observed between any of these three regions for inanimate stimuli (Fig 6 a-c, *center*).

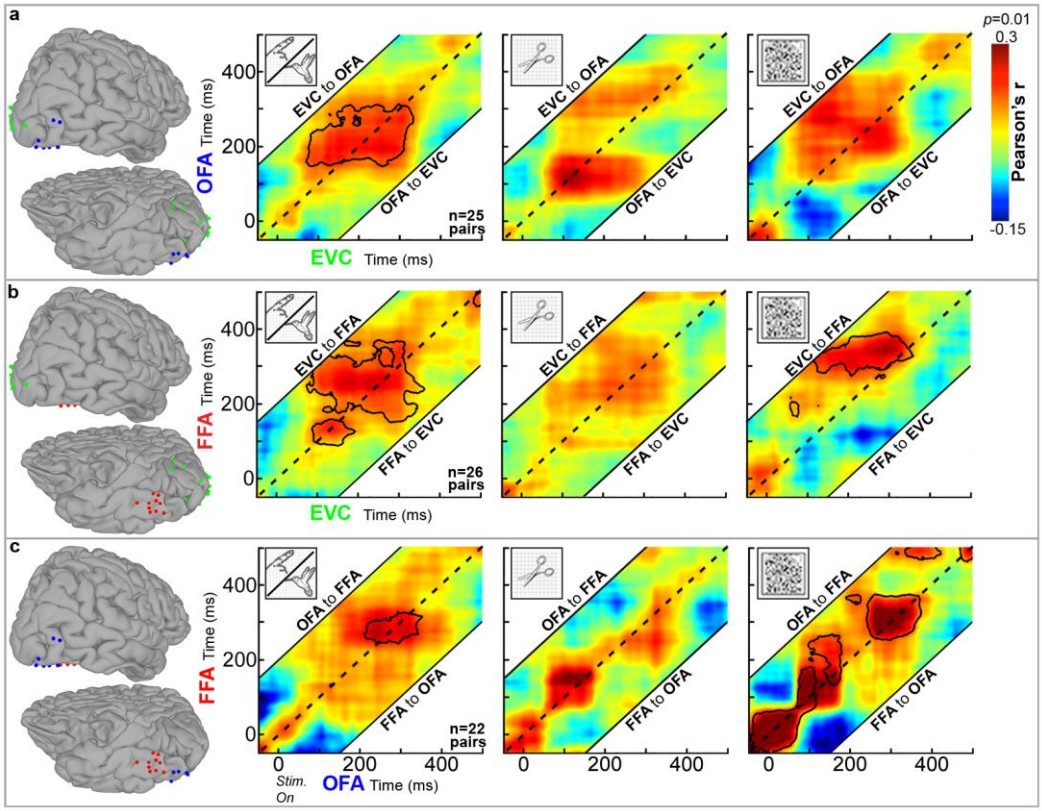

Figure IV-6. Grouped Functional Connectivity: Non-Face Stimuli

a) Group temporal cross correlograms of EVC-OFA connectivity for animate (*left)*, inanimate (*middle),* and scrambled (*right*) stimuli (*n*=25 total pairs of SDEs, contours denote significant connectivity, *p*=0.01, two-sided Wilcoxon signed-rank test, FDR corrected).

b) Connectivity between EVC and the FFA (*n*=26 SDE pairs).

c) Connectivity between OFA and the FFA (*n*=22 pairs).

For animate stimuli, no early (<100 ms) connectivity was observed between any of the three regions (Fig 6 a-c, *left)*. Significant positive correlations were observed between both EVC⇔FFA and EVC⇔OFA, beginning ~100 ms and subsequently ending by ~350 ms. Between the OFA⇔FFA, brief connectivity was observed from ~250 ms to ~350 ms.

For scramble stimuli (Fig 6 a-c, *right*), no significant connectivity between EVC⇔OFA was observed, while weakly significant correlations were observed from EVC⇒FFA beginning ~200 ms. Between OFA⇔FFA, significant positive baseline correlations were observed for scrambled stimuli, which persisted until ~200 ms after stimulus onset. A subsequent period of brief OFA⇔FFA connectivity re-emerged from ~250 ms to ~350 ms. We note here that the observed patterns of OFA⇔FFA connectivity for scrambled stimuli are consistent with prior fMRI studies that have shown the OFA and FFA to be strongly correlated during rest, and this correlation modulated in a category-specific manner during perceptual tasks [291-293].

Experiment 3 – Structural connectivity through cortico-cortical evoked potentials (CCEPs):

Of the three subjects included in the AEC analysis, two also underwent CCEP recordings during FFA stimulation (subjects 1 and 2). An additional participant (subject 11), who did not undergo ECoG recordings during face naming, was included in this study because he did undergo CCEP stimulation at FFA and EVC electrodes, and also underwent CSM at both the OFA and FFA electrodes.

CCEPs recorded during FFA stimulation in these three subjects revealed distributed N1 responses across much of the ventro-temporal occipital cortex (Fig 7 a). The shortest response latencies were identified in electrodes over early visual and inferior occipital cortex, indicative of direct connectivity between the FFA and these regions [278, 279, 294]. Stimulation of EVC electrodes in subject 11 produced short latency CCEP responses in the FFA and OFA (Fig 7 b).

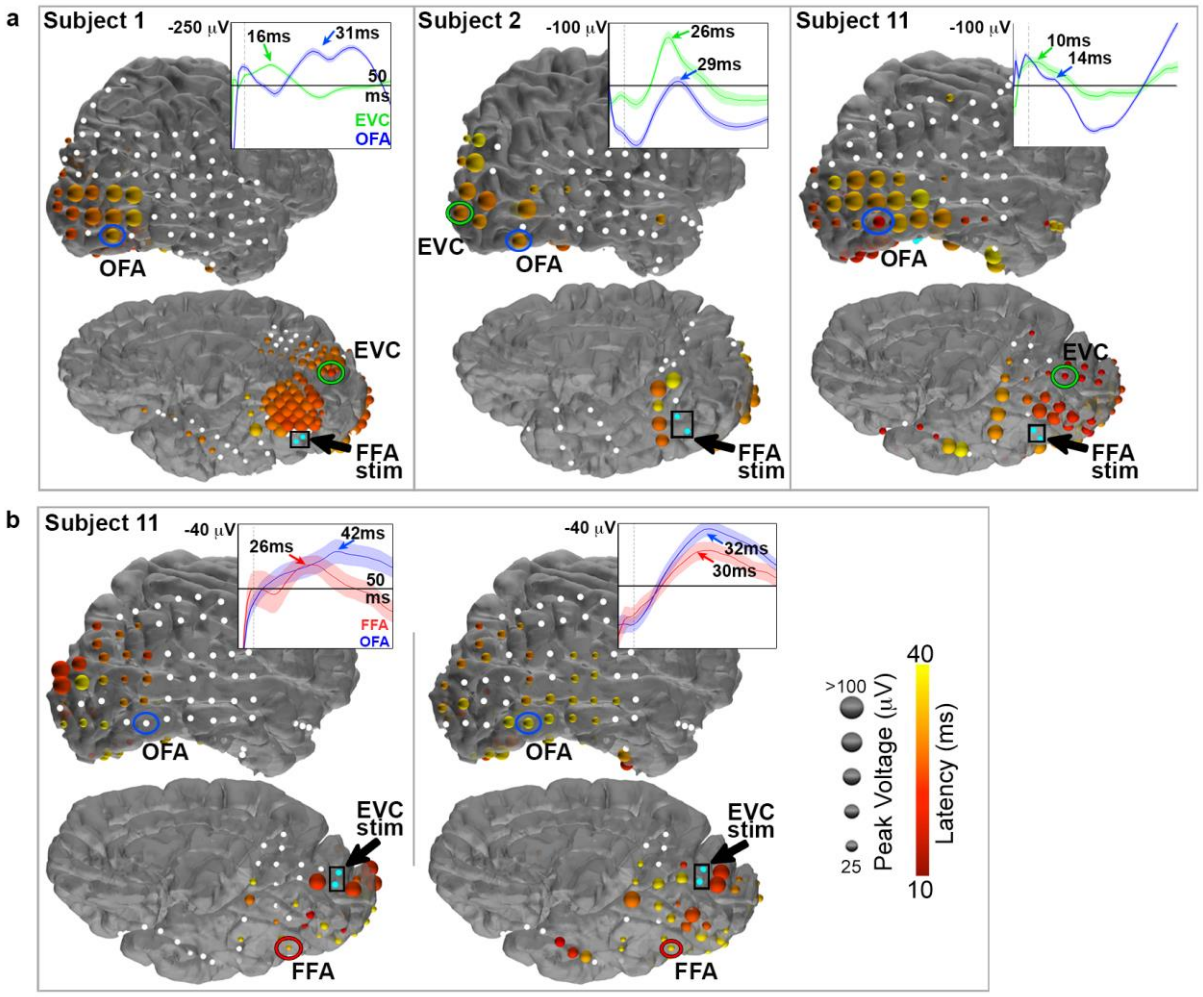

Figure IV-7. Individual Structural Connectivity

a) Cortico-cortical evoked potentials (CCEPs) in three subjects visualized on cortical surface models. Cyan electrodes denote stimulation pairs (bipolar pulses; 10 mA, 500 micro-second pulse width; 1 Hz for 50s). Amplitude (radius of electrode) and latency (color) of the N1 responses are represented. Distributed N1 responses are observed across ventro-temporal occipital cortex, with shortest response latencies in electrodes over early visual and inferior occipital regions. Electrodes without CCEP responses are white spheres. Representative CCEPs are shown for the encircled OFA and EVC electrodes (*insets*). Shadings represent 1 SEM (mean, *n*=50 trials)

b) CCEPs recorded with stimulation of two pairs of EVC electrodes in a single subject (no. 11). N1 responses for the encircled FFA and OFA electrodes in this subject are displayed (*insets)*.

Experiment 4 – Functional disruption through cortical stimulation mapping (CSM):

CSM of electrodes over EVC (subjects 1 and 11) and of the OFA (subjects 1 and 2) consistently produced elementary and intermediary visual hallucinations, respectively (i.e. phosphenes and geometric forms; Fig 8) [262, 263, 268, 285, 295-298].

CSM in subject 11 performed in electrodes situated over the OFA* and the FFA* produced unique, complex perceptual disturbances. Stimulation of OFA* electrodes consistently produced a visual distortion involving a focal region of the experimenter's face. The subject reported "*There is something on your forehead."* On further questioning, the subject elaborated, "*Something is moving on your forehead"*, while simultaneously tracing curved lines in the air in front of him with his hands. Upon stimulation of an adjacent pair of OFA* electrodes, the subject saw, "*An empty space on your cheek.*" When the experimenter held a pen up to the spot, the subject reported that the pen disappeared along with the cheek. Importantly, during stimulation at either pairs of OFA* SDEs, the subject did not report a visual disturbance of the experimenter's entire face, but consistently of only a portion of the experimenter's face (Fig 8, bottom). The focal nature of these visual disturbances is consistent with the smaller receptive field size of this region [56, 235, 299].

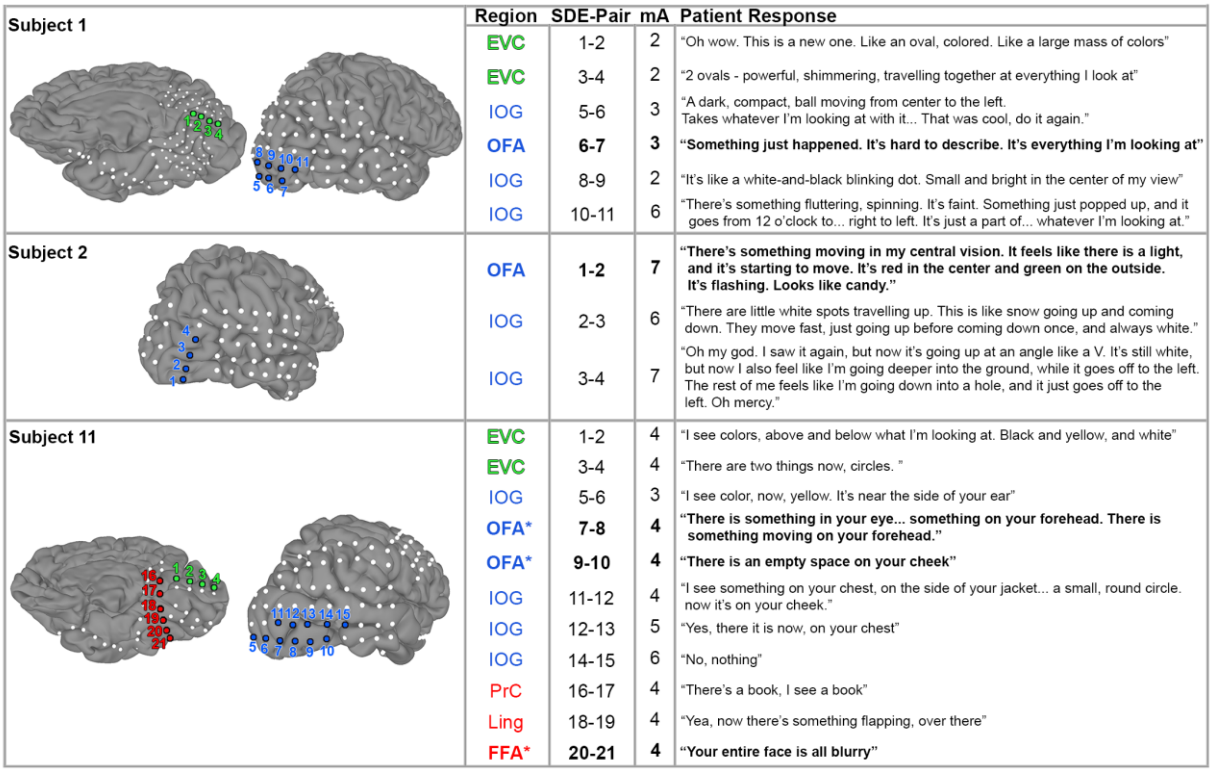

Region	SDE-Pair	mA	Patient Response
EVC	1-2	2	"Oh wow. This is a new one. Like an oval, colored. Like a large mass of colors"
EVC	3-4	2	"2 ovals - powerful, shimmering, travelling together at everything I look at"
IOG	5-6	3	"A dark, compact, ball moving from center to the left. Takes whatever I'm looking at with it... That was cool, do it again."
OFA	**6-7**	**3**	**"Something just happened. It's hard to describe. It's everything I'm looking at"**
IOG	8-9	2	"It's like a white-and-black blinking dot. Small and bright in the center of my view"
IOG	10-11	6	"There's something fluttering, spinning. It's faint. Something just popped up, and it goes from 12 o'clock to... right to left. It's just a part of... whatever I'm looking at."
OFA	**1-2**	**7**	**"There's something moving in my central vision. It feels like there is a light, and it's starting to move. It's red in the center and green on the outside. It's flashing. Looks like candy."**
IOG	2-3	6	"There are little white spots travelling up. This is like snow going up and coming down. They move fast, just going up before coming down once, and always white."
IOG	3-4	7	"Oh my god. I saw it again, but now it's going up at an angle like a V. It's still white, but now I also feel like I'm going deeper into the ground, while it goes off to the left. The rest of me feels like I'm going down into a hole, and it just goes off to the left. Oh mercy."
EVC	1-2	4	"I see colors, above and below what I'm looking at. Black and yellow, and white"
EVC	3-4	4	"There are two things now, circles. "
IOG	5-6	3	"I see color, now, yellow. It's near the side of your ear"
OFA*	**7-8**	**4**	**"There is something in your eye... something on your forehead. There is something moving on your forehead."**
OFA*	**9-10**	**4**	**"There is an empty space on your cheek"**
IOG	11-12	4	"I see something on your chest, on the side of your jacket... a small, round circle. now it's on your cheek."
IOG	12-13	5	"Yes, there it is now, on your chest"
IOG	14-15	6	"No, nothing"
PrC	16-17	4	"There's a book, I see a book"
Ling	18-19	4	"Yea, now there's something flapping, over there"
FFA*	**20-21**	**4**	**"Your entire face is all blurry"**

Figure IV-8. Individual Cortical Stimulation Mapping

Stimulated subdural electrode (SDE)-pairs, the current (mA) at which perceptual effects were evoked, and subject descriptions are presented for the three subjects that underwent CSM. (*Top)* Cortical stimulation mapping (CSM) of the OFA in this subject produced intermediary visual hallucinations (10mA; 3s, 50 Hz trains; alternating polarity square-wave pulses, 0.3 ms). (*Middle)* CSM in this subject's OFA also produced low-level visual hallucinations. (*Bottom)* CSM of the OFA* resulted in focal face-perception disturbances in specific portions of the experimenters face. In contrast, CSM of the FFA* produced a complete perceptual distortion of the experimenter's face. *EVC* – early visual cortex; *IOG* – inferior occipital gyrus; *OFA* – occipital face area; *PrC* – Precuneus; *Ling* – Lingual gyrus; *FFA* – fusiform face area. * denotes regions determined to be face-selective through CSM alone (i.e. no ECoG data).

CSM performed in SDEs adjacent to subject 11's OFA* SDEs produced additional intermediate and high-level visual disturbances that involved portions of the experimenter's body, as well as in one instance his cheek (Fig 8). These disturbances were also focal and confined to the subject's central visual field, and are consistent with reports of sparsely distributed and alternating face- and body-part specific functional

clusters in the inferior occipital gyrus [33, 166]. Importantly, despite the large portions of inferior occipital cortex mapped in subject 11 (almost in its entirety), no complete disruptions to face-perception were reported [300].

In contrast, CSM performed in FFA* electrodes for subject 11 evoked an abrupt visual distortion of the entire experimenter's face (Fig 8). The subject reported, "*Your entire face is all blurry."* On repeat stimulation, the subject was asked if the entire face was "*nice and blurry*", to which he replied, "*Yes"*. The subject did not report visual disturbances to anything other than the experimenter's face. Stimulation in adjacent SDEs produced other intermediate and high-level visual disturbances that did not involve face-perception. This confirmed the unique-face-related perceptual distortions evoked during FFA* stimulation were a result of disruption to face-sensitive fusiform cortex.

It is important to mention that ideally functional imaging and electrophysiology data would be collected in every subject that also receives CSM of functionally defined cortical regions (e.g. OFA and FFA). However, strict clinical limitations do not always permit the opportunity to do so. Nevertheless, while recent studies have demonstrated that electrophysiological and functional imaging data complement direct electrical stimulation [301, 302], CSM remains the gold standard for pre-resection localization of eloquent cortex in these subjects [83, 283]. Importantly, in the most complete CSM study of face perception to date [270], only 2 of the 5 patients had perfect concordance of functionally defined FFA (ECoG) and CSM evoked face-distortions. Of the 3 remaining subjects, one did not receive ECoG testing and two had double dissociations between ECoG face-selectivity and stimulation-evoked face distortions [270]. Therefore, while

CSM at an electrode over functionally localized OFA/FFA may be highly correlated with the production of face-specific distortions, it is not assured.

Conclusions

Our work suggests that the feed-forward model (FFM) of face perception is likely incorrect based on four distinct findings during a face-naming task: (1) onset of face selective responses in the FFA occur prior to the OFA; (2) EVC⇒FFA functional connectivity precedes OFA⇒FFA connectivity; (3) independent EVC⇒FFA structural connectivity; and (4) complete distortions of face-perception during FFA* CSM, but only focal face-distortions during OFA* CSM within the same individual. Together, these findings are more consistent with Non-Hierarchical Model (NHM) interpretations of face perception [74].

Parallel, distributed information flow to the core face network

Given the OFA's posterior location, the FFM has implicitly assumed that EVC input is first delivered to the OFA, which initiates a parts-based face analysis prior to relaying information to the FFA [40, 49]. The OFA is therefore predicted to exhibit earliest face-selectivity [266]. However, although our comparisons of ECoG activity integrated over the epoch reveal OFA and FFA face-selectivity, our time-series analyses contradict this FFM prediction. Specifically, robust dissociations between face and non-face stimuli are only visible in the FFA, beginning ~180 ms after stimulus onset (Fig 5 a). In contrast, the OFA exhibits comparable responses to salient stimuli that preclude face-selectivity at any given time point [33, 50]. Moreover, the only significant conditional contrast observed in the OFA time-series (scrambled images) does not precede but coincides with face-selectivity onset in the FFA (~180 ms). Finally, the increases in

broadband gamma power across the occipito-temporal cortex (~130-140 ms; Movie 1) provide compelling visual evidence against the FFA's dependency on OFA input to initiate activity. In sum, these findings do not support OFA face-detection prior to downstream FFA processing. Instead, our results suggest that during visual naming input to these two regions occurs independently and in parallel [303], and that face-selectivity in the FFA precedes the OFA [286].

The Fusiform Face Area detects faces and initiates face processing

The NHM posits that the FFA, not the OFA, detects faces through coarse, global stimulus configuration (holistic processing) via direct inputs from EVC [72, 304]. In a coarse-to-fine manner, reentrant OFA-FFA interactions then progressively refine facial representations to facilitate individuation [74]. While our time-series analyses support an earlier face-sensitivity in the FFA, an elaboration of the functional connectivity between these regions was crucial to validate NHM predictions. Critically, AEC revealed feed-forward EVC⇒FFA connectivity prior to the onset of bidirectional OFA⇔FFA connectivity (Fig 5 b). This finding stands in stark contrast to FFM predictions, and provides novel empirical evidence of EVC⇒FFA input independent of the OFA [42, 305]. The early (<100 ms) and face-selective nature of EVC⇒FFA connectivity, together with its absence between EVC⇒OFA, furthermore supports NHM predictions regarding the FFA's role in face-detection. Given the timing (<100 ms) at which early EVC⇒FFA connectivity begins, if face-detection is mediated through these early interactions, it likely reflects an automatic process prior to conscious perception [206, 306-311].

Notably, changes in EVC activity appear to mediate task-related processes in the other two core face regions. Specifically, a break in EVC⇒FFA connectivity

(~70ms) occurs prior to EVC broadband gamma onset (~85 ms), while the reemergence of EVC⇒FFA connectivity and the onset of EVC⇒OFA connectivity (~80 & ~100 ms, respectively) both precede broadband gamma onsets in the FFA and OFA (~140 & ~130 ms, respectively). Importantly, the intense, task-dependent onset in broadband gamma activity is believed to reflect a rapid and large increase in regional neural activity, which mediates higher-level face processing and is coupled to perceptual awareness [179, 196, 198, 201, 254]. Taken together, these results would then implicate EVC input as the match that "ignites" perceptual face processing in these core face-regions [196]. Similarly, the onset of OFA⇔FFA connectivity (~150 ms) precedes both FFA face-selectivity (~180 ms) and the significant face vs. scramble contrast in the OFA time-series (~180 ms). The (relatively) later onsets and bidirectional nature of OFA⇔FFA connectivity are consistent with NHM predictions of reentrant OFA-FFA interactions mediating higher-level face processing through feature refinement [74, 223, 312].

Structural connectivity between EVC and the core face network

Given that individual subject electrode placement is both sparse and variable, connectivity between EVC and the OFA and FFA might reflect interactions from unrecorded neural substrates (i.e. hidden/common-source correlations). We therefore used cortico-cortical evoked potentials (CCEPs) - a task-independent measure of structural connectivity - to validate our results. The demonstration of short-latency, bidirectional N1 responses between these three regions confirms the existence of independent connections that mediate rapid, parallel information flow [278, 279]. These results are further supported by recent tractography studies demonstrating direct white-matter connections between EVC and the FFA [60, 62, 249, 305, 313, 314].

Stimulation of FFA, but not OFA, disrupts face perception

In our final experiment, we transiently impair OFA and FFA function using high-frequency cortical stimulation mapping (CSM). Assuming feed-forward mechanisms described by the FFM, stimulation of the OFA would disrupt all stages of face processing, while FFA stimulation would disrupt just the later stages (i.e. individuation) [300].

Currently, the existent literature on OFA CSM is entirely derived from a single subject [182, 268, 269]. However, both studies on this patient demonstrated a clear disruption only to ***individuation*** in contrast to FFM predictions. Similarly, non-invasive TMS studies of OFA stimulation have reported reduced accuracy rates during *individuation* tasks, but not basic-level face categorization [300, 315]. In contrast, prior studies of FFA stimulation have consistently disrupted the earliest-stages of face perception [152, 184, 230, 270, 284, 316, 317].

To the best of our knowledge, no study has ever reported the effects of CSM in a subject with simultaneous OFA and FFA coverage. This is important, given the close approximation of OFA and FFA, to confirm that the behavioral effects of CSM in one region do not occur because of current spread to the other [184]. Here, we demonstrate that within the same subject, while OFA* stimulation produced focal perceptual disturbances of the experimenter's face, FFA* stimulation induced a complete perceptual loss (i.e. blurring) of the entire experimenter's face (and nothing else). In our remaining two subjects OFA stimulation failed to evoke anything other than intermediary visual hallucinations. When taken into consideration with the findings from our other three experiments, the differential CSM effects reported here provide strong

causal support to implicate the cortical substrates in fusiform, but not inferior occipital cortex as the neural circuitry most critical to face-perception [269, 270].

In summary, we integrate measures of cortical activation, connectivity, and functional disruption to demonstrate that the neural mechanisms that underpin face perception cannot be adequately explained by the current FFM. Rather, the core face-network appears to operate in a parallel, distributed manner much more in line with NHM predictions [74].

Inherent limitations of invasive studies in humans - small subject numbers, sites of electrode placements and stimulation parameters determined by clinical rather than research criteria - preclude a more comprehensive validation of the NHM. Furthermore, our results may not be relevant beyond the visual naming paradigm that we have tested, as face processing involves complex interactions across many more cortical regions than the three investigated here. However, our findings do generate specific predictions regarding the timing and regional interactions of critical stages of face-perception, which can be validated through chronometric [318] or real-time stimulation by future studies causally evaluating the NHM mechanisms implicated here.

Our results add to a growing body of literature that implicate higher visual areas as active participants in object processing [209, 303, 319, 320], consistent with predictive coding, reverse-hierarchical, and top-down interpretations of visual recognition [66, 71, 321-323]. Our findings also highlight the need to critically evaluate existing and future cognitive network models using both cortical activity and inter-areal connectivity captured at sufficient spatio-temporal resolution. Improvements in our ability to accurately model cognitive function will have important implications for understanding

and developing treatments for disease states, such as prosopagnosia [324], that arise from the disruption of these complex networks.

Summary

Understanding the neural mechanisms that govern face perception is a major focus of cognitive neuroscience. Prevailing theory suggests that cortical face networks operate in a feed-forward, hierarchical manner. Here, we utilize invasive human electrophysiology to test face-processing model predictions via measurements of cortical activation, functional connectivity, and disruption through electrical stimulation. We demonstrate that during a face-naming task, onset of face-selective responses in the Fusiform Face Area (FFA) occur prior to the Occipital Face Area (OFA). Furthermore, functional coupling between early visual cortex (EVC) and the FFA appears prior to OFA-FFA connectivity, and electrophysiological connectivity reveals direct cortico-cortical connections between EVC and FFA. Finally, direct disruption of the FFA, but not the OFA, produces complete impairment of face perception. These findings are incompatible with the traditional feed-forward model of face processing. They instead support arguments for the existence of a parallel, distributed network underlying face perception, and a critical role for the FFA in face detection.

Chapter V: Conclusions and Future Directions

Visual object recognition is mediated by a dynamic cortical network, whose successful function is fundamental to our survival. After decades of study, putative regions that may serve category-specific visual functions, such as the recognition of faces, places, and tools, have just begun to be identified. However, debate continues over the exact location of these regions and the nature of information flow between them. These issues remain unresolved due to a lack of appropriate animal models, as well as the poor spatio-temporal resolution of non-invasive imaging modalities (e.g. fMRI and scalp EEG). Our lack of knowledge in these matters has precluded the formation of effective strategies for modeling and treating injuries to these regions, which produce debilitating diseases, such as agnosia (e.g. face-blindness), that may have devastating impacts on social, vocational, and professional life.

The goal of this research project has been to address two outstanding questions in the field of object recognition: a) what is the functional organization of category-specific regions within higher-level visual cortex and b) whether the networks they form operate in a feed-forward, hierarchical or parallel, distributed fashion. To address these questions, we studied high spatiotemporal resolution intracranial EEG data, which was collected across a large cohort of patients (n=42) as they performed the visual naming of five ecologically relevant object categories: faces, animate non-faces (i.e. animate), tools, places, and words.

To relate electrophysiological activity to its underlying cortical sources, icEEG data are often depicted on 3D models of individual brain surfaces. However, current techniques to spatially represent icEEG data have been unable to overcome difficulties resulting from the brain's complex folding patterns (i.e. inverse problem). A more serious challenge arises with respect to inter-subject comparisons. Due to the discrete

nature of SDE placement, single-subject recordings cannot sample from all cortical regions of interest (i.e. sparse-sampling), necessitating the combination of datasets across large numbers of subjects. However, current approaches used to spatially normalize datasets across individuals (e.g. affine/volumetric normalizations) are unable to preserve the topological alignment of homologous functional regions, due to the highly folded (nonlinear) cortical geometry[75, 80-83].

To overcome these limitations, we developed a pipeline to generate surface-based datasets of SDE coverage and icEEG activity, using geodesic metrics to correct for local gyral and sulcal folding patterns. We applied surface-based co-registration algorithms to accurately align datasets across subjects and resolve sparse-sampling issues. We then integrated these methods with a statistically robust mixed-effects multilevel analysis (MEMA) analysis to correct for variable effect sizes and missing data. In this fashion, our surface-based MEMA (SB-MEMA) was able to generate continuous brain activity maps that fully leveraged icEEG's unique spatio-temporal properties toward the study of higher-level visual networks[80].

The first question we addressed was whether category-selective regions in the VTC and LOC formed distinct functional modules or were topologically organized with respect to cortical folding patterns[4, 41]. Our hypothesis was that these regions were organized around specific sulcal landmarks – the mid-fusiform sulcus (MFS) in the VTC and the lateral occipital sulcus (LOS) in the LOC – to form larger-scale functional maps. SB-MEMA revealed overlapping regions of category-selective activity, suggesting that these regions were distributed across the VTC and LOC, rather than confined to isolated functional modules. Looking at the spatial organization of category-selective SDEs on the cortical surface, we observed that, in the VTC, face and animate selective

regions were constrained lateral to the MFS, while place and tool selective regions were constrained medially. Similarly, in the LOC, face and animate selective regions were constrained ventral to the LOS, while place and tools-selective regions were constrained dorsally. Thus, distinct sulcal landmarks – the MSF and LOS – could reliably predict functional transitions in selectivity for living (face and animate) and non-living (place and tool) object classes. These findings confirmed our original hypothesis, and provided novel electrophysiological support for the hierarchical coding model of higher-level visual organization.

The topological organization of functional representations in higher-level visual cortex has been hypothesized to facilitate the rapid extraction of category information. Specifically, the convergence of category-selective regions sharing similar preferences along one side of a sulcus (e.g. faces and animals lateral to MFS), while simultaneously segregating differentially selective regions on the other side (e.g. places and tools medial to MFS), would generate an implicit nesting of small-scale representations (category-selectivity) within a larger scale functional map (e.g. living vs. non-living). This would provide a mechanism for the visual system (and other cognitive systems, e.g. speech centers) to automatically read out different levels of categorical detail at different spatial scales (i.e. small scale for face information, larger scale for animacy information)[4].

Such organization may speed up the process of visual categorization by allowing independent stimulus information (e.g. scene and face information) to be processed in a parallel fashion within their respective networks. Additionally, the spatial clustering of related category-specific regions (i.e. face and animals lateral to MFS) likely minimizes wiring cost to thereby increase the speed of neural interactions, as these regions would

likely share neural circuitry due to the statistical regularity with which their object categories may co-occur in the world[4, 66].

Notably, this hierarchical information structuring may already be implemented at the anatomical level, since the same sulci (MFS and LOS) also predict transitions in cortical micro- and macro-architecture (e.g. cyto- and receptor architectonics and white-matter structural networks, respectively). This is consistent with the idea that the locations of these category-specific regions are tied to the neural hardware of the higher-level visual cortex that contains the neural circuits optimized for their necessary computations[4, 46, 58, 60, 62, 63, 65, 166].

To date, direct evidence for the topological organization of category-selective regions has been limited by the indirect nature of non-invasive neuroimaging methods, which report hemodynamic changes rather than direct neural activity. Our findings here provide important electrophysiological evidence, from a large number of individuals, to support hierarchical information structuring within the higher-level visual cortex[67].

The second question we addressed was related to competing models of information flow within category-specific networks. The decision to constrain the scope of the current analysis to network models of face-perception was made because they are (by far) the most clearly articulated[70]. We note, however, that faces are considered to be a special class of objects. This is because each face, though similar in shape to all other faces, is nevertheless unique and requires differentiation from all other faces. Therefore, insight gleaned about the visual processing of faces should extend to other categories, which likely use a subset of these processes[40, 68].

The two competing models we evaluated hypothesize fundamentally different mechanism for how information in early visual cortex (EVC) reaches two core regions responsible for different aspects of face perception: the occipital face area (OFA) and fusiform face area (FFA). The feed-forward, hierarchical model argues that EVC input is first delivered to the OFA for feature detection (e.g. detect face-parts), and then relayed to the FFA for structural encoding and identity representation[40]. In contrast, based on subjects with uni- or bilateral OFA lesions, the non-hierarchical model states that EVC input is delivered independently and in parallel to both the FFA and OFA. The FFA then detects faces in a holistic fashion, using an initially coarse representation. Following face detection, re-entrant interactions between the OFA and FFA refine the facial detail for identity discrimination[74].

In support of non-hierarchical model, connectivity analyses revealed functional and structural (i.e. white-matter) connectivity between EVC and both the FFA and OFA, as well as bidirectional connectivity between the OFA and FFA. Critically, and in direct contradiction to the feed-forward hierarchical model, EVC-FFA functional connectivity was observed prior to the onset of re-entrant OFA-FFA connectivity, indicating that FFA receives independent visual input directly from EVC. Furthermore, cortical stimulation mapping (CSM) provided causal support for the non-hierarchical model. Only CSM at FFA sites produced a complete disruption in face perception. In contrast, stimulation of EVC and OFA produced only low-level or intermediate visual hallucinations, without complete impairment of face perception. These results provide strong evidence in favor of the non-hierarchical model of face-perception.

Although our results here support the hypothesis that information flow to higher-level visual cortex occurs via parallelized, distributed networks, our sample size was

very small, raising concerns that the analysis may be underpowered. However, preliminary analysis from 4 subjects with left hemisphere coverage of EVC, OFA, and FFA show consistent results, which alleviate these concerns.

A second issue relates to the applicability of these results to other category-specific networks. From our analysis into the organization of higher-level visual cortex, few tool, animate, or word-selective SDEs were found within both VTC and LOC (although within a single region, there may be a larger number). The count becomes far smaller when we can only consider subjects with concurrent coverage over both or all three regions (including EVC). To be able to fully extend non-hierarchical predictions of parallelized, distributed information flow to other categories, more subjects with sufficient coverage will be required. Unfortunately, the dependence on single-subject coverage in this fashion is an intrinsic limitation of icEEG, due to the invasive nature of the procedure, as well as the relative rarity of the disease that requires it (i.e. focal epilepsy, see Appendix B). An alternative hypothesis, however, is the possibility that other categories do not require as extensive a network as face-selective regions. Nevertheless, subjects with sufficient coverage would still be required to validate this interpretation.

Future Plans:

Previous work studying the visual naming of common nouns (all categories), suggests that ~100-150ms prior to the onset of speech production, in the left inferior frontal gyrus (LIFG, e.g. Broca's area), pars orbitalis (POr) facilitates semantic processing by inhibiting pars triangularis (PT)[97]. This inhibition provides a plausible mechanism for controlled retrieval, in which POr enables the uninterrupted processing of higher-level visual regions responsible for object recognition by stalling response

selection in the LIFG (e.g. choosing the final word for articulation). Once visual object recognition processing is completed, PT inhibition is released and speech processing begins (i.e. response articulation).

These findings provide temporal and anatomical constraints within which to frame investigations of how perceptual information from higher-level visual regions (VTC/LOC) reaches prefrontal articulatory centers (LIFG) during object name selection. However, the functional coupling between the higher-level visual regions (VTC and LOC) responsible for object recognition and prefrontal speech centers (LIFG) is still vastly unknown. If POr and PT do perform different functions (controlled retrieval and response selection, respectively), they should exhibit unique patterns of functional connectivity with temporal and occipital regions. Specifically, POr should exhibit positive coupling with the visual semantic regions, while PT may not. Furthermore, changes in this long-range coupling will likely be the signal for POr to end inhibition of response selection.

In order to confirm or reject this model, network analysis of intra and inter- areal dynamics will be employed to investigate information flow between category-specific regions in VTC and LOC sub-serving object recognition and the subcomponents of the left inferior frontal gyrus. The following questions will be addressed:

a) Do pars orbitalis (POr) and/or pars triangularis (PT) exhibit functional connectivity with ventro-lateral occipito-temporal regions within 400 ms of stimulus onset? Are their respective patterns of connectivity with the ventro-lateral occipito-temporal regions similar or different?

b) Is functional connectivity between the prefrontal and occipito-temporal cortices unidirectional or bidirectional? Does ascending input from the occipito-temporal cortical region provide a signal for the end of semantic processing, allowing POr to end inhibition of PT and initiate response selection? Does the end of functional coupling between occipito-temporal regions and POr act as this signal?

c) Are there differences in functional connectivity characteristics for different categories?

Appendix A: The History of Visual Cortex

As I began my research, I found myself surprised to discover that the field of object recognition research was less than 100 years old. And the idea that a discrete brain region could mediate any visual subroutine (i.e. object recognition) had only been proposed in the mid-1930s – when Henrich Kluver's interest in mescaline-induced hallucinations led him to recruit Paul Bucy, a neurosurgeon, to help him perform some experiments by resecting monkey temporal lobe[24, 325]. In fact, modern neuroscience itself – the scientific study of structure-function relationships in the cerebral cortex – traces its origins back only 200 years to Franz Joseph Gall's radical proposal of his phrenological system[326].

Given the importance of perception to nearly every philosophical and scientific enterprise, it seemed implausible that the relatively young field of object recognition could have developed without some lingering influence from the beliefs of the pre-"modern neuroscience" era. For this reason, I've included this historical sketch on the evolution of perceptual theory; since understanding the broader historical context within which my research questions were developed should aid in generating an adequate framework with which to interpret my results. I note, however, that this is (by necessity) only a crude sketch. Much has been left out, though I wish it could have been otherwise. Unfortunately, in the fashion of non-invasive brain imaging, time and space are limited.

Broadly, this following history of visual object recognition is divided into four periods:

1) 400 BCE – 1810 CE: Ventricular localization and the *Sensus Communis*

2) 1810 – 1890: Cortical localization and the discovery of sensory motor brain

3) 1890 – 1930: The discovery of association cortex and visual agnosia

4) 1930 – present: The discovery of inferotemporal cortex and category-specificity

Ventricular localization and the *Sensus Communis*

At each step the metaphysicians come in, to retard the progress of the naturalists; and, in general, it is to the metaphysicians, that we must attribute the ignorance in which we are still involved..."

Franz Joseph Gall, 1835

Prior to the 19th century, the cerebral cortex was rarely assumed to have any role in cognitive or sensory function[k]. Most theories of mind, in fact, were still derivations of epistemological, metaphysical, and medical doctrines dating back to the 5th century BCE, all of which placed great importance on adequately explaining how the immortal soul interfaced with the organ of thought, be it the heart (e.g. Aristotle) or the brain (e.g. Alcmaeon, Galen)[326, 327].

In the 5th century CE, the most influential theory had become the doctrine of ventricular localization, teaching that all mental and sensory functions were localized

[k] As in all things, there are exceptions – specifically Thomas Willis (1664) and Emanuel Swedenborg (1740).

within the three ventricular spaces of the brain. Developed by early church fathers, this doctrine loosely integrated Aristotle's 'mental faculties' with Galen's depictions of the brain ventricles as storage sites for 'psychic pneuma'[l] – the animal spirits that served as active principles for peripheral and central nervous activity[328, 329]. But little-to-no significance was given to the cortex itself, which was viewed to be too dirty an organ to serve as intermediary between the body and the soul[330].

The dominance of ventricular localization persisted for nearly 1200 years, until its decline with the onset of the Enlightenment movement in the 17th century. Nevertheless, lasting damage to the cortex had been done. Nearly every theory of mind to be proposed for the next 200 years would harbor implicit prejudice against any possible role for the cortex in psychological or sensorimotor function.

Matters were made worse in the mid-1700s, when an important discovery lent powerful, empirical support toward anti-cortical beliefs – specifically with respect to sensorimotor function. Albrecht von Haller, an influent German physiology professor, published a series of animal experiments in which he demonstrated cortical insensitivity and inexcitability to mechanical and chemical stimulation. He further reported that pain

[l] Galen (129-199 CE) was one of the most important figures in ancient medicine, and his works influenced views of the brain through the Renaissance. His integration of animal dissection with his experience from treating gladiatorial injuries led him to record highly accurate and detailed anatomical descriptions of the brain. Although the ventricles were important to Galen, he localized the soul and higher cognitive functions in the solid portions of the brain. However, his disbelief that the size of the cerebral convolutions was related to intelligence – a proposition from a Ptolemaic anatomist, Erasistratus (ca 260) – had an incredibly long-lasting and negative impact. Following his death, and the decline of Greek medicine, his work became dogma. In the 4th and 5th centuries, the Church Fathers drew upon Galen's ideas of the brain, but, believing the solid portion too dirty to act as intermediary between body and soul, they located mental faculties to the ventricles, the empty spaces in the brain. It was believed that the five sensory organs went to the first ventricles, where sensory information was integrated across modalities by the common sense (*sensus communis)*.

and convulsions could, in fact, be elicited by subcortical stimulation (in the thalamus and cortical striatum/basal ganglia, respectively). Haller's immense prestige gave these findings long-lasting influence, and it became a ground truth until 1870 that the cortex was silent while sensorimotor function lived within the midbrain[330].

Cortical localization and the discovery of the sensory-motor brain

"*This apparent inexcitability of the cerebral cortex greatly retarded the progress of cerebral physiology… Everywhere doubt and discrepancy prevailed.*"

David Ferrier, 1868

At the beginning of the 19th century, the introduction of phrenology by Franz Joseph Gall brought punctate cortical localization into the realm of serious scientific discourse for the first time. It was the first systematic proposal to argue that the cerebral cortex comprised a set of organs with distinct psychological functions (though not sensorimotor)[331]. Although Gall's ideas faced fierce opposition from religious and scientific establishments, the concept of cerebral localization continued to be actively debated, even after phrenology was made obsolete. Finally, in 1861, Paul Broca decisively ended the debate in favor of the localizationists. His case presentation of M. Leborgne provided the evidence necessary to demonstrate the association between speech deficits and frontal lobar damage[332, 333].

Nevertheless, the localizationist victory still did not extend beyond higher intellectual faculties to include sensorimotor function. It was not until 1870 that the notion of an "insensitive cortex" was finally and unequivocally refuted by Gustav Fritsch and Edouard Hitzig, who used electrical stimulation to map out the motor cortex in dogs. On the implications of their results, they stated[332]:

> *It further appears, from the sum of all our experiments … certainly some psychological functions and perhaps all of them … need certain circumscribed centers of the cortex (1870, pg. 6).*

The findings of Fritsch and Hitzig cleared the last crucial impediment to localizing sensorimotor function in the brain.

Shortly after, an English physiologist named David Ferrier began to systematically search for visual (and other sensory) cortex in dogs and monkeys[334] using the electrical stimulation technique of Fritsch and Hitzig[m]. However, Ferrier incorrectly localized vision within the angular gyrus, stating that the occipital lobe played (at most) a supporting role[n]. Thus it was not until in 1879, following another series of dog and monkey lesional studies, that a German physiology professor named Hermann Munk correctly localized vision in the occipital cortex[o].

Munk's success was due in part to his surgical skills, which were more refined than Ferrier's, and which incorporated a newly described antiseptic techniques[p] that

---

[m] Ferrier published his findings relating to the localization of sensory brain regions in *The Functions of the Brain* in 1876. Although he was incorrect about many of his conclusions, his work on localizing motor and sensory regions in the brain had a major impact on the prevailing scientific community. This impact extended to the development of modern neurosurgical approaches, which use functional localization to guide surgical strategies.

[n] The discrepancy in Ferrier's findings with current knowledge is attributed to the fact that in removing the "occipital cortex", Ferrier spared enough residual striate cortex to account for the apparent lack of blindness. In contrast, his angular dissections were deeper and more complete, likely affecting the optic radiations. Ferrier's results were a result of poor surgical technique and short observational periods (only a few days) prior to sacrificing his animals, which were a main source of criticism.

[o] The first person to systematically argue for the discrete localization of cortical visual function was actually Bartolomeo Panizza (~1855). At that point, however, the cortex was still considered to be inexcitable, and the highest sensory regions localized in the thalamus. His work had little impact and was largely forgotten until Munk's rediscovery of the occipital lobe in the 1880s.

[p] Just prior to this period, Joseph Lister, an English surgeon, had revealed his novel antiseptic surgical technique, developed after he learned of the recent microbiological discoveries made by Louis Pasteur.

permitted Munk to observe his animals for much longer periods of time (up to five years)[330]. As a result, Munk not only localized visual cortex correctly, but he also chanced to observe an entirely novel and unusual type of visual deficit in one of his dogs with extensive occipital damage:

> *No abnormalities of hearing, taste, smell, or sensation. The dog walks freely about the room without bumping into objects… But within they psychic domain of vision a distinctive defect exists: he pays no attention to water or food, even if he is hungry and thirsty. He seems indifferent to everything he sees; threats do not frighten him. One can bring a match up to his eyes without him backing away. . . he no longer knows or recognizes what he sees.*

Munk termed this peculiar deficit *Seelenblindheit* – which literally translates to "soul-blind-sight", and what he called "psychic blindness"[q].

Munk's findings received conclusive support in follow-up studies performed by Edward Schafer and Sanger Brown in 1887. And similar to Munk, Schafer and Brown's experimentation with bilateral temporal lobectomies in monkeys produced unusual visual deficits[331]. Interestingly, because their lesions were much more extensive than Munk's, the deficits produced by Schafer and Brown's included additional emotional and intellectual changes as well. On publishing their findings in 1888, they described the changes in their monkey:

> *He voluntarily approaches all persons indifferently, allows himself to be handled, or even to be teased or slapped without making any attempt at retaliation or endeavoring to escape. His memory and intelligence seem deficient. He gives evidence of hearing, seeing and of his senses*

[q] The concept of "psychic blindness" fit with the British associationist theories in psychology at that time, resulting in its delivery to a wide audience in 1890 by William James' *Principles of Psychology*. This likely led to the term's adoption by the neurologist, Heinrich Lissauer, who published the first detailed report of psychic blindness in humans, and whose division of the condition into apperceptive and associative sub-classes is still widely followed by neurologist and neuropsychiatrists today. The term "psychic blindness" was later replaced with "visual agnosia" by Sigmund Freud in 1891.

generally, but it is clear that he no longer clearly understands the meanings of the sights, sounds and other impressions that reach him [italics my own]… Even after having examined an object in this way with the utmost care and deliberation, he will, on again coming across the same object accidentally… go through exactly the same process, as if he had forgotten his previous experiments. He appears no longer to discriminate between the different kinds of food … devours everything just as it happens to come.

It wasn't until much later that these descriptions would be recognized as the very first case of Klüver-Bucy syndrome[24]. However, at that time, Schafer and Brown were more focused on their quarrels with David Ferrier over the location of visual (and other) sensory cortical regions. They dismissed these deficits as a type of "idiocy" and never mentioned again[330].

Discovery of association cortex and visual agnosia

"*As I reported earlier, there is good evidence that visual habits are dependent upon the striate cortex and upon no other part of the cerebral cortex"*

Karl Lashley, 1950

By 1890, the cortical localization of primary sensorimotor regions was essentially complete, and interest began to shift towards the remaining "silent areas" of cortex[332]. At this time, these regions had been labeled as the "association cortex", based on the myelogenesis work of Paul Flechsig in 1876. Flechsig chose the term believing that myelination in these regions occurred as children began to associate the different senses with each other[331, 332] .

The appeal of Flechsig's terminology to the dominant psychological movement at the time – British associationism – quickly led to the adaptation of these regions to the task of associating sensory information into perceptions, images, and memories[330]. The terms "visuosensory" and "visuopsychic" were developed to distinguish the striate

cortex's primary sensory function from the more abstract functions of the surrounding associative cortical areas (including the peri- and para-striate cortex, i.e. Brodmann areas 18 & 19, respectively)[21]. By 1890, cases of "psychic blindness" (e.g. Munk's dog) were believed to result from the failure to associate the "optical sensations" (from visuosensory cortex) with what they signify, due to the damage in the visuopsychic areas of the brain.

As more cases of psychic blindness were reported – now relabeled as "visual agnosia" after 1891 (by Sigmund Freud) – the damage was typically attributed to the visual association cortex. However, due to the methodological constraints of the time, this did not mean much more than assigning the injury to a generally posterior location[331]. By the 1920s, the inconsistencies in lesion locations, coupled with the fall of British associationism and rise of Gestalt psychology (with its holistic view of cortical function), led to an increase of attacks on the link between visual association cortex and visual agnosias. Eventually belief in visual agnosia began to fade. It remained in doubt until the 1930s, when a series of publications by Heinrich Klüver and Paul Bucy reignited the debate, setting vision neuroscientists on the path toward discovering object recognition centers in the brain.

Discovery of inferotemporal cortex and its role in object recognition

Around 1933, Heinrich Klüver, a University of Chicago professor, approached a neurosurgeon named Paul Bucy to ask for his assistance in performing some experiments. Klüver had been studying visual cognition in monkeys for some time, but also maintained a personal interested in the effects of mescaline on perception[325]. Based off of personal, clinical, and experimental experience, Klüver began to suspect that the hallucinations reported by patients with temporal lobe epilepsy had a similar

mechanism of action as hallucinations induced by mescaline consumption[24, 335]. To test his hypothesis, he asked Bucy to perform bilateral temporal lobectomies in monkeys so that he could see whether postoperative mescaline administration produced the same hallucinogenic effects (they did). But it was in this context, in 1937, that Klüver and Bucy were able to observe and categorize the strange visual and behavioral changes that resulted from the surgeries in these monkeys, which today are still grouped under the psychological syndrome that bears their name[r]. Importantly, the very first deficit listed in Klüver-Bucy syndrome was "psychic blindness or visual agnosia", which they described as the inability to recognize objects by sight in the absence of any impairment in visual acuity[24].

This re-emergence of visual agnosia in the wake of the Gestalt's attacks received great attention. Notably, this included the attention of prominent psychologist, Karl Lashley, a friend of Kluver's, who became determined to resolve the questions surrounding visual agnosia[331]. Lashley began a series of monkey lesional studies in 1948, but ultimately concluded that the "comparison of the experimental and clinical evidence indicates that visual agnosia cannot be ascribed to uncomplicated loss of prestriate tissue"[336]. Lashley's negative findings, which were due to the shallow extent of his lesions, were quickly reversed following the arrival of a neurosurgeon, Karl Pribram, who had trained with Paul Bucy in Chicago. And in 1948, Pribram, working with two graduate students from Lashley's lab – Josephine Semmes (Blum) and Kao Chow – successfully managed to decouple visual agnosia from the remainder of the

[r] Following one of his lectures in 1930s, Klüver was asked by an audience member – Egas Moniz – if his technique could be used to treat incurably violent individuals. Klüver later expressed his extreme discomfort at the interaction. Moniz, in contrast, won the Nobel Prize in 1949 for his invention of the prefrontal lobotomy.

Klüver-Bucy deficits through careful and deeper incisions in the ventral temporal lobe[19, 337, 338].

Finally, in 1954, Pribram, who had now by this time recruited a new graduate student named Mortimer Mishkin, managed to precisely localize the crucial cortical regions of visual agnosia to the middle and inferior temporal gyri[339, 340]. Following their publications, research into these regions –together labeled as the inferotemporal cortex (IT) – rapidly spread across the country. At that time, however, visual agnosia was still considered to be a psychological rather than sensory dysfunction, and IT was considered to be association cortex whose function was mostly still a mystery [330]. Moreover, in the mid-1950s, visual processing was still thought to be completely contained within the occipital striate (V1 today) [336]. As such, it was unclear how any visual information could reach IT from the distant occipital striate [331].

The first link between IT and striate cortex was established by Mishkin in 1966, who used a series of crossed-lesion experiments to demonstrate that visual input to IT depended on a bilateral network of multi-synaptic cortico-cortical connections [341]. Shortly afterward, a multitude of topographically organized visual areas (e.g. V2, V3, V4) began to be discovered, filling the "empty" cortical mantle from striate to IT cortex [11, 342]. And then, in 1969, the final link to confirm IT's role in visual object recognition was confirmed by Charles[s], who used single-neuron electrophysiology to demonstration the first recordings of category-specific neural activity in visual cortex (for hands and faces) [14, 16, 18].

[s] As described in Chapter 1, Gross' decision to test complex visual shapes (e.g. faces) was inspired by Jerzy Konorski, who had been building on Hubel and Wiesel's new and revelatory logic of hierarchical sensory processing.

By 1980, more than a dozen visual areas in both the dorsal and ventral aspects of the occipital and temporal lobes had been identified. At this time, Mishkin had started his own laboratory at the National Institute of Mental Health, where he was joined by another post-doctorate student from Pribram's lab, Leslie Ungerleider. Together, Mishkin and Ungerleider proposed a powerful theory of vision that reconciled the rapidly fractionating visual literature. Their theory – whose origins trace back to the behavioral deficits reported in Ferrier's angular gyrus and Munk's occipito-temporal lesion experiments – proposed that the numerous extrastriate visual regions could be hierarchically organized into two separate visual streams: a dorsal stream specialized for 'spatial' vision, and a ventral stream specialized for 'object' perception. Today, the "dual visual stream" theory of Mishkin and Ungerleider has since demonstrated great explanatory power, serving as a crucial foundation of modern object recognition research[13, 343].

Appendix B: Disease Profile of Drug-Resistant Epilepsy

Introduction

Epilepsy is one of the oldest conditions known to mankind, and it remains the most common neurological condition to affect individual of all ages – with an estimated 50 million people (~0.5 – 1% of the population) impacted worldwide [344]. Epilepsy encompasses a diverse group of neurological disorders characterized by recurrent seizures (two or more) resulting from disordered neuronal discharge [345].

It is important to clarify that "seizures" and "epilepsy" are *not* synonymous. A **seizure** is a single, transient event, classified as an uncontrolled, excessive, and hyper-synchronous discharge of cortical neurons. As such, seizures can be provoked by external factors that disrupt the normal inhibitory tone of cortical circuits (e.g. alcohol-withdrawal, fever, concussion). In contrast, **epilepsy** is defined in patients presenting with a tendency towards *unprovoked* and *recurrent* seizures. More formally, epilepsy is a disease of the brain defined by any of the following conditions [346]:

1) At least two unprovoked (or reflex) seizures occurring > 24 hours apart

2) One unprovoked (or reflex) seizure and a probability of further seizures similar to the general recurrence risk (at least 60%) after two unprovoked seizures, occurring over the next 10 years.

3) Diagnosis of an epilepsy syndrome (e.g. juvenile myoclonic epilepsy or Lennox-Gastaut)

A patient's treatment and prognosis depends in large part upon the type of epilepsy diagnosed. For this reason, a great deal of effort has been made to create a consistent and accurate classification system for epilepsy – the most widely accepted of which is determined by the International League Against Epilepsy (ILAE) [347].

Currently, epilepsies are divided into two broad classes – generalized and partial – determined by the location of seizure onset (i.e. epileptogenic zone). **Generalized epilepsies** are characterized by seizures originating within/across both cerebral hemispheres, and often present with a strong genetic component. In contrast, **partial (focal or localization-related) epilepsies** are characterized by seizures originating in one or more localized (i.e. focal) regions of the brain, generally within a single hemisphere. Despite this imposed dichotomy, seizure classifications fall along continuum between these two extremes. Epilepsies that do not adhere to either category (e.g. spasms – which appear generalized, but are focal in origin) are grouped by the ILAE into a third, "unknown" class [347, 348].

While most patients diagnosed with epilepsy (~70%) eventually achieve some degree of seizure-control, about one-third of patients remain resistant to conventional antiepileptic drug (AED) therapy [349]. Patients with drug-resistant epilepsy (DRE, i.e. refractory or intractable) suffer the greatest burden of this disease, facing increased risks of premature death, injury, psychosocial and neuropsychiatric dysfunction, and impaired quality of life [350]. Although these patients reflect a minority of all individuals with epilepsy, they occupy the majority of the focus of epileptologist and of research aimed at prevention and treatment of this disease [351].

Epidemiology

Given the heterogeneous and complex nature of the disease, epidemiological studies of epilepsy have faced some difficulties, resulting in a wide range of prevalence and incidence estimates typically reported [345, 352, 353]. Prevalence here refers to the number of people diagnosed with epilepsy as a proportion of the total population (expressed as a number of cases per 1000 persons). Incidence refers to the number of

new cases of epilepsy during a 1 year time period in a well-defined population (expressed as number of cases per 100,000 people per year).

Worldwide estimates for epilepsy prevalence range from 2.2 – 41.0 per 1000, while incidence estimates range from 16 – 51 per 100,000 per year [345, 352]. Typically, more developed countries report a lower prevalence (~5 – 8 per 1000) of epilepsy, while resource-poor (i.e. developing) countries often report higher values [345, 352, 353]. In developed countries, the highest incidence of epilepsy occurs at the extremes of life (early childhood and after age 60). Studies reporting gender differences often suggest a predominance of epilepsy in males over females [345, 354], although the significance of these findings has also been debated [352]. No significant association with ethnicity has ever been reported, however a higher incidence of epilepsies has been linked with lower socioeconomic status [345, 352, 355].

In the United States, there exist a 3.6 percent risk of experiencing at least a single seizure in a normal 80-year life span [356]. About 1.5% of the population (~2.9 million people, adults and children) has active epilepsy, of which ~30% have been diagnosed with DRE and are refractory to medical therapy[350, 357].

Etiology

While virtually any insult to the cerebral cortex can cause a seizure, less than half of epilepsy cases are diagnosed with an identifiable cause. Of those with identifiable causes, common precipitating factors include: head trauma, brain tumors, stroke, infection, and inborn errors of metabolism or congenital malformations [358, 359]. In the remaining idiopathic cases, diagnostic advances (specifically in neuroimaging and genetics) have revealed that a majority are associated with underlying genetic factors,

while others can be attributed to autoimmune disease and/or cortical lesions. However, even when a single, dominant etiology has been identified, a patient's predisposition for developing epilepsy will still depend on the complex interaction of multiple additional factors [358]. Contributing factors can be found at multiple spatial scales (micro to macro), which generally interact to enhance an individual's predisposition to developing epilepsy. The complex, multifactorial nature of epilepsy makes identifying and treating a root cause prohibitively difficult. As such, treatment plans have shifted towards treating the disease as a complex system.

Symptoms and Diagnosis

Given the etiological complexity of epilepsy, a five-tier classification system has been developed to help standardize diagnostic approaches [358, 360]. Two of these five tiers focus on defining seizure symptoms while the other three tiers focus on defining the etiology and location of the brain abnormality.

The current mainstay of epilepsy management is antiepileptic drug (AED) therapy. The majority of patients diagnosed with epilepsy respond positively to AEDs (~70%) - with ~47% responding to one drug alone, 13% to two, and 5-10% to three or more drugs [361-363]. In fact, the major contributing factor to recurrence of seizures (>50%) is non-adherence to AED treatment regimens[364].

For the remaining patients (~30%), the diagnosis of drug-resistant/intractable epilepsy is recommend following the failure of two tolerated, appropriately chosen and administered AEDs (monotherapy or in combination) [365]. Predictors of intractability include a lack of efficacy after the first AED therapy, early age at seizure onset, high seizure frequency prior to treatment, and a diagnosis of non-idiopathic epilepsy. Partial

epilepsies with a lesional focus contribute to more than half of the diagnoses of intractable epilepsy in adults, among which those with mesial temporal lobe (MTL) sclerosis have the highest rates of intractability (~40 to 80%) [366, 367]. Idiopathic (genetic) epilepsies present with the least risk of becoming drug resistant [362, 363, 367, 368].

Risk factors for drug resistance appear to be multifactorial in nature, and are currently poorly understood. Research efforts have focused extensively on decreased drug penetration, drug target insensitivity, and impaired ion channel function in epileptogenic brain tissue as likely mechanisms[350].

Surgical Treatment

[Note: This section focuses on adult DRE patients eligible for epilepsy surgery, specifically those with mesial temporal lobe sclerosis as this is the predominant patient population in my field of research. Alternative therapies (increasing AEDs regimen, vagus nerve stimulation, cortical stimulation) are available for adult DRE patients in whom surgery is not an option (e.g. bilateral or multifocal seizure onset, medical comorbidities, generalized epilepsies), but these are beyond the scope of this report. Surgical therapies for pediatric DRE patients involving removal or cortical isolation of a diseased hemisphere (e.g. hemispherectomy, corpus callosotomy, and multiple subpial transections) are also not discussed here.]

In order for a DRE patient to be eligible for epilepsy surgery, a pre-surgical evaluation is first undertaken to accurately localize the epileptogenic zone, and determine the extent to which it can be resected without introducing new, unacceptable handicaps [369]. To achieve this, DRE patients are typically referred to a comprehensive epilepsy center in which they receive [370]:

1) A detailed history and neurological exam, and video-EEG monitoring, to characterize seizure semiology and rule out misclassification.

2) High-resolution MRI scan to document presence of sclerosis or other brain lesions

3) Repeated interictal EEGs to grossly evaluate seizure onset location

4) A detailed neuropsychological evaluation to determine baseline cognitive function, as well as identify any functional abnormalities that may assist in identifying seizure onset zones.

In general, the potential effectiveness of focal resections depends on the concordance of seizure semiology with EEG and structural MRI findings. If noninvasive measures remain inconclusive, or if they suggest the involvement of highly functional neocortical regions (e.g. cortex involved in auditory or visual or language function), additional neuroimaging may be required. This may include: functional MRI (fMRI, non-invasive), intracarotid sodium amobarbital/methohexital tests (WADA, minimally invasive), and intracranial EEG (icEEG, highly invasive) to assist in localizing high-level cognitive functions mediated by the cortical regions in question. It should be noted that icEEG non-trivially increases patient risk (infection, hemorrhage, or mass-shift effects), as it requires an extra surgical procedure, in which the skull is removed, so that electrodes can be implant directly upon or within the pial surface. When indicated, however, icEEG greatly improves the chances of seizure localization and surgical outcome [83, 369].

In MTL patients with a seizure focus localized to the amygdala and/or hippocampus, focal surgical resection of epileptogenic cortex has been demonstrated to be the safest and most effective course of action [371-373]. The most common surgical approach for MTL patients involves the removal of the anterior temporal pole (~one to two-thirds), hippocampus, and parts of the amygdala – either all together or in different

combinations [374]. The posterior aspects of the temporal lobe (~4 – 4.5 cm from the pole) are typically avoided to prevent damage to visual radiations [375].

If seizure focus does not appear to involve the neocortex, an alternative approach is selective amygdalohippocampectomy to remove the amygdala and hippocampus while sparing neocortical aspects of the temporal lobe. Depending on the patient's specific disease profile, different surgical approaches have been developed to facilitate access to the lesion (e.g. transsylvian vs. transcortical vs. subtemporal). Regardless of approach, however, the end goal is the same: minimal but efficacious removal of pathological tissue while preserving cognitive function as much as possible[374].

Prognosis

Preoperatively, the most important predictors of seizure freedom include: the presence of an MRI-localized focal brain lesion, the presence of unilateral mesial temporal sclerosis in the temporal lobe of seizure origin, and shorter preoperative seizure durations. Postoperatively, the strongest predictor of long-term seizure control is the absence of any seizures in the first year after surgery [376-378]. EEG-identified epileptiform activity within the first few years after surgery is associated with ~3x higher risk of seizure recurrence [379].

In general, the best surgical outcomes are obtained when seizure semiology, interictal and seizure onset focus (determined by EEG), and MRI lesional results are all functionally and anatomically concordant [369]. In such patients, ~65 – 75% achieve complete seizure freedom, or present with auras only for up to 10 years after surgery. For an additional 10-15% of patients, complete remission is achieved following a

transient period of post-operative seizure activity. For MTL patients with normal brain MRIs, rates of seizure freedom are slightly decreased, ranging from 50 – 60 %. Of these patients, most (70 – 80%) achieve a decrease in seizure frequency by at least 75% [376, 380-385].

In general, mortality and morbidity of epilepsy surgery are small. Risk of surgical death following anterior temporal lobectomy is < 1%, and epilepsy surgery presents with an overall morbidity of ~10% [369, 386]. The greatest risks are often to cognitive functions, especially when seizure foci are localized around functionally important cortical regions. However, this risk must often be weighed against the consequences of failing to achieve seizure control - decreased memory and cognitive function; psychosocial stigma; increased risk for depression, injury, or death; difficulty in finding or maintaining employment; and difficulty in achieving independence for day-to-day activities [387, 388].

Despite the conventional belief that surgery should remain an option of last-resort, MTL patients are strongly encouraged to consider surgical options as soon as drug resistance is reached. As seizure activity remains uncontrolled, risks to quality of life and cognitive health increase constantly. To date, epilepsy surgery in MTL patients has been demonstrated to provide the most effective treatment in terms of seizure control as well as cost, and the greatest improvement in quality-of-life in comparison to any other alternative [371, 389].

Translational Need

Research efforts into the neurological mechanisms of epilepsy have enabled unique insights to be gained into the biology of human cognitive function and its

organization in various disease states [83, 282]. Early studies by Penfield and Foerster, investigating functional localization, led to the creation of the sensorimotor homunculus maps that are so widely taught in every basic neuroscience course. The opportunity to obtain high spatiotemporal resolution recordings of cognitive function from directly on or within the human cortex has led to massive advances in our understanding of how the brain operates. These advances have radically altered our understanding of critical functions such as language, object recognition, and sensorimotor systems. With the small amount of knowledge we have gained thus far, paralyzed patients are currently able to control robotic limbs, using nothing but their thoughts, to regain the ability to walk and interact with their environment and loved ones. Nevertheless, we are only now beginning to realize the depth of the challenges that still remain. The pathophysiology and neurobiology behind diseases such as epilepsy have only become more complex the more we have learned. We still do not understand many of the basic principles of epilepsy, or even the mechanisms of action of many conventional AEDs. Massive inter-disciplinary efforts, entirely translational in nature, will be required to overcome the challenges of these multi-scale-multi-factorial diseases[390].

References

1. Pinker, S. The Mind's Eye. in *How The Mind Works* (W. W. Norton & Company, New York, 1997).

2. DiCarlo, J.J., Zoccolan, D. & Rust, N.C. How does the brain solve visual object recognition? *Neuron* **73**, 415-434 (2012).

3. Felleman, D.J. & Van Essen, D.C. Distributed hierarchical processing in the primate cerebral cortex. *Cereb Cortex* **1**, 1-47 (1991).

4. Grill-Spector, K. & Weiner, K.S. The functional architecture of the ventral temporal cortex and its role in categorization. *Nat Rev Neurosci* **15**, 536-548 (2014).

5. Hubel, D.H. & Wiesel, T.N. Receptive fields, binocular interaction and functional architecture in the cat's visual cortex. *J Physiol* **160**, 106-154 (1962).

6. Hubel, D.H. & Wiesel, T.N. Receptive Fields and Functional Architecture in Two Nonstriate Visual Areas (18 and 19) of the Cat. *J Neurophysiol* **28**, 229-289 (1965).

7. Ungerleider, L.G. & Mishkin, M. Two cortical visual systems. in *Analysis of visual behavior* (ed. D.J. Ingle, M.A. Goodale & R.J.W. Mansfield) 549-586 (MIT Press, Cambridge, MA, 1982).

8. Farah, M.J. *Visual Agnosia* (MIT Press, Cambridge, MA, 2004).

9. Hubel, D.H. & Wiesel, T.N. Receptive fields of single neurones in the cat's striate cortex. *J Physiol* **148**, 574-591 (1959).

10. Wurtz, R.H. Recounting the impact of Hubel and Wiesel. *J Physiol* **587**, 2817-2823 (2009).

11. Allman, J.M. & Kaas, J.H. A representation of the visual field in the caudal third of the middle tempral gyrus of the owl monkey (Aotus trivirgatus). *Brain Res* **31**, 85-105 (1971).

12. Zeki, S.M. Functional organization of a visual area in the posterior bank of the superior temporal sulcus of the rhesus monkey. *J Physiol* **236**, 549-573 (1974).

13. Mishkin, M.U., L.G.; Macko, K.A. Object vision and spatial vision: two cortical pathways. *Trends in Neuroscience* **6**, 414 - 417 (1983).

14. Gross, C.G., Bender, D.B. & Rocha-Miranda, C.E. Visual receptive fields of neurons in inferotemporal cortex of the monkey. *Science* **166**, 1303-1306 (1969).

15. Gross, C.G., Cowey, A. & Manning, F.J. Further analysis of visual discrimination deficits following foveal prestriate and inferotemporal lesions in rhesus monkeys. *Journal of comparative and physiological psychology* **76**, 1-7 (1971).

16. Gross, C.G., Rocha-Miranda, C.E. & Bender, D.B. Visual properties of neurons in inferotemporal cortex of the Macaque. *J Neurophysiol* **35**, 96-111 (1972).

17. Konorski, J. *Integrative Activity of the Brain: An Interdisciplinary Approach* (University of Chicago Press, Chicago, 1967).

18. Gross, C.G. Single neuron studies of inferior temporal cortex. *Neuropsychologia* **46**, 841-852 (2008).

19. Blum, J.S., Chow, K.L. & Pribram, K.H. A behavioral analysis of the organization of the parieto-temporo-preoccipital cortex. *J Comp Neurol* **93**, 53-100 (1950).

20. Freud, S. *On aphasia; a critical study* (International Universities Press, New York,, 1953).

21. James, W. *The principles of psychology* (H. Holt and company, New York,, 1890).

22. Munk, H. Of the visual area of the cerebral cortex and its relation to eye movements. *Brain* **13**, 450-469 (1890).

23. Pribram, K.B., M. Further Analysis of the Temporal Lobe Syndrome Utilizing Fronto-Temporal Ablations. *J Comp Neurol* **99**, 347-375 (1953).

24. Kluver, H.B., P.C. An Analysis of Certain Effects of Bilateral Temporal Lobectomy in the Rhesus Monkey, with Special Reference to "Psychic Blindness". *J Psychology* **5**, 33-54 (1938).

25. Gross, C.G. Genealogy of the "grandmother cell". *Neuroscientist* **8**, 512-518 (2002).

26. Koch, C. *The Quest for Consciousness: A Neurobiological Approach* (Roberts and Company Publishers, Engelwood, Co, 2004).

27. Kwong, K.K., Belliveau, J.W., Chesler, D.A., Goldberg, I.E., Weisskoff, R.M., Poncelet, B.P., Kennedy, D.N., Hoppel, B.E., Cohen, M.S., Turner, R., Cheng, H.-M., Brady, T.J. & Rosen, B.R. Dynamic magnetic resonance imaging of human brain activity during primary sensory stimulation. *Proceding of the National Academy of Sciences* **89**, 5675-5679 (1992).

28. Ogawa, S., Tank, D.W., Menon, R., Ellermann, J.M., Kim, S.-G., Merkle, H. & Ugurbil, K. Intrinsic signal changes accompanying sensory stimulation: functional brain mapping with magnetic resonance imaging. *Proceedings of the National Academy of Sciences*, 5951-5955 (1992).

29. Petersen, S.E., Fox, P.T., Posner, M.I., Mintun, M. & Raichle, M.E. Positron emission tomographic studies of the cortical anatomy of single-word processing. *Nature* **331**, 585-589 (1988).

30. Posner, M.I., Petersen, S.E., Fox, P.T. & Raichle, M.E. Localization of cognitive operations in the human brain. *Science* **240**, 1627-1631 (1988).

31. Raichle, M.E. Positron emission tomography. *Annu Rev Neurosci* **6**, 249-267 (1983).

32. Ungerleider, L.G. & Haxby, J.V. 'What' and 'where' in the human brain. *Curr Opin Neurobiol* **4**, 157-165 (1994).

33. Weiner, K.S. & Grill-Spector, K. Neural representations of faces and limbs neighbor in human high-level visual cortex: evidence for a new organization principle. *Psychol Res* **77**, 74-97 (2013).

34. Kanwisher, N., McDermott, J. & Chun, M.M. The fusiform face area: a module in human extrastriate cortex specialized for face perception. *J Neurosci* **17**, 4302-4311 (1997).

35. Kanwisher, N. Functional specificity in the human brain: a window into the functional architecture of the mind. *Proc Natl Acad Sci U S A* **107**, 11163-11170 (2010).

36. Epstein, R. & Kanwisher, N. A cortical representation of the local visual environment. *Nature* **392**, 598-601 (1998).

37. Downing, P.E., Jiang, Y., Shuman, M. & Kanwisher, N. A cortical area selective for visual processing of the human body. *Science* **293**, 2470-2473 (2001).

38. Friston, K.J., Rotshtein, P., Geng, J.J., Sterzer, P. & Henson, R.N. A critique of functional localisers. *Neuroimage* **30**, 1077-1087 (2006).

39. Gauthier, I., Tarr, M.J., Moylan, J., Skudlarski, P., Gore, J.C. & Anderson, A.W. The fusiform "face area" is part of a network that processes faces at the individual level. *J Cogn Neurosci* **12**, 495-504 (2000).

40. Haxby, J.V., Hoffman, E.A. & Gobbini, M.I. The distributed human neural system for face perception. *Trends Cogn Sci* **4**, 223-233 (2000).

41. Op de Beeck, H.P., Dicarlo, J.J., Goense, J.B., Grill-Spector, K., Papanastassiou, A., Tanifuji, M. & Tsao, D.Y. Fine-scale spatial organization of face and object selectivity in the temporal lobe: do functional magnetic resonance imaging, optical imaging, and electrophysiology agree? *J Neurosci* **28**, 11796-11801 (2008).

42. Rossion, B. Constraining the cortical face network by neuroimaging studies of acquired prosopagnosia. *Neuroimage* **40**, 423-426 (2008).

43. Rossion, B., Caldara, R., Seghier, M., Schuller, A.M., Lazeyras, F. & Mayer, E. A network of occipito-temporal face-sensitive areas besides the right middle fusiform gyrus is necessary for normal face processing. *Brain* **126**, 2381-2395 (2003).

44. Weiner, K.S. & Grill-Spector, K. The improbable simplicity of the fusiform face area. *Trends Cogn Sci* **16**, 251-254 (2012).

45. Puce, A., Allison, T., Bentin, S., Gore, J.C. & McCarthy, G. Temporal cortex activation in humans viewing eye and mouth movements. *J Neurosci* **18**, 2188-2199 (1998).

46. Nasr, S., Liu, N., Devaney, K.J., Yue, X., Rajimehr, R., Ungerleider, L.G. & Tootell, R.B. Scene-selective cortical regions in human and nonhuman primates. *J Neurosci* **31**, 13771-13785 (2011).

47. Orlov, T., Makin, T.R. & Zohary, E. Topographic representation of the human body in the occipitotemporal cortex. *Neuron* **68**, 586-600 (2010).

48. Peelen, M.V. & Downing, P.E. The neural basis of visual body perception. *Nat Rev Neurosci* **8**, 636-648 (2007).

49. Kanwisher, N.B.J. The Functional Architecture of the Face System: Integrating Evidence from fMRI and Patient Studies. in *The Oxford Handbook of Face Perception* 111 - 129 (Oxford University Press, 2011).

50. Weiner, K.S. & Grill-Spector, K. Sparsely-distributed organization of face and limb activations in human ventral temporal cortex. *Neuroimage* **52**, 1559-1573 (2010).

51. Grill-Spector, K. The neural basis of object perception. *Curr Opin Neurobiol* **13**, 159-166 (2003).

52. Grill-Spector, K., Golarai, G. & Gabrieli, J. Developmental neuroimaging of the human ventral visual cortex. *Trends Cogn Sci* **12**, 152-162 (2008).

53. Grill-Spector, K., Kourtzi, Z. & Kanwisher, N. The lateral occipital complex and its role in object recognition. *Vision Res* **41**, 1409-1422 (2001).

54. Grill-Spector, K. & Malach, R. The human visual cortex. *Annu Rev Neurosci* **27**, 649-677 (2004).

55. Hasson, U., Levy, I., Behrmann, M., Hendler, T. & Malach, R. Eccentricity bias as an organizing principle for human high-order object areas. *Neuron* **34**, 479-490 (2002).

56. Levy, I., Hasson, U., Avidan, G., Hendler, T. & Malach, R. Center-periphery organization of human object areas. *Nat Neurosci* **4**, 533-539 (2001).

57. Malach, R., Levy, I. & Hasson, U. The topography of high-order human object areas. *Trends Cogn Sci* **6**, 176-184 (2002).

58. Caspers, J., Palomero-Gallagher, N., Caspers, S., Schleicher, A., Amunts, K. & Zilles, K. Receptor architecture of visual areas in the face and word-form recognition region of the posterior fusiform gyrus. *Brain Struct Funct* **220**, 205-219 (2015).

59. Caspers, J., Zilles, K., Eickhoff, S.B., Schleicher, A., Mohlberg, H. & Amunts, K. Cytoarchitectonical analysis and probabilistic mapping of two extrastriate areas of the human posterior fusiform gyrus. *Brain Struct Funct* **218**, 511-526 (2013).

60. Gomez, J., Pestilli, F., Witthoft, N., Golarai, G., Liberman, A., Poltoratski, S., Yoon, J. & Grill-Spector, K. Functionally defined white matter reveals segregated pathways in human ventral temporal cortex associated with category-specific processing. *Neuron* **85**, 216-227 (2015).

61. Lorenz, S., Weiner, K.S., Caspers, J., Mohlberg, H., Schleicher, A., Bludau, S., Eickhoff, S.B., Grill-Spector, K., Zilles, K. & Amunts, K. Two New Cytoarchitectonic Areas on the Human Mid-Fusiform Gyrus. *Cereb Cortex* (2015).

62. Yeatman, J.D., Weiner, K.S., Pestilli, F., Rokem, A., Mezer, A. & Wandell, B.A. The vertical occipital fasciculus: A century of controversy resolved by in vivo measurements. *Proc Natl Acad Sci U S A* **111**, E5214-5223 (2014).

63. Kujovic, M., Zilles, K., Malikovic, A., Schleicher, A., Mohlberg, H., Rottschy, C., Eickhoff, S.B. & Amunts, K. Cytoarchitectonic mapping of the human dorsal extrastriate cortex. *Brain Struct Funct* **218**, 157-172 (2013).

64. Pyles, J.A., Verstynen, T.D., Schneider, W. & Tarr, M.J. Explicating the face perception network with white matter connectivity. *PLoS One* **8**, e61611 (2013).

65. Saygin, Z.M., Osher, D.E., Koldewyn, K., Reynolds, G., Gabrieli, J.D. & Saxe, R.R. Anatomical connectivity patterns predict face selectivity in the fusiform gyrus. *Nat Neurosci* **15**, 321-327 (2012).

66. Marr, D. *Vision* (The MIT Press, 1982).

67. Jacques, C., Witthoft, N., Weiner, K.S., Foster, B.L., Rangarajan, V., Hermes, D., Miller, K.J., Parvizi, J. & Grill-Spector, K. Corresponding ECoG and fMRI category-selective signals in human ventral temporal cortex. *Neuropsychologia* (2015).

68. Sergent, J. & Signoret, J.L. Functional and anatomical decomposition of face processing: evidence from prosopagnosia and PET study of normal subjects. *Philos Trans R Soc Lond B Biol Sci* **335**, 55-61; discussion 61-52 (1992).

69. Atkinson, A.P. & Adolphs, R. The neuropsychology of face perception: beyond simple dissociations and functional selectivity. *Philos Trans R Soc Lond B Biol Sci* **366**, 1726-1738 (2011).

70. Haxby, J.V.G., M.I. Distributed Neural Systems for Face Perception. in *The Oxford Handbook of Face Perception* 93 - 110 (Oxford University Press, 2011).

71. Lamme, V.A. & Roelfsema, P.R. The distinct modes of vision offered by feedforward and recurrent processing. *Trends Neurosci* **23**, 571-579 (2000).

72. Rossion, B., Dricot, L., Goebel, R. & Busigny, T. Holistic face categorization in higher order visual areas of the normal and prosopagnosic brain: toward a non-hierarchical view of face perception. *Front Hum Neurosci* **4**, 225 (2011).

73. Steeves, J., Dricot, L., Goltz, H.C., Sorger, B., Peters, J., Milner, A.D., Goodale, M.A., Goebel, R. & Rossion, B. Abnormal face identity coding in the middle fusiform gyrus of two brain-damaged prosopagnosic patients. *Neuropsychologia* **47**, 2584-2592 (2009).

74. Rossion, B. Understanding face perception by means of prosopagnosia and neuroimaging. *Frontiers in bioscience* **6**, 258-307 (2014).

75. Lachaux, J.P., Axmacher, N., Mormann, F., Halgren, E. & Crone, N.E. High-frequency neural activity and human cognition: past, present and possible future of intracranial EEG research. *Prog Neurobiol* **98**, 279-301 (2012).

76. Lachaux, J.P., Rudrauf, D. & Kahane, P. Intracranial EEG and human brain mapping. *J Physiol Paris* **97**, 613-628 (2003).

77. Farah, M.J. *Visual agnosia, 2nd Ed.* (MIT Press, Cambridge, MA, 2004).

78. Haxby, J.V., Grady, C.L., Ungerleider, L.G. & Horwitz, B. Mapping the functional neuroanatomy of the intact human brain with brain work imaging. *Neuropsychologia* **29**, 539-555 (1991).

79. Jerbi, K., Ossandon, T., Hamame, C.M., Senova, S., Dalal, S.S., Jung, J., Minotti, L., Bertrand, O., Berthoz, A., Kahane, P. & Lachaux, J.P. Task-related gamma-band dynamics from an intracerebral perspective: review and implications for surface EEG and MEG. *Hum Brain Mapp* **30**, 1758-1771 (2009).

80. Kadipasaoglu, C.M., Baboyan, V.G., Conner, C.R., Chen, G., Saad, Z.S. & Tandon, N. Surface-based mixed effects multilevel analysis of grouped human electrocorticography. *Neuroimage* **101**, 215-224 (2014).

81. Kadipasaoglu, C.M., Forseth, K., Whaley, M., Conner, C.R., Rollo, M.J., Baboyan, V.G. & Tandon, N. Development of grouped icEEG for the study of cognitive processing. *Frontiers in psychology* **6**, 1008 (2015).

82. Mukamel, R. & Fried, I. Human intracranial recordings and cognitive neuroscience. *Annu Rev Psychol* **63**, 511-537 (2012).

83. Tandon, N. Cortical Mapping by Electrical Stimulation of Subdural Electrodes: Language areas. in *Textbook of Epilepsy Surgery* (ed. H. Luders) 1001-1015 (Informa Healthcare, 2008).

84. Damasio, H., Tranel, D., Grabowski, T., Adolphs, R. & Damasio, A. Neural systems behind word and concept retrieval. *Cognition* **92**, 179-229 (2004).

85. Mahon, B.Z. & Caramazza, A. Concepts and categories: a cognitive neuropsychological perspective. *Annu Rev Psychol* **60**, 27-51 (2009).

86. Watrous, A.J., Tandon, N., Conner, C.R., Pieters, T. & Ekstrom, A.D. Frequency-specific network connectivity increases underlie accurate spatiotemporal memory retrieval. *Nat Neurosci* **16**, 349-356 (2013).

87. Chang, E.F., Rieger, J.W., Johnson, K., Berger, M.S., Barbaro, N.M. & Knight, R.T. Categorical speech representation in human superior temporal gyrus. *Nat Neurosci* **13**, 1428-1432 (2011).

88. Sahin, N.T., Pinker, S., Cash, S.S., Schomer, D. & Halgren, E. Sequential processing of lexical, grammatical, and phonological information within Broca's area. *Science* **326**, 445-449 (2009).

89. Rutishauser, U., Tudusciuc, O., Neumann, D., Mamelak, A.N., Heller, A.C., Ross, I.B., Philpott, L., Sutherling, W.W. & Adolphs, R. Single-unit responses selective for whole faces in the human amygdala. *Curr Biol* **21**, 1654-1660 (2011).

90. Crone, N.E., Sinai, A. & Korzeniewska, A. High-frequency gamma oscillations and human brain mapping with electrocorticography. *Prog Brain Res* **159**, 275-295 (2006).

91. Crone, N.E., Hao, L., Hart, B.J., Boatman, D., Lesser, R.P., Irizarry, R. & Gordon, B. Electrocorticographic gamma activity during word production in spoken and sign language. *Neurology* **57**, 2045-2053 (2001).

92. Ojemann, G.A., Ojemann, J. & Ramsey, N.F. Relation between functional magnetic resonance imaging (fMRI) and single neuron, local field potential (LFP) and electrocorticography (ECoG) activity in human cortex. *Front Hum Neurosci* **7**, 34 (2013).

93. Gaillard, R., Naccache, L., Pinel, P., Clemenceau, S., Volle, E., Hasboun, D., Dupont, S., Baulac, M., Dehaene, S., Adam, C. & Cohen, L. Direct intracranial, FMRI, and lesion evidence for the causal role of left inferotemporal cortex in reading. *Neuron* **50**, 191-204 (2006).

94. Cervenka, M.C., Boatman-Reich, D.F., Ward, J., Franaszczuk, P.J. & Crone, N.E. Language mapping in multilingual patients: electrocorticography and cortical stimulation during naming. *Front Hum Neurosci* **5**, 13.

95. Buzsaki, G. & Draguhn, A. Neuronal oscillations in cortical networks. *Science* **304**, 1926-1929 (2004).

96. Conner, C.R., Ellmore, T.M., Pieters, T.A., Disano, M.A. & Tandon, N. Variability of the Relationship between Electrophysiology and BOLD-fMRI across Cortical Regions in Humans. *J Neurosci* **31**, 12855-12865 (2011).

97. Conner, C.R., Chen, G., Pieters, T.A. & Tandon, N. Category Specific Spatial Dissociations of Parallel Processes Underlying Visual Naming. *Cereb Cortex* (2013).

98. Logothetis, N.K. & Pfeuffer, J. On the nature of the BOLD fMRI contrast mechanism. *Magn Reson Imaging* **22**, 1517-1531 (2004).

99. Lachaux, J.P., Fonlupt, P., Kahane, P., Minotti, L., Hoffmann, D., Bertrand, O. & Baciu, M. Relationship between task-related gamma oscillations and BOLD signal: new insights from combined fMRI and intracranial EEG. *Hum Brain Mapp* **28**, 1368-1375 (2007).

100. Ojemann, G.A., Corina, D.P., Corrigan, N., Schoenfield-McNeill, J., Poliakov, A., Zamora, L. & Zanos, S. Neuronal correlates of functional magnetic resonance imaging in human temporal cortex. *Brain* **133**, 46-59 (2010).

101. Khursheed, F., Tandon, N., Tertel, K., Pieters, T.A., Disano, M.A. & Ellmore, T.M. Frequency-Specific Electrocorticographic Correlates of Working Memory Delay Period fMRI Activity. *Neuroimage* **3**, 1773-1782 (2011).

102. Nir, Y., Fisch, L., Mukamel, R., Gelbard-Sagiv, H., Arieli, A., Fried, I. & Malach, R. Coupling between neuronal firing rate, gamma LFP, and BOLD fMRI is related to interneuronal correlations. *Curr Biol* **17**, 1275-1285 (2007).

103. Hermes, D., Miller, K.J., Vansteensel, M.J., Aarnoutse, E.J., Leijten, F.S. & Ramsey, N.F. Neurophysiologic correlates of fMRI in human motor cortex. *Hum Brain Mapp* (2011).

104. Mukamel, R., Gelbard, H., Arieli, A., Hasson, U., Fried, I. & Malach, R. Coupling between neuronal firing, field potentials, and FMRI in human auditory cortex. *Science* **309**, 951-954 (2005).

105. Esposito, F., Singer, N., Podlipsky, I., Fried, I., Hendler, T. & Goebel, R. Cortex-based inter-subject analysis of iEEG and fMRI data sets: Application to sustained task-related BOLD and gamma responses. *Neuroimage* **66C**, 457-468 (2012).

106. Logothetis, N.K., Pauls, J., Augath, M., Trinath, T. & Oeltermann, A. Neurophysiological investigation of the basis of the fMRI signal. *Nature* **412**, 150-157 (2001).

107. Halgren, E., Marinkovic, K. & Chauvel, P. Generators of the late cognitive potentials in auditory and visual oddball tasks. *Electroencephalogr Clin Neurophysiol* **106**, 156-164 (1998).

108. Alivisatos, A.P., Chun, M., Church, G.M., Deisseroth, K., Donoghue, J.P., Greenspan, R.J., McEuen, P.L., Roukes, M.L., Sejnowski, T.J., Weiss, P.S. & Yuste, R. Neuroscience. The brain activity map. *Science* **339**, 1284-1285 (2013).

109. Pieters, T.A., Conner, C.R. & Tandon, N. Recursive grid partitioning on a cortical surface model: an optimized technique for the localization of implanted subdural electrodes. *J Neurosurg* **118**, 1086-1097 (2013).

110. Miller, K.J., Leuthardt, E.C., Schalk, G., Rao, R.P., Anderson, N.R., Moran, D.W., Miller, J.W. & Ojemann, J.G. Spectral changes in cortical surface potentials during motor movement. *J Neurosci* **27**, 2424-2432 (2007).

111. Dykstra, A.R., Chan, A.M., Quinn, B.T., Zepeda, R., Keller, C.J., Cormier, J., Madsen, J.R., Eskandar, E.N. & Cash, S.S. Individualized localization and cortical surface-based registration of intracranial electrodes. *Neuroimage* **59**, 3563-3570 (2012).

112. Oosterhof, N.N., Wiestler, T., Downing, P.E. & Diedrichsen, J. A comparison of volume-based and surface-based multi-voxel pattern analysis. *Neuroimage* **56**, 593-600 (2011).

113. Saad, Z.S. & Reynolds, R.C. Suma. *Neuroimage* **62**, 768-773 (2012).

114. Anticevic, A., Dierker, D.L., Gillespie, S.K., Repovs, G., Csernansky, J.G., Van Essen, D.C. & Barch, D.M. Comparing surface-based and volume-based analyses of

functional neuroimaging data in patients with schizophrenia. *Neuroimage* **41**, 835-848 (2008).

115. Fischl, B., Sereno, M.I., Tootell, R.B. & Dale, A.M. High-resolution intersubject averaging and a coordinate system for the cortical surface. *Hum Brain Mapp* **8**, 272-284 (1999).

116. Groppe, D.M., Bickel, S., Keller, C.J., Jain, S.K., Hwang, S.T., Harden, C. & Mehta, A.D. Dominant frequencies of resting human brain activity as measured by the electrocorticogram. *Neuroimage* **79**, 223-233 (2013).

117. Mukamel, E.A., Pirondini, E., Babadi, B., Wong, K.F., Pierce, E.T., Harrell, P.G., Walsh, J.L., Salazar-Gomez, A.F., Cash, S.S., Eskandar, E.N., Weiner, V.S., Brown, E.N. & Purdon, P.L. A transition in brain state during propofol-induced unconsciousness. *J Neurosci* **34**, 839-845 (2014).

118. Woolrich, M. Robust group analysis using outlier inference. *Neuroimage* **41**, 286-301 (2008).

119. Chen, G., Saad, Z.S., Nath, A.R., Beauchamp, M.S. & Cox, R.W. FMRI group analysis combining effect estimates and their variances. *Neuroimage* **60**, 747-765 (2011).

120. Vidal, J.R., Ossandon, T., Jerbi, K., Dalal, S.S., Minotti, L., Ryvlin, P., Kahane, P. & Lachaux, J.P. Category-Specific Visual Responses: An Intracranial Study Comparing Gamma, Beta, Alpha, and ERP Response Selectivity. *Front Hum Neurosci* **4**, 195 (2010).

121. Kojima, K., Brown, E.C., Matsuzaki, N., Rothermel, R., Fuerst, D., Shah, A., Mittal, S., Sood, S. & Asano, E. Gamma activity modulated by picture and auditory naming tasks: Intracranial recording in patients with focal epilepsy. *Clin Neurophysiol* (2013).

122. Burke, J.F., Zaghloul, K.A., Jacobs, J., Williams, R.B., Sperling, M.R., Sharan, A.D. & Kahana, M.J. Synchronous and asynchronous theta and gamma activity during episodic memory formation. *J Neurosci* **33**, 292-304 (2013).

123. Davidesco, I., Harel, M., Ramot, M., Kramer, U., Kipervasser, S., Andelman, F., Neufeld, M.Y., Goelman, G., Fried, I. & Malach, R. Spatial and object-based attention modulates broadband high-frequency responses across the human visual cortical hierarchy. *J Neurosci* **33**, 1228-1240 (2013).

124. Dalal, S.S., Edwards, E., Kirsch, H.E., Barbaro, N.M., Knight, R.T. & Nagarajan, S.S. Localization of neurosurgically implanted electrodes via photograph-MRI-radiograph coregistration. *J Neurosci Methods* **174**, 106-115 (2008).

125. Hermes, D., Miller, K.J., Noordmans, H.J., Vansteensel, M.J. & Ramsey, N.F. Automated electrocorticographic electrode localization on individually rendered brain surfaces. *J Neurosci Methods* **185**, 293-298 (2010).

126. Dale, A.M., Fischl, B. & Sereno, M.I. Cortical surface-based analysis. I. Segmentation and surface reconstruction. *Neuroimage* **9**, 179-194 (1999).

127. Cox, R.W. AFNI: software for analysis and visualization of functional magnetic resonance neuroimages. *Comput Biomed Res* **29**, 162-173 (1996).

128. R Core Team. R: A Language and Environment for Statistical Computing. (R Foundation for Statistical Computing, 2012).

129. Viechtbauer, W. Conducting meta-analyses in R with the metafor package. *Journal of Statistical Software* **36**, 1-48 (2010).

130. Knapp, G. & Hartung, J. Improved tests for a random effects meta-regression with a single covariate. *Stat Med* **22**, 2693-2710 (2003).

131. Logothetis, N.K., Kayser, C. & Oeltermann, A. In vivo measurement of cortical impedance spectrum in monkeys: implications for signal propagation. *Neuron* **55**, 809-823 (2007).

132. Nathan, S.S., Sinha, S.R., Gordon, B., Lesser, R.P. & Thakor, N.V. Determination of current density distributions generated by electrical stimulation of the human cerebral cortex. *Electroencephalogr Clin Neurophysiol* **86**, 183-192 (1993).

133. Nunez, P.L. & Srinivasan, R. *Electric Fields of the Brain* (Oxford University Press, 2006).

134. Bijsterbosch, J.D., Barker, A.T., Lee, K.H. & Woodruff, P.W.R. Where does transcranial magnetic stimulation (TMS) stimulate? Modelling of induced field maps for some common cortical and cerebellar targets. *Med Biol Eng Comput* **50**, 671-681 (2012).

135. Buzsáki, G. *Rhythms of the Brain* (Oxford University Press, Oxford, 2006).

136. Travis, K.E., Leonard, M.K., Chan, A.M., Torres, C., Sizemore, M.L., Qu, Z., Eskandar, E., Dale, A.M., Elman, J.L., Cash, S.S. & Halgren, E. Independence of early speech processing from word meaning. *Cereb Cortex* **23**, 2370-2379 (2013).

137. Acar, Z.A., Palmer, J., Worrell, G. & Makeig, S. Electrocortical source imaging of intracranial EEG data in epilepsy. *Conf Proc IEEE Eng Med Biol Soc* **2011**, 3909-3912 (2011).

138. Buzsaki, G., Anastassiou, C.A. & Koch, C. The origin of extracellular fields and currents--EEG, ECoG, LFP and spikes. *Nat Rev Neurosci* **13**, 407-420 (2012).

139. Acar, Z.A., Worrell, G. & Makeig, S. Patch-basis electrocortical source imaging in epilepsy. *Conf Proc IEEE Eng Med Biol Soc* **2009**, 2930-2933 (2009).

140. Acar, Z.A., Makeig, S. & Worrell, G. Head modeling and cortical source localization in epilepsy. *Conf Proc IEEE Eng Med Biol Soc* **2008**, 3763-3766 (2008).

141. Argall, B.D., Saad, Z.S. & Beauchamp, M.S. Simplified intersubject averaging on the cortical surface using SUMA. *Hum Brain Mapp* **27**, 14-27 (2006).

142. Fischl, B., Sereno, M.I. & Dale, A.M. Cortical surface-based analysis. II: Inflation, flattening, and a surface-based coordinate system. *Neuroimage* **9**, 195-207 (1999).

143. Ritzl, E.K., Wohlschlaeger, A.M., Crone, N.E., Wohlschlaeger, A., Gingis, L., Bowers, C.W. & Boatman, D.F. Transforming electrocortical mapping data into standardized common space. *Clinical EEG and neuroscience* **38**, 132-136 (2007).

144. Kanwisher, N. & Yovel, G. The fusiform face area: a cortical region specialized for the perception of faces. *Philos Trans R Soc Lond B Biol Sci* **361**, 2109-2128 (2006).

145. McGugin, R.W., Gatenby, J.C., Gore, J.C. & Gauthier, I. High-resolution imaging of expertise reveals reliable object selectivity in the fusiform face area related to perceptual performance. *Proc Natl Acad Sci U S A* **109**, 17063-17068 (2012).

146. Joseph, J.E. Functional neuroimaging studies of category specificity in object recognition: a critical review and meta-analysis. *Cognitive, affective & behavioral neuroscience* **1**, 119-136 (2001).

147. Herrmann, C.S., Munk, M.H. & Engel, A.K. Cognitive functions of gamma-band activity: memory match and utilization. *Trends Cogn Sci* **8**, 347-355 (2004).

148. Mesgarani, N. & Chang, E.F. Selective cortical representation of attended speaker in multi-talker speech perception. *Nature* **485**, 233-236 (2012).

149. Bouchard, K.E., Mesgarani, N., Johnson, K. & Chang, E.F. Functional organization of human sensorimotor cortex for speech articulation. *Nature* **495**, 327-332 (2013).

150. He, B., Yang, L., Wilke, C. & Yuan, H. Electrophysiological imaging of brain activity and connectivity-challenges and opportunities. *IEEE Trans Biomed Eng* **58**, 1918-1931 (2011).

151. Barton, J.J. Higher cortical visual deficits. *Continuum* **20**, 922-941 (2014).

152. Allison, T., Ginter, H., McCarthy, G., Nobre, A.C., Puce, A., Luby, M. & Spencer, D.D. Face recognition in human extrastriate cortex. *J Neurophysiol* **71**, 821-825 (1994).

153. Desimone, R., Albright, T.D., Gross, C.G. & Bruce, C. Stimulus-selective properties of inferior temporal neurons in the macaque. *J Neurosci* **4**, 2051-2062 (1984).

154. Haxby, J.V., Grady, C.L., Horwitz, B., Ungerleider, L.G., Mishkin, M., Carson, R.E., Herscovitch, P., Schapiro, M.B. & Rapoport, S.I. Dissociation of object and spatial visual processing pathways in human extrastriate cortex. *Proc Natl Acad Sci U S A* **88**, 1621-1625 (1991).

155. Peelen, M.V. & Downing, P.E. Selectivity for the human body in the fusiform gyrus. *J Neurophysiol* **93**, 603-608 (2005).

156. Sergent, J., Ohta, S. & MacDonald, B. Functional neuroanatomy of face and object processing. A positron emission tomography study. *Brain* **115 Pt 1**, 15-36 (1992).

157. Tanaka, K. Inferotemporal cortex and object vision. *Annu Rev Neurosci* **19**, 109-139 (1996).

158. Chao, L.L., Haxby, J.V. & Martin, A. Attribute-based neural substrates in temporal cortex for perceiving and knowing about objects. *Nat Neurosci* **2**, 913-919 (1999).

159. Cohen, L., Dehaene, S., Naccache, L., Lehericy, S., Dehaene-Lambertz, G., Henaff, M.A. & Michel, F. The visual word form area: spatial and temporal characterization of an initial stage of reading in normal subjects and posterior split-brain patients. *Brain* **123 (Pt 2)**, 291-307 (2000).

160. Nobre, A.C., Allison, T. & McCarthy, G. Word recognition in the human inferior temporal lobe. *Nature* **372**, 260-263 (1994).

161. Malach, R., Reppas, J.B., Benson, R.R., Kwong, K.K., Jiang, H., Kennedy, W.A., Ledden, P.J., Brady, T.J., Rosen, B.R. & Tootell, R.B. Object-related activity revealed by functional magnetic resonance imaging in human occipital cortex. *Proc Natl Acad Sci U S A* **92**, 8135-8139 (1995).

162. Op de Beeck, H.P., Haushofer, J. & Kanwisher, N.G. Interpreting fMRI data: maps, modules and dimensions. *Nat Rev Neurosci* **9**, 123-135 (2008).

163. Brants, M., Baeck, A., Wagemans, J. & de Beeck, H.P. Multiple scales of organization for object selectivity in ventral visual cortex. *Neuroimage* **56**, 1372-1381 (2011).

164. Dilks, D.D., Julian, J.B., Paunov, A.M. & Kanwisher, N. The occipital place area is causally and selectively involved in scene perception. *J Neurosci* **33**, 1331-1336a (2013).

165. Martin, A., Wiggs, C.L., Ungerleider, L.G. & Haxby, J.V. Neural correlates of category-specific knowledge. *Nature* **379**, 649-652 (1996).

166. Weiner, K.S., Golarai, G., Caspers, J., Chuapoco, M.R., Mohlberg, H., Zilles, K., Amunts, K. & Grill-Spector, K. The mid-fusiform sulcus: a landmark identifying both cytoarchitectonic and functional divisions of human ventral temporal cortex. *Neuroimage* **84**, 453-465 (2014).

167. Konkle, T. & Caramazza, A. Tripartite organization of the ventral stream by animacy and object size. *J Neurosci* **33**, 10235-10242 (2013).

168. Hasson, U., Harel, M., Levy, I. & Malach, R. Large-scale mirror-symmetry organization of human occipito-temporal object areas. *Neuron* **37**, 1027-1041 (2003).

169. Sha, L., Haxby, J.V., Abdi, H., Guntupalli, J.S., Oosterhof, N.N., Halchenko, Y.O. & Connolly, A.C. The animacy continuum in the human ventral vision pathway. *J Cogn Neurosci* **27**, 665-678 (2015).

170. Konkle, T. & Oliva, A. A real-world size organization of object responses in occipitotemporal cortex. *Neuron* **74**, 1114-1124 (2012).

171. Kriegeskorte, N., Mur, M., Ruff, D.A., Kiani, R., Bodurka, J., Esteky, H., Tanaka, K. & Bandettini, P.A. Matching categorical object representations in inferior temporal cortex of man and monkey. *Neuron* **60**, 1126-1141 (2008).

172. Haxby, J.V., Gobbini, M.I., Furey, M.L., Ishai, A., Schouten, J.L. & Pietrini, P. Distributed and overlapping representations of faces and objects in ventral temporal cortex. *Science* **293**, 2425-2430 (2001).

173. Huth, A.G., Nishimoto, S., Vu, A.T. & Gallant, J.L. A continuous semantic space describes the representation of thousands of object and action categories across the human brain. *Neuron* **76**, 1210-1224 (2012).

174. O'Toole, A.J., Jiang, F., Abdi, H., Penard, N., Dunlop, J.P. & Parent, M.A. Theoretical, statistical, and practical perspectives on pattern-based classification approaches to the analysis of functional neuroimaging data. *J Cogn Neurosci* **19**, 1735-1752 (2007).

175. Saxe, R., Brett, M. & Kanwisher, N. Divide and conquer: a defense of functional localizers. *Neuroimage* **30**, 1088-1096; discussion 1097-1089 (2006).

176. Dubois, J., de Berker, A.O. & Tsao, D.Y. Single-unit recordings in the macaque face patch system reveal limitations of fMRI MVPA. *J Neurosci* **35**, 2791-2802 (2015).

177. Haxby, J.V. Multivariate pattern analysis of fMRI: the early beginnings. *Neuroimage* **62**, 852-855 (2012).

178. Allison, T., Puce, A., Spencer, D.D. & McCarthy, G. Electrophysiological studies of human face perception. I: Potentials generated in occipitotemporal cortex by face and non-face stimuli. *Cereb Cortex* **9**, 415-430 (1999).

179. Davidesco, I., Zion-Golumbic, E., Bickel, S., Harel, M., Groppe, D.M., Keller, C.J., Schevon, C.A., McKhann, G.M., Goodman, R.R., Goelman, G., Schroeder, C.E., Mehta, A.D. & Malach, R. Exemplar selectivity reflects perceptual similarities in the human fusiform cortex. *Cereb Cortex* **24**, 1879-1893 (2014).

180. Engell, A.D. & McCarthy, G. The relationship of gamma oscillations and face-specific ERPs recorded subdurally from occipitotemporal cortex. *Cereb Cortex* **21**, 1213-1221 (2011).

181. Engell, A.D. & McCarthy, G. Face, eye, and body selective responses in fusiform gyrus and adjacent cortex: an intracranial EEG study. *Front Hum Neurosci* **8**, 642 (2014).

182. Jonas, J., Descoins, M., Koessler, L., Colnat-Coulbois, S., Sauvee, M., Guye, M., Vignal, J.P., Vespignani, H., Rossion, B. & Maillard, L. Focal electrical intracerebral stimulation of a face-sensitive area causes transient prosopagnosia. *Neuroscience* **222**, 281-288 (2012).

183. Liu, H., Agam, Y., Madsen, J.R. & Kreiman, G. Timing, timing, timing: fast decoding of object information from intracranial field potentials in human visual cortex. *Neuron* **62**, 281-290 (2009).

184. Parvizi, J., Jacques, C., Foster, B.L., Witthoft, N., Rangarajan, V., Weiner, K.S. & Grill-Spector, K. Electrical stimulation of human fusiform face-selective regions distorts face perception. *J Neurosci* **32**, 14915-14920 (2012).

185. Privman, E., Nir, Y., Kramer, U., Kipervasser, S., Andelman, F., Neufeld, M.Y., Mukamel, R., Yeshurun, Y., Fried, I. & Malach, R. Enhanced category tuning revealed

by intracranial electroencephalograms in high-order human visual areas. *J Neurosci* **27**, 6234-6242 (2007).

186. Bastin, J., Vidal, J.R., Bouvier, S., Perrone-Bertolotti, M., Benis, D., Kahane, P., David, O., Lachaux, J.P. & Epstein, R.A. Temporal components in the parahippocampal place area revealed by human intracerebral recordings. *J Neurosci* **33**, 10123-10131 (2013).

187. Snodgrass, J.G. & Vanderwart, M. A standardized set of 260 pictures: norms for name agreement, image agreement, familiarity, and visual complexity. *Journal of Experimental Psychology: Human Learning & Memory* **6**, 174-215 (1980).

188. McCandliss, B.D., Cohen, L. & Dehaene, S. The visual word form area: expertise for reading in the fusiform gyrus. *Trends Cogn Sci* **7**, 293-299 (2003).

189. Wandell, B.A., Rauschecker, A.M. & Yeatman, J.D. Learning to see words. *Annu Rev Psychol* **63**, 31-53 (2012).

190. Yeatman, J.D., Rauschecker, A.M. & Wandell, B.A. Anatomy of the visual word form area: adjacent cortical circuits and long-range white matter connections. *Brain Lang* **125**, 146-155 (2013).

191. Ellmore, T.M., Beauchamp, M.S., O'Neill, T.J., Dreyer, S. & Tandon, N. Relationships between essential cortical language sites and subcortical pathways. *J Neurosurg* **111**, 755-766 (2009).

192. Talairach, J. & Tournoux, P. *Co-Planar Stereotaxic Atlas of the Human Brain* (Theime Medical Publishers, Inc., New York, 1988).

193. Fischl, B., Sereno, M., Tootell, R.B.H. & Dale, A.M. High-resolution intersubject averaging and a coordinate system for the cortical surface. *Hum Brain Mapp* **8**, 272-284 (1999).

194. Holmes, C.J., Hoge, R., Collins, L., Woods, R., Toga, A.W. & Evans, A.C. Enhancement of MR images using registration for signal averaging. *J Comput Assist Tomogr* **22**, 324-333 (1998).

195. Crone, N.E., Boatman, D., Gordon, B. & Hao, L. Induced electrocorticographic gamma activity during auditory perception. Brazier Award-winning article, 2001. *Clin Neurophysiol* **112**, 565-582 (2001).

196. Fisch, L., Privman, E., Ramot, M., Harel, M., Nir, Y., Kipervasser, S., Andelman, F., Neufeld, M.Y., Kramer, U., Fried, I. & Malach, R. Neural "ignition": enhanced activation linked to perceptual awareness in human ventral stream visual cortex. *Neuron* **64**, 562-574 (2009).

197. Rodriguez, E., George, N., Lachaux, J.P., Martinerie, J., Renault, B. & Varela, F.J. Perception's shadow: long-distance synchronization of human brain activity. *Nature* **397**, 430-433 (1999).

198. Hermes, D., Miller, K.J., Wandell, B.A. & Winawer, J. Stimulus Dependence of Gamma Oscillations in Human Visual Cortex. *Cereb Cortex* (2014).

199. Miller, K.J., Honey, C.J., Hermes, D., Rao, R.P., denNijs, M. & Ojemann, J.G. Broadband changes in the cortical surface potential track activation of functionally diverse neuronal populations. *Neuroimage* **85 Pt 2**, 711-720 (2014).

200. Kreiman, G., Hung, C.P., Kraskov, A., Quiroga, R.Q., Poggio, T. & DiCarlo, J.J. Object selectivity of local field potentials and spikes in the macaque inferior temporal cortex. *Neuron* **49**, 433-445 (2006).

201. Manning, J.R., Jacobs, J., Fried, I. & Kahana, M.J. Broadband shifts in local field potential power spectra are correlated with single-neuron spiking in humans. *J Neurosci* **29**, 13613-13620 (2009).

202. Miller, K.J., Sorensen, L.B., Ojemann, J.G. & den Nijs, M. Power-law scaling in the brain surface electric potential. *PLoS Comput Biol* **5**, e1000609 (2009).

203. He, B.J., Snyder, A.Z., Zempel, J.M., Smyth, M.D. & Raichle, M.E. Electrophysiological correlates of the brain's intrinsic large-scale functional architecture. *Proc Natl Acad Sci U S A* **105**, 16039-16044 (2008).

204. Winawer, J., Kay, K.N., Foster, B.L., Rauschecker, A.M., Parvizi, J. & Wandell, B.A. Asynchronous broadband signals are the principal source of the BOLD response in human visual cortex. *Curr Biol* **23**, 1145-1153 (2013).

205. Afraz, S.R., Kiani, R. & Esteky, H. Microstimulation of inferotemporal cortex influences face categorization. *Nature* **442**, 692-695 (2006).

206. Ghuman, A.S., Brunet, N.M., Li, Y., Konecky, R.O., Pyles, J.A., Walls, S.A., Destefino, V., Wang, W. & Richardson, R.M. Dynamic encoding of face information in the human fusiform gyrus. *Nature communications* **5**, 5672 (2014).

207. Green, D.M. & Swets, J.A. *Signal Detection Theory and Psychophysics* (Wiley, New York, 1966).

208. Matsuo, T., Kawasaki, K., Kawai, K., Majima, K., Masuda, H., Murakami, H., Kunii, N., Kamitani, Y., Kameyama, S., Saito, N. & Hasegawa, I. Alternating Zones Selective to Faces and Written Words in the Human Ventral Occipitotemporal Cortex. *Cereb Cortex* (2013).

209. Tang, H., Buia, C., Madhavan, R., Crone, N.E., Madsen, J.R., Anderson, W.S. & Kreiman, G. Spatiotemporal dynamics underlying object completion in human ventral visual cortex. *Neuron* **83**, 736-748 (2014).

210. Rouse, A.G., Williams, J.J., Wheeler, J.J. & Moran, D.W. Cortical adaptation to a chronic micro-electrocorticographic brain computer interface. *J Neurosci* **33**, 1326-1330 (2013).

211. Benjamini, Y.H.Y. Controlling the False Discovery Rate: A Practical and Powerful Approach to Multiple Testing. *Journal of the Royal Statistical Society B* **57**, 289 - 300 (1995).

212. Wickham, H. *ggplot2: elegant graphics for data analysis* (Springer New York, 2009).

213. Bates D., M.M.B.B.M.W.S. Fitting Linear Mixed-Effects Models using lme4. *Journal of Statistical Software* (2015).

214. Bates, D.M., M.; Bolker, B.; Walker, S. lme4: Linear mixed-effects models using Eigen and S4. *R package version 1.1-8* (2015).

215. Kuznetsova, A.B., B.; Christensen, H.B;. lmerTest: Tests in Linear Mixed Effects Modles. *R package version 2.0-29* (2015).

216. Baayen, R.H.D.D.J.B., D.M. Mixed-effects modeling with crossed random effects for subjects and items. *Journal of memory and language*, 390-412 (2008).

217. Falk, E.B., O'Donnell, M.B., Cascio, C.N., Tinney, F., Kang, Y., Lieberman, M.D., Taylor, S.E., An, L., Resnicow, K. & Strecher, V.J. Self-affirmation alters the brain's response to health messages and subsequent behavior change. *Proc Natl Acad Sci U S A* **112**, 1977-1982 (2015).

218. Price, C.J. & Devlin, J.T. The interactive account of ventral occipitotemporal contributions to reading. *Trends Cogn Sci* **15**, 246-253 (2011).

219. Dehaene, S. & Cohen, L. The unique role of the visual word form area in reading. *Trends Cogn Sci* **15**, 254-262.

220. Pourtois, G., Peelen, M.V., Spinelli, L., Seeck, M. & Vuilleumier, P. Direct intracranial recording of body-selective responses in human extrastriate visual cortex. *Neuropsychologia* **45**, 2621-2625 (2007).

221. Weiner, K.S. & Grill-Spector, K. Not one extrastriate body area: using anatomical landmarks, hMT+, and visual field maps to parcellate limb-selective activations in human lateral occipitotemporal cortex. *Neuroimage* **56**, 2183-2199 (2011).

222. Lingnau, A. & Downing, P.E. The lateral occipitotemporal cortex in action. *Trends Cogn Sci* **19**, 268-277 (2015).

223. Bentin, S., Allison, T., Puce, A., Perez, E. & McCarthy, G. Electrophysiological Studies of Face Perception in Humans. *J Cogn Neurosci* **8**, 551-565 (1996).

224. Caramazza, A. & Mahon, B.Z. The organization of conceptual knowledge: the evidence from category-specific semantic deficits. *Trends Cogn Sci* **7**, 354-361 (2003).

225. Chan, A.M., Baker, J.M., Eskandar, E., Schomer, D., Ulbert, I., Marinkovic, K., Cash, S.S. & Halgren, E. First-pass selectivity for semantic categories in human anteroventral temporal lobe. *J Neurosci* **31**, 18119-18129 (2011).

226. Drane, D.L., Ojemann, G.A., Aylward, E., Ojemann, J.G., Johnson, L.C., Silbergeld, D.L., Miller, J.W. & Tranel, D. Category-specific naming and recognition deficits in temporal lobe epilepsy surgical patients. *Neuropsychologia* **46**, 1242-1255 (2008).

227. Gauthier, I., Skudlarski, P., Gore, J.C. & Anderson, A.W. Expertise for cars and birds recruits brain areas involved in face recognition. *Nat Neurosci* **3**, 191-197 (2000).

228. Kojima, K., Brown, E.C., Matsuzaki, N. & Asano, E. Animal category-preferential gamma-band responses in the lower- and higher-order visual areas: intracranial recording in children. *Clin Neurophysiol* **124**, 2368-2377 (2013).

229. Martin, A. The representation of object concepts in the brain. *Annu Rev Psychol* **58**, 25-45 (2007).

230. Puce, A., Allison, T. & McCarthy, G. Electrophysiological studies of human face perception. III: Effects of top-down processing on face-specific potentials. *Cereb Cortex* **9**, 445-458 (1999).

231. Privman, E., Fisch, L., Neufeld, M.Y., Kramer, U., Kipervasser, S., Andelman, F., Yeshurun, Y., Fried, I. & Malach, R. Antagonistic relationship between gamma power and visual evoked potentials revealed in human visual cortex. *Cereb Cortex* **21**, 616-624 (2011).

232. Capitani, E., Laiacona, M., Mahon, B. & Caramazza, A. What are the facts of semantic category-specific deficits? A critical review of the clinical evidence. *Cognitive neuropsychology* **20**, 213-261 (2003).

233. Avidan, G., Harel, M., Hendler, T., Ben-Bashat, D., Zohary, E. & Malach, R. Contrast sensitivity in human visual areas and its relationship to object recognition. *J Neurophysiol* **87**, 3102-3116 (2002).

234. Davidenko, N., Remus, D.A. & Grill-Spector, K. Face-likeness and image variability drive responses in human face-selective ventral regions. *Hum Brain Mapp* **33**, 2334-2349 (2012).

235. Grill-Spector, K., Kushnir, T., Edelman, S., Itzchak, Y. & Malach, R. Cue-invariant activation in object-related areas of the human occipital lobe. *Neuron* **21**, 191-202 (1998).

236. Kourtzi, Z. & Kanwisher, N. Representation of perceived object shape by the human lateral occipital complex. *Science* **293**, 1506-1509 (2001).

237. Mendola, J.D., Dale, A.M., Fischl, B., Liu, A.K. & Tootell, R.B. The representation of illusory and real contours in human cortical visual areas revealed by functional magnetic resonance imaging. *J Neurosci* **19**, 8560-8572 (1999).

238. Moutoussis, K. & Zeki, S. The relationship between cortical activation and perception investigated with invisible stimuli. *Proc Natl Acad Sci U S A* **99**, 9527-9532 (2002).

239. Vinberg, J. & Grill-Spector, K. Representation of shapes, edges, and surfaces across multiple cues in the human visual cortex. *J Neurophysiol* **99**, 1380-1393 (2008).

240. Walther, D.B., Chai, B., Caddigan, E., Beck, D.M. & Fei-Fei, L. Simple line drawings suffice for functional MRI decoding of natural scene categories. *Proc Natl Acad Sci U S A* **108**, 9661-9666 (2011).

241. Andrews, T.J., Clarke, A., Pell, P. & Hartley, T. Selectivity for low-level features of objects in the human ventral stream. *Neuroimage* **49**, 703-711 (2010).

242. Baldassi, C., Alemi-Neissi, A., Pagan, M., Dicarlo, J.J., Zecchina, R. & Zoccolan, D. Shape similarity, better than semantic membership, accounts for the structure of visual object representations in a population of monkey inferotemporal neurons. *PLoS Comput Biol* **9**, e1003167 (2013).

243. Rice, G.E., Watson, D.M., Hartley, T. & Andrews, T.J. Low-level image properties of visual objects predict patterns of neural response across category-selective regions of the ventral visual pathway. *J Neurosci* **34**, 8837-8844 (2014).

244. Mahon, B.Z., Anzellotti, S., Schwarzbach, J., Zampini, M. & Caramazza, A. Category-specific organization in the human brain does not require visual experience. *Neuron* **63**, 397-405 (2009).

245. Khaligh-Razavi, S.M. & Kriegeskorte, N. Deep supervised, but not unsupervised, models may explain IT cortical representation. *PLoS Comput Biol* **10**, e1003915 (2014).

246. Connolly, A.C., Guntupalli, J.S., Gors, J., Hanke, M., Halchenko, Y.O., Wu, Y.C., Abdi, H. & Haxby, J.V. The representation of biological classes in the human brain. *J Neurosci* **32**, 2608-2618 (2012).

247. Bruce, V. & Young, A. Understanding face recognition. *Br J Psychol* **77 (Pt 3)**, 305-327 (1986).

248. Fairhall, S.L. & Ishai, A. Effective connectivity within the distributed cortical network for face perception. *Cereb Cortex* **17**, 2400-2406 (2007).

249. Catani, M., Jones, D.K., Donato, R. & Ffytche, D.H. Occipito-temporal connections in the human brain. *Brain* **126**, 2093-2107 (2003).

250. McCarthy, G., Puce, A., Belger, A. & Allison, T. Electrophysiological studies of human face perception. II: Response properties of face-specific potentials generated in occipitotemporal cortex. *Cereb Cortex* **9**, 431-444 (1999).

251. Halgren, E., Baudena, P., Heit, G., Clarke, J.M., Marinkovic, K. & Clarke, M. Spatio-temporal stages in face and word processing. I. Depth-recorded potentials in the human occipital, temporal and parietal lobes [corrected]. *J Physiol Paris* **88**, 1-50 (1994).

252. Pourtois, G., Schwartz, S., Spiridon, M., Martuzzi, R. & Vuilleumier, P. Object representations for multiple visual categories overlap in lateral occipital and medial fusiform cortex. *Cereb Cortex* **19**, 1806-1819 (2009).

253. Hamame, C.M., Vidal, J.R., Perrone-Bertolotti, M., Ossandon, T., Jerbi, K., Kahane, P., Bertrand, O. & Lachaux, J.P. Functional selectivity in the human occipitotemporal cortex during natural vision: Evidence from combined intracranial EEG and eye-tracking. *Neuroimage* (2014).

254. Lachaux, J.P., George, N., Tallon-Baudry, C., Martinerie, J., Hugueville, L., Minotti, L., Kahane, P. & Renault, B. The many faces of the gamma band response to complex visual stimuli. *Neuroimage* **25**, 491-501 (2005).

255. Tsuchiya, N., Kawasaki, H., Oya, H., Howard, M.A., 3rd & Adolphs, R. Decoding face information in time, frequency and space from direct intracranial recordings of the human brain. *PLoS One* **3**, e3892 (2008).

256. Barbeau, E.J., Taylor, M.J., Regis, J., Marquis, P., Chauvel, P. & Liegeois-Chauvel, C. Spatio temporal dynamics of face recognition. *Cereb Cortex* **18**, 997-1009 (2008).

257. Bruns, A., Eckhorn, R., Jokeit, H. & Ebner, A. Amplitude envelope correlation detects coupling among incoherent brain signals. *Neuroreport* **11**, 1509-1514 (2000).

258. Vidal, J.R., Freyermuth, S., Jerbi, K., Hamame, C.M., Ossandon, T., Bertrand, O., Minotti, L., Kahane, P., Berthoz, A. & Lachaux, J.P. Long-distance amplitude correlations in the high gamma band reveal segregation and integration within the reading network. *J Neurosci* **32**, 6421-6434 (2012).

259. Matsumoto, R., Nair, D.R., LaPresto, E., Najm, I., Bingaman, W., Shibasaki, H. & Luders, H.O. Functional connectivity in the human language system: a cortico-cortical evoked potential study. *Brain* **127**, 2316-2330 (2004).

260. Ojemann, G., Ojemann, J., Lettich, E. & Berger, M. Cortical language localization in left, dominant hemisphere. An electrical stimulation mapping investigation in 117 patients. *J Neurosurg* **71**, 316-326 (1989).

261. Wang, L., Mruczek, R.E., Arcaro, M.J. & Kastner, S. Probabilistic Maps of Visual Topography in Human Cortex. *Cereb Cortex* (2014).

262. Murphey, D.K., Maunsell, J.H., Beauchamp, M.S. & Yoshor, D. Perceiving electrical stimulation of identified human visual areas. *Proc Natl Acad Sci U S A* **106**, 5389-5393 (2009).

263. Yoshor, D., Bosking, W.H., Ghose, G.M. & Maunsell, J.H. Receptive fields in human visual cortex mapped with surface electrodes. *Cereb Cortex* **17**, 2293-2302 (2007).

264. Wandell, B.A. & Winawer, J. Imaging retinotopic maps in the human brain. *Vision Res* **51**, 718-737 (2011).

265. Rossion, B., Hanseeuw, B. & Dricot, L. Defining face perception areas in the human brain: a large-scale factorial fMRI face localizer analysis. *Brain Cogn* **79**, 138-157 (2012).

266. Pitcher, D., Walsh, V. & Duchaine, B. The role of the occipital face area in the cortical face perception network. *Exp Brain Res* **209**, 481-493 (2011).

267. Tsao, D.Y., Moeller, S. & Freiwald, W.A. Comparing face patch systems in macaques and humans. *Proc Natl Acad Sci U S A* **105**, 19514-19519 (2008).

268. Jonas, J., Frismand, S., Vignal, J.P., Colnat-Coulbois, S., Koessler, L., Vespignani, H., Rossion, B. & Maillard, L. Right hemispheric dominance of visual phenomena evoked by intracerebral stimulation of the human visual cortex. *Hum Brain Mapp* **35**, 3360-3371 (2014).

269. Jonas, J., Rossion, B., Krieg, J., Koessler, L., Colnat-Coulbois, S., Vespignani, H., Jacques, C., Vignal, J.P., Brissart, H. & Maillard, L. Intracerebral electrical stimulation of a face-selective area in the right inferior occipital cortex impairs individual face discrimination. *Neuroimage* **99**, 487-497 (2014).

270. Rangarajan, V., Hermes, D., Foster, B.L., Weiner, K.S., Jacques, C., Grill-Spector, K. & Parvizi, J. Electrical stimulation of the left and right human fusiform gyrus causes different effects in conscious face perception. *J Neurosci* **34**, 12828-12836 (2014).

271. Pitcher, D., Goldhaber, T., Duchaine, B., Walsh, V. & Kanwisher, N. Two critical and functionally distinct stages of face and body perception. *J Neurosci* **32**, 15877-15885 (2012).

272. Aru, J., Axmacher, N., Do Lam, A.T., Fell, J., Elger, C.E., Singer, W. & Melloni, L. Local category-specific gamma band responses in the visual cortex do not reflect conscious perception. *J Neurosci* **32**, 14909-14914 (2012).

273. Varela, F., Lachaux, J.P., Rodriguez, E. & Martinerie, J. The brainweb: phase synchronization and large-scale integration. *Nat Rev Neurosci* **2**, 229-239 (2001).

274. Canolty, R.T., Edwards, E., Dalal, S.S., Soltani, M., Nagarajan, S.S., Kirsch, H.E., Berger, M.S., Barbaro, N.M. & Knight, R.T. High gamma power is phase-locked to theta oscillations in human neocortex. *Science* **313**, 1626-1628 (2006).

275. Hipp, J.F., Hawellek, D.J., Corbetta, M., Siegel, M. & Engel, A.K. Large-scale cortical correlation structure of spontaneous oscillatory activity. *Nat Neurosci* (2012).

276. Adhikari, A., Sigurdsson, T., Topiwala, M.A. & Gordon, J.A. Cross-correlation of instantaneous amplitudes of field potential oscillations: a straightforward method to estimate the directionality and lag between brain areas. *J Neurosci Methods* **191**, 191-200 (2010).

277. Conner, C.R. Network Dynamics of Visual Naming. in *Neuroscience* 123 (University of Texas Graduate School of Biomedical Sciences at Houston, Digital Commons at Texas Medical Center, 2013).

278. Keller, C.J., Honey, C.J., Megevand, P., Entz, L., Ulbert, I. & Mehta, A.D. Mapping human brain networks with cortico-cortical evoked potentials. *Philos Trans R Soc Lond B Biol Sci* **369** (2014).

279. Conner, C.R., Ellmore, T.M., Disano, M.A., Pieters, T.A., Potter, A.W. & Tandon, N. Anatomic and electro-physiologic connectivity of the language system: A combined DTI-CCEP study. *Comput Biol Med* (2011).

280. Swann, N.C., Cai, W., Conner, C.R., Pieters, T.A., Claffey, M.P., George, J.S., Aron, A.R. & Tandon, N. Roles for the pre-supplementary motor area and the right inferior frontal gyrus in stopping action: electrophysiological responses and functional and structural connectivity. *Neuroimage* **59**, 2860-2870 (2012).

281. Keller, C.J., Bickel, S., Entz, L., Ulbert, I., Milham, M.P., Kelly, C. & Mehta, A.D. Intrinsic functional architecture predicts electrically evoked responses in the human brain. *Proc Natl Acad Sci U S A* (2011).

282. Tandon, N. Mapping of Human Language. in *Clinical Brain Mapping* (ed. D. Yoshor) 203-218 (McGraw Hill, 2012).

283. Desmurget, M., Song, Z., Mottolese, C. & Sirigu, A. Re-establishing the merits of electrical brain stimulation. *Trends Cogn Sci* **17**, 442-449 (2013).

284. Penfield, W. & Perot, P. The Brain's Record of Auditory and Visual Experience. A Final Summary and Discussion. *Brain* **86**, 595-696 (1963).

285. Selimbeyoglu, A. & Parvizi, J. Electrical stimulation of the human brain: perceptual and behavioral phenomena reported in the old and new literature. *Front Hum Neurosci* **4**, 46 (2010).

286. Jiang, F., Dricot, L., Weber, J., Righi, G., Tarr, M.J., Goebel, R. & Rossion, B. Face categorization in visual scenes may start in a higher order area of the right fusiform gyrus: evidence from dynamic visual stimulation in neuroimaging. *J Neurophysiol* **106**, 2720-2736 (2011).

287. Rayner, K. Eye movements and attention in reading, scene perception, and visual search. *Quarterly journal of experimental psychology* **62**, 1457-1506 (2009).

288. Summerfield, C. & Egner, T. Expectation (and attention) in visual cognition. *Trends Cogn Sci* **13**, 403-409 (2009).

289. Esterman, M. & Yantis, S. Perceptual expectation evokes category-selective cortical activity. *Cereb Cortex* **20**, 1245-1253 (2010).

290. Puri, A.M., Wojciulik, E. & Ranganath, C. Category expectation modulates baseline and stimulus-evoked activity in human inferotemporal cortex. *Brain Res* **1301**, 89-99 (2009).

291. Zhang, H., Tian, J., Liu, J., Li, J. & Lee, K. Intrinsically organized network for face perception during the resting state. *Neurosci Lett* **454**, 1-5 (2009).

292. Davies-Thompson, J. & Andrews, T.J. Intra- and interhemispheric connectivity between face-selective regions in the human brain. *J Neurophysiol* **108**, 3087-3095 (2012).

293. Zhu, Q., Zhang, J., Luo, Y.L., Dilks, D.D. & Liu, J. Resting-state neural activity across face-selective cortical regions is behaviorally relevant. *J Neurosci* **31**, 10323-10330 (2011).

294. Matsuzaki, N., Juhasz, C. & Asano, E. Cortico-cortical evoked potentials and stimulation-elicited gamma activity preferentially propagate from lower- to higher-order visual areas. *Clin Neurophysiol* **124**, 1290-1296 (2013).

295. Lee, H.W., Hong, S.B., Seo, D.W., Tae, W.S. & Hong, S.C. Mapping of functional organization in human visual cortex: electrical cortical stimulation. *Neurology* **54**, 849-854 (2000).

296. Brindley, G.S. & Lewin, W.S. The sensations produced by electrical stimulation of the visual cortex. *J Physiol* **196**, 479-493 (1968).

297. Matsuzaki, N.S., R.F.; Nishida, M.; Ofen, N.; Asano, E. Upright face-preferential high-gamma responses in lower-order visual areas: evidence from intracranial recordings in children. *Neuroimage* (2015).

298. Tandon, N., Alexopoulos, A.V., Warbel, A., Najm, I.M. & Bingaman, W.E. Occipital epilepsy: spatial categorization and surgical management. *J Neurosurg* **110**, 306-318 (2009).

299. Schwarzlose, R.F., Swisher, J.D., Dang, S. & Kanwisher, N. The distribution of category and location information across object-selective regions in human visual cortex. *Proc Natl Acad Sci U S A* **105**, 4447-4452 (2008).

300. Solomon-Harris, L.M., Mullin, C.R. & Steeves, J.K. TMS to the "occipital face area" affects recognition but not categorization of faces. *Brain Cogn* **83**, 245-251 (2013).

301. Genetti, M., Tyrand, R., Grouiller, F., Lascano, A.M., Vulliemoz, S., Spinelli, L., Seeck, M., Schaller, K. & Michel, C.M. Comparison of high gamma electrocorticography and fMRI with electrocortical stimulation for localization of somatosensory and language cortex. *Clin Neurophysiol* **126**, 121-130 (2015).

302. Sinai, A., Bowers, C.W., Crainiceanu, C.M., Boatman, D., Gordon, B., Lesser, R.P., Lenz, F.A. & Crone, N.E. Electrocorticographic high gamma activity versus electrical cortical stimulation mapping of naming. *Brain* **128**, 1556-1570 (2005).

303. Rudrauf, D., David, O., Lachaux, J.P., Kovach, C.K., Martinerie, J., Renault, B. & Damasio, A. Rapid interactions between the ventral visual stream and emotion-related structures rely on a two-pathway architecture. *J Neurosci* **28**, 2793-2803 (2008).

304. Keil, A., Muller, M.M., Ray, W.J., Gruber, T. & Elbert, T. Human gamma band activity and perception of a gestalt. *J Neurosci* **19**, 7152-7161 (1999).

305. Weiner, K.S.M., L.; Jonas, J.; Brissart, H.; Hossu, G.; Jacques, C.; Loftus, D.; Gomez, J.; Grill-Spector, K.; Rossion, B.;. The resiliency of cortical networks: Stable functional organization of the face processing network after surgical resection of the right inferior occipital gyrus. in *Society for Neuroscience* (Washington, D.C., 2014).

306. Rossion, B. & Caharel, S. ERP evidence for the speed of face categorization in the human brain: Disentangling the contribution of low-level visual cues from face perception. *Vision Res* **51**, 1297-1311 (2011).

307. Braeutigam, S., Bailey, A.J. & Swithenby, S.J. Task-dependent early latency (30-60 ms) visual processing of human faces and other objects. *Neuroreport* **12**, 1531-1536 (2001).

308. Johnson, M.H. Subcortical face processing. *Nat Rev Neurosci* **6**, 766-774 (2005).

309. Kiani, R., Esteky, H. & Tanaka, K. Differences in onset latency of macaque inferotemporal neural responses to primate and non-primate faces. *J Neurophysiol* **94**, 1587-1596 (2005).

310. Sugase, Y., Yamane, S., Ueno, S. & Kawano, K. Global and fine information coded by single neurons in the temporal visual cortex. *Nature* **400**, 869-873 (1999).

311. Seeck, M., Michel, C.M., Mainwaring, N., Cosgrove, R., Blume, H., Ives, J., Landis, T. & Schomer, D.L. Evidence for rapid face recognition from human scalp and intracranial electrodes. *Neuroreport* **8**, 2749-2754 (1997).

312. Rossion, B. Understanding face perception by means of human electrophysiology. *Trends Cogn Sci* **18**, 310-318 (2014).

313. Gschwind, M., Pourtois, G., Schwartz, S., Van De Ville, D. & Vuilleumier, P. White-matter connectivity between face-responsive regions in the human brain. *Cereb Cortex* **22**, 1564-1576 (2012).

314. Kim, M., Ducros, M., Carlson, T., Ronen, I., He, S., Ugurbil, K. & Kim, D.S. Anatomical correlates of the functional organization in the human occipitotemporal cortex. *Magn Reson Imaging* **24**, 583-590 (2006).

315. Pitcher, D., Walsh, V., Yovel, G. & Duchaine, B. TMS evidence for the involvement of the right occipital face area in early face processing. *Curr Biol* **17**, 1568-1573 (2007).

316. Chong, S.C., Jo, S., Park, K.M., Joo, E.Y., Lee, M.J., Hong, S.C. & Hong, S.B. Interaction between the electrical stimulation of a face-selective area and the perception of face stimuli. *Neuroimage* **77**, 70-76 (2013).

317. Megevand, P., Groppe, D.M., Goldfinger, M.S., Hwang, S.T., Kingsley, P.B., Davidesco, I. & Mehta, A.D. Seeing scenes: topographic visual hallucinations evoked by direct electrical stimulation of the parahippocampal place area. *J Neurosci* **34**, 5399-5405 (2014).

318. Wessel, J.R., Conner, C.R., Aron, A.R. & Tandon, N. Chronometric electrical stimulation of right inferior frontal cortex increases motor braking. *J Neurosci* **33**, 19611-19619 (2013).

319. Moldakarimov, S., Bazhenov, M. & Sejnowski, T.J. Perceptual priming leads to reduction of gamma frequency oscillations. *Proc Natl Acad Sci U S A* **107**, 5640-5645 (2010).

320. Bar, M., Kassam, K.S., Ghuman, A.S., Boshyan, J., Schmid, A.M., Dale, A.M., Hamalainen, M.S., Marinkovic, K., Schacter, D.L., Rosen, B.R. & Halgren, E. Top-down facilitation of visual recognition. *Proc Natl Acad Sci U S A* **103**, 449-454 (2006).

321. Hochstein, S. & Ahissar, M. View from the top: hierarchies and reverse hierarchies in the visual system. *Neuron* **36**, 791-804 (2002).

322. Friston, K. A theory of cortical responses. *Philos Trans R Soc Lond B Biol Sci* **360**, 815-836 (2005).

323. Bever, T.G.P., D. Analysis by Synthesis: A (Re-Emerging Program of Research for Language and Vision. *Biolinguistics* **4** (2010).

324. Damasio, A.R., Tranel, D. & Damasio, H. Face agnosia and the neural substrates of memory. *Annu Rev Neurosci* **13**, 89-109 (1990).

325. Kluver, H. *Mescal, The 'Divine' Plant and Its Psychological Effects* (K. Paul, Trent and Trubner & Company Limited, London, 1928).

326. Finger, S. *Origins of Neuroscience* (Oxford University Press, New York, 1994).

327. Gross, C.G. Aristotle on the Brain. *Neuroscientist* **1**, 245-250 (1995).

328. Bennett, M.R. & Hacker, P.M. The motor system in neuroscience: a history and analysis of conceptual developments. *Prog Neurobiol* **67**, 1-52 (2002).

329. Green, C.D. Where did the ventricular localization of mental faculties come from? *J Hist Behav Sci* **39**, 131-142 (2003).

330. Gross, C.G. From Imhotep to Hubel and Wiesel: The Story of Visual Cortex. in *Cerebral Cortex: Volume 12: Extrastriate Cortex in Primates* (ed. K.S.K. Rockand, J.H. Peters, A.) 1-58 (Plenum Press, New York, 1997).

331. Gross, C.G. How inferior temporal cortex became a visual area. *Cereb Cortex* **4**, 455-469 (1994).

332. Finger, S. The Era of Cortical Localization. in *Origins of Neuroscience* (Oxford University Press, New York, 1994).

333. Broca, P. Remarques sur le siège de la faculté du langage articulé; suivies d'une observation d'aphémie (perte de la parole). *Bulletins de la Société Anatomique (Paris)* **6**, 330-357, 398-407 (1861).

334. Ferrier, D. The Functions of the Brain. . *Smith, Elder, & Co., London.* (1886).

335. Nahm, F.K. & Pribram, K.H. Heinrich Kluver: May 25, 1897-February 8, 1979. *Biographical memoirs. National Academy of Sciences* **73**, 289-305 (1998).

336. Lashley, K.S. The mechanism of vision; effects of destroying the visual associative areas of the monkey. *Genetic psychology monographs* **37**, 107-166 (1948).

337. Chow, K.L. Effects of partial extirpations of the posterior association cortex on visually mediated behavior. *Comp Psychol Monogr* **20**, 187-217 (1951).

338. Chow, K.L. & Hutt, P.J. The association cortex of Macaca mulatta: a review of recent contributions to its anatomy and functions. *Brain* **76**, 625-677 (1953).

339. Mishkin, M. Visual discrimination performance following partial ablations of the temporal lobe. II. Ventral surface vs. hippocampus. *Journal of comparative and physiological psychology* **47**, 187-193 (1954).

340. Mishkin, M. & Pribram, K.H. Visual discrimination performance following partial ablations of the temporal lobe. I. Ventral vs. lateral. *Journal of comparative and physiological psychology* **47**, 14-20 (1954).

341. Mishkin, M. Visual mechanims beyond the striate cortex. in *Frontiers in physiological psychology* (ed. R.W. Russell) (Academic Press, New York, 1966).

342. Woolsey, C.N. Comparative studies on cortical representation of vision. *Vision Res* **Suppl 3**, 365-382 (1971).

343. Ungerleider, L.M., M. Two cortical visual systems. in *Analysis of Visual Behavior* (ed. D.G. Ingle, M.A.; Mansfield, R.J.W.) 549-586 (MIT Press, Cambridge, MA, 1982).

344. WHO. Epilepsy: aetiology, epidemiology and prognosis **Fact Sheet No 999** (2015).

345. Banerjee, P.N., Filippi, D. & Allen Hauser, W. The descriptive epidemiology of epilepsy-a review. *Epilepsy Res* **85**, 31-45 (2009).

346. Fisher, R.S., Acevedo, C., Arzimanoglou, A., Bogacz, A., Cross, J.H., Elger, C.E., Engel, J., Jr., Forsgren, L., French, J.A., Glynn, M., Hesdorffer, D.C., Lee, B.I., Mathern, G.W., Moshe, S.L., Perucca, E., Scheffer, I.E., Tomson, T., Watanabe, M. & Wiebe, S. ILAE official report: a practical clinical definition of epilepsy. *Epilepsia* **55**, 475-482 (2014).

347. Berg, A.T., Berkovic, S.F., Brodie, M.J., Buchhalter, J., Cross, J.H., van Emde Boas, W., Engel, J., French, J., Glauser, T.A., Mathern, G.W., Moshe, S.L., Nordli, D., Plouin, P. & Scheffer, I.E. Revised terminology and concepts for organization of seizures and epilepsies: report of the ILAE Commission on Classification and Terminology, 2005-2009. *Epilepsia* **51**, 676-685 (2010).

348. Chang, B.S. & Lowenstein, D.H. Epilepsy. *N Engl J Med* **349**, 1257-1266 (2003).

349. Sisodiya, S. Etiology and management of refractory epilepsies. *Nature clinical practice. Neurology* **3**, 320-330 (2007).

350. Kwan, P., Schachter, S.C. & Brodie, M.J. Drug-resistant epilepsy. *N Engl J Med* **365**, 919-926 (2011).

351. Berg, A.T. Epidemiology of the intractable generalized epilepsies. in *Textbook of Epilepsy Surgery* (ed. H. Luders) 207-214 (Informa Healthcare, United Kingdom, 2008).

352. Neligan, A., Hauser, W.A. & Sander, J.W. The epidemiology of the epilepsies. *Handbook of clinical neurology* **107**, 113-133 (2012).

353. Sander, J.W. The epidemiology of epilepsy revisited. *Curr Opin Neurol* **16**, 165-170 (2003).

354. McHugh, J.C. & Delanty, N. Epidemiology and classification of epilepsy: gender comparisons. *Int Rev Neurobiol* **83**, 11-26 (2008).

355. Russ, S.A., Larson, K. & Halfon, N. A national profile of childhood epilepsy and seizure disorder. *Pediatrics* **129**, 256-264 (2012).

356. Murphy, C.C., Trevathan, E. & Yeargin-Allsopp, M. Prevalence of epilepsy and epileptic seizures in 10-year-old children: results from the Metropolitan Atlanta Developmental Disabilities Study. *Epilepsia* **36**, 866-872 (1995).

357. Centers for Disease, C. & Prevention. Epilepsy in adults and access to care--United States, 2010. *MMWR. Morbidity and mortality weekly report* **61**, 909-913 (2012).

358. Luders, H. Classification of epileptic seizures and epilepsies. in *Textbook of Epilepsy Surgery* (ed. H. Luders) 245-248 (Informa Healthcare, United Kingdom, 2008).

359. Schachter, S.C. Iatrogenic seizures. *Neurologic clinics* **16**, 157-170 (1998).

360. Loddenkemper, T., Kellinghaus, C., Wyllie, E., Najm, I.M., Gupta, A., Rosenow, F. & Luders, H.O. A proposal for a five-dimensional patient-oriented epilepsy classification. *Epileptic Disord* **7**, 308-316 (2005).

361. Devinsky, O. Patients with refractory seizures. *N Engl J Med* **340**, 1565-1570 (1999).

362. Kwan, P. & Brodie, M.J. Early identification of refractory epilepsy. *N Engl J Med* **342**, 314-319 (2000).

363. Lardizabal, D.V. Medical intractability in epilepsy. in *Textbook of Epilepsy Surgery* (ed. H. Luders) 203-206 (Informa Healthcare, United Kingdom, 2008).

364. Ettinger, A.B., Manjunath, R., Candrilli, S.D. & Davis, K.L. Prevalence and cost of nonadherence to antiepileptic drugs in elderly patients with epilepsy. *Epilepsy Behav* **14**, 324-329 (2009).

365. Kwan, P., Arzimanoglou, A., Berg, A.T., Brodie, M.J., Allen Hauser, W., Mathern, G., Moshe, S.L., Perucca, E., Wiebe, S. & French, J. Definition of drug resistant epilepsy: consensus proposal by the ad hoc Task Force of the ILAE Commission on Therapeutic Strategies. *Epilepsia* **51**, 1069-1077 (2010).

366. Berg, A.T., Shinnar, S., Levy, S.R., Testa, F.M., Smith-Rapaport, S. & Beckerman, B. Early development of intractable epilepsy in children: a prospective study. *Neurology* **56**, 1445-1452 (2001).

367. Dlugos, D.J., Sammel, M.D., Strom, B.L. & Farrar, J.T. Response to first drug trial predicts outcome in childhood temporal lobe epilepsy. *Neurology* **57**, 2259-2264 (2001).

368. Brodie, M.J. & Kwan, P. Staged approach to epilepsy management. *Neurology* **58**, S2-8 (2002).

369. Morris, H.N., I.; Kahane, P. Epilepsy surgery: patient selection. in *Textbook of Epilepsy Surgery* (ed. H. Luders) 230-237 (Informa Healthcare, United Kingdom, 2008).

370. Schuele, S.U. & Luders, H.O. Intractable epilepsy: management and therapeutic alternatives. *Lancet neurology* **7**, 514-524 (2008).

371. Campos, M.G.W.S. Epilepsy surgery: access, costs, and quality of life. in *Textbook of Epilepsy Surgery* (ed. H. Luders) 223-229 (Informa Healthcare, United Kingdom, 2008).

372. Wiebe, S., Blume, W.T., Girvin, J.P., Eliasziw, M., Effectiveness & Efficiency of Surgery for Temporal Lobe Epilepsy Study, G. A randomized, controlled trial of surgery for temporal-lobe epilepsy. *N Engl J Med* **345**, 311-318 (2001).

373. Wieser, H.G. & Epilepsy, I.C.o.N.o. ILAE Commission Report. Mesial temporal lobe epilepsy with hippocampal sclerosis. *Epilepsia* **45**, 695-714 (2004).

374. Binder, D.K.S., J. Resective surgical techniques: mesial temporal lobe epilepsy. in *Textbook of Epilepsy Surgery* (ed. H. Luders) 1083-1092 (Informa Healthcare, United Kingdom, 2008).

375. Josephson, C.B., Dykeman, J., Fiest, K.M., Liu, X., Sadler, R.M., Jette, N. & Wiebe, S. Systematic review and meta-analysis of standard vs selective temporal lobe epilepsy surgery. *Neurology* **80**, 1669-1676 (2013).

376. Jeha, L.E., Najm, I.M., Bingaman, W.E., Khandwala, F., Widdess-Walsh, P., Morris, H.H., Dinner, D.S., Nair, D., Foldvary-Schaeffer, N., Prayson, R.A., Comair, Y., O'Brien, R., Bulacio, J., Gupta, A. & Luders, H.O. Predictors of outcome after temporal lobectomy for the treatment of intractable epilepsy. *Neurology* **66**, 1938-1940 (2006).

377. McIntosh, A.M., Kalnins, R.M., Mitchell, L.A., Fabinyi, G.C., Briellmann, R.S. & Berkovic, S.F. Temporal lobectomy: long-term seizure outcome, late recurrence and risks for seizure recurrence. *Brain* **127**, 2018-2030 (2004).

378. Radhakrishnan, K., So, E.L., Silbert, P.L., Jack, C.R., Jr., Cascino, G.D., Sharbrough, F.W. & O'Brien, P.C. Predictors of outcome of anterior temporal lobectomy for intractable epilepsy: a multivariate study. *Neurology* **51**, 465-471 (1998).

379. Rathore, C. & Radhakrishnan, K. Prognostic significance of interictal epileptiform discharges after epilepsy surgery. *J Clin Neurophysiol* **27**, 255-262 (2010).

380. Alarcon, G., Valentin, A., Watt, C., Selway, R.P., Lacruz, M.E., Elwes, R.D., Jarosz, J.M., Honavar, M., Brunhuber, F., Mullatti, N., Bodi, I., Salinas, M., Binnie, C.D. & Polkey, C.E. Is it worth pursuing surgery for epilepsy in patients with normal neuroimaging? *J Neurol Neurosurg Psychiatry* **77**, 474-480 (2006).

381. de Tisi, J., Bell, G.S., Peacock, J.L., McEvoy, A.W., Harkness, W.F., Sander, J.W. & Duncan, J.S. The long-term outcome of adult epilepsy surgery, patterns of seizure remission, and relapse: a cohort study. *Lancet* **378**, 1388-1395 (2011).

382. Elliott, R.E., Bollo, R.J., Berliner, J.L., Silverberg, A., Carlson, C., Geller, E.B., Barr, W.B., Devinsky, O. & Doyle, W.K. Anterior temporal lobectomy with

amygdalohippocampectomy for mesial temporal sclerosis: predictors of long-term seizure control. *J Neurosurg* **119**, 261-272 (2013).

383. Fong, J.S., Jehi, L., Najm, I., Prayson, R.A., Busch, R. & Bingaman, W. Seizure outcome and its predictors after temporal lobe epilepsy surgery in patients with normal MRI. *Epilepsia* **52**, 1393-1401 (2011).

384. Hemb, M., Palmini, A., Paglioli, E., Paglioli, E.B., Costa da Costa, J., Azambuja, N., Portuguez, M., Viuniski, V., Booij, L. & Nunes, M.L. An 18-year follow-up of seizure outcome after surgery for temporal lobe epilepsy and hippocampal sclerosis. *J Neurol Neurosurg Psychiatry* **84**, 800-805 (2013).

385. Holmes, M.D., Born, D.E., Kutsy, R.L., Wilensky, A.J., Ojemann, G.A. & Ojemann, L.M. Outcome after surgery in patients with refractory temporal lobe epilepsy and normal MRI. *Seizure* **9**, 407-411 (2000).

386. McClelland, S., 3rd, Guo, H. & Okuyemi, K.S. Population-based analysis of morbidity and mortality following surgery for intractable temporal lobe epilepsy in the United States. *Arch Neurol* **68**, 725-729 (2011).

387. Davies, K.G., Maxwell, R.E., Beniak, T.E., Destafney, E. & Fiol, M.E. Language function after temporal lobectomy without stimulation mapping of cortical function. *Epilepsia* **36**, 130-136 (1995).

388. Ivnik, R.J., Sharbrough, F.W. & Laws, E.R., Jr. Effects of anterior temporal lobectomy on cognitive function. *Journal of clinical psychology* **43**, 128-137 (1987).

389. Engel, J., Jr. The timing of surgical intervention for mesial temporal lobe epilepsy: a plan for a randomized clinical trial. *Arch Neurol* **56**, 1338-1341 (1999).

390. Lytton, W.W. Computer modelling of epilepsy. *Nat Rev Neurosci* **9**, 626-637 (2008).

Vita

Mehmet Cihan Kadipasaoglu was born in Anderson, SC on May 22, 1986, the son of Kamuran Kadipasaoglu and Sukran Kadipasaoglu. After completing high school at Awty International School, Houston, TX, in 2004, he entered Carnegie Mellon University in Pittsburgh, PA. He received the degree of Bachelor of Science in Mechanical Engineering and Bachelor of Science in Philosophy, graduating with honors in both majors from Carnegie Mellon University in December 2008. For the next year and a half, he worked as an equipment manager and senior research technician in The Department of Cardiovascular Pathology and The Cullen Cardiovascular Research Laboratory at The Texas Heart Institute, Houston, TX. In August of 2010 he entered the MD program at The University of Texas Medical School at Houston. He completed two years of medical education, at which time he entered the University of Texas MD/PhD Program at Houston. In June of 2012 he began his PhD studies in The University of Texas Graduate School of Biomedical Sciences, working in Dr. Nitin Tandon's Neuroimaging and Electrophysiology Lab in the Department of Neurosurgery. In June of 2015 he was married to the love of his life, Jamie Robin Chu.

Permanent address:

2601 Bellefontaine Street, Apt. B212
Houston, Texas 77025